INSTITUTO POTOSINO DE INVESTIGACIÓN CIENTÍFICA Y TECNOLÓGICA, A.C.

POSGRADO EN CIENCIAS AMBIENTALES

“Study of nano-ZnO/Graphene-based photocatalyst to degrade Triclosan under UV and visible light”

Tesis presentada por:

M. en C. Nancy Ayerim Cervantes Rincón

Para obtener el grado de:

Doctora en Ciencias Ambientales

San Luis Potosí, S.L.P., 21 de Febrero de 2020

Constancia de aprobación de la tesis

La tesis “Study of nano-ZnO/Graphene-based photocatalyst to degrade Triclosan under UV and visible light” presentada para obtener el Grado de Doctora en Ciencias Ambientales fue elaborada por **Nancy Ayerim Cervantes Rincón** y aprobada el **día 21 de febrero de 2020** por los suscritos, designados por el Colegio de Profesores de la División de Ciencias Ambientales del Instituto Potosino de Investigación Científica y Tecnológica, A.C.

Dr. Vladimir Alonso Escobar Barrios _____

Director de Tesis

Dr. Monserrat Bizarro Sordo _____

Miembro del Comité Tutor

Dr. Luis Felipe Cházaro Ruíz _____

Miembro del Comité Tutor

Dr. Cesar Nieto Delgado _____

Miembro del Comité Tutor

IPICYT

Constancia de aprobación de la tesis

La tesis ***"Study of nano-ZnO/Graphene-based photocatalyst to degrade Triclosan under UV and visible light"*** presentada para obtener el Grado de Doctora en Ciencias Ambientales fue elaborada por **Nancy Ayerim Cervantes Rincón** y aprobada el veintiuno de febrero del dos mil veinte por los suscritos, designados por el Colegio de Profesores de la División de Ciencias Ambientales del Instituto Potosino de Investigación Científica y Tecnológica, A.C.

Dr. Vladimir Alonso Escobar Barrios
Director de la tesis

Dra. Monserrat Bizarro Sordo
Miembro del Comité Tutoral

Dr. Vicente Rodríguez González
Miembro del Comité Tutoral

IPICYT

Instituto Potosino de Investigación Científica y Tecnológica, A.C.

Acta de Examen de Grado

El Secretario Académico del Instituto Potosino de Investigación Científica y Tecnológica, A.C., certifica que en el Acta 024 del Libro Primero de Actas de Exámenes de Grado del Programa de Doctorado en Ciencias Ambientales está asentado lo siguiente:

En la ciudad de San Luis Potosí a los 21 días del mes de febrero del año 2020, se reunió a las 11:10 horas en las instalaciones del Instituto Potosino de Investigación Científica y Tecnológica, A.C., el Jurado integrado por:

Dr. Luis Felipe Cházaro Ruiz	**Presidente**	**IPICYT**
Dra. Monserrat Bizarro Sordo	**Secretaria**	**UNAM**
Dr. Cesar Nieto Delgado	**Sinodal**	**IPICYT**
Dr. Vladimir Alonso Escobar Barrios	**Sinodal**	**IPICYT**

a fin de efectuar el examen, que para obtener el Grado de:

DOCTORA EN CIENCIAS AMBIENTALES

sustentó la C.

Nancy Ayerim Cervantes Rincón

sobre la Tesis intitulada:

Study of nano-ZnO/Graphene-based photocatalyst to degrade Triclosan under UV and visible light

que se desarrolló bajo la dirección de

Dr. Vladimir Alonso Escobar Barrios

El Jurado, después de deliberar, determinó

APROBARLA

Dándose por terminado el acto a las 13:35 horas, procediendo a la firma del Acta los integrantes del Jurado. Dando fe el Secretario Académico del Instituto.

A petición de la interesada y para los fines que a la misma convengan, se extiende el presente documento en la ciudad de San Luis Potosí, S.L.P., México, a los 21 días del mes de febrero de 2020.

Dr. Marcial Bonilla Marín
Secretario Académico

Mtra. Ivonne Lizette Cuevas Vélez
Jefa del Departamento del Posgrado

INSTITUTO POTOSINO DE INVESTIGACIÓN CIENTÍFICA Y TECNOLÓGICA, A.C.
IPICYT
SECRETARIA ACADEMICA

IPICYT
INSTITUTO POTOSINO DE INVESTIGACIÓN CIENTÍFICA Y TECNOLÓGICA, A.C.

Department of Environmental Science

M.Sc. Nancy Ayerim Cervantes Rincón

Study of nano-ZnO/Graphene-based photocatalyst to degrade Triclosan under UV and visible light

Thesis for the degree of Doctor of Science (Environmental Sciences) to be presented with due permission for public examination and criticism in the Instituto Potosino de Investigacion Cientifica y Tecnologica (IPICYT), San Luis Potosi, Mexico on 21st of February, 2020.

Supervisor Dr. Vladimir Alonso Escobar Barrios
Department of Advanced Materials
Instiuto Potosino de Investigacion Cientifica y Tecnologica A.C. (IPICYT)
Mexico

Reviewers Dr. Monserrat Bizarro Sordo
Materials Research Institute
Universidad Nacional Autonoma de Mexico (UNAM)
Mexico

Dr. Luis Felipe Cházaro Ruíz
Department of Environmental Science
Instiuto Potosino de Investigacion Cientifica y Tecnologica A.C. (IPICYT)
Mexico

Dr. Cesar Nieto Delgado
Department of Environmental Science
Instiuto Potosino de Investigacion Cientifica y Tecnologica A.C. (IPICYT)
Mexico

San Lui Potosi, Mexico
February, 2020

Abstract

In recent years, a growing problem with water treatment has arisen due to the presence of endocrine-disrupting compounds (EDC), which persist in surface, waste, and drinking water. A significant example of EDC is triclosan (TCS), a bactericidal widely used in deodorant formulations, toothpaste, soaps, powders, cosmetics, textiles, plastics, polymers, fibers, and medical implant devices. Then, given the use of these products, triclosan has been directly discharged into wastewater, although it has also been detected in surface water, sludge, sediment, and drinking water. The treatment of water, by conventional methods, removes in some cases up to 90% of EDC. However, with such residual concentrations of triclosan, it is necessary to develop methods to remove even trace concentrations of these pollutants. Heterogeneous photocatalysis, which is usually carried out under ultraviolet radiation to activate the semiconductor and thereby to trigger reduction and oxidation reactions that are responsible for degrading and mineralizing organic compounds, such as triclosan. Nano ZnO is a semiconductor that has demonstrated potential photocatalytic activity to degrade EDC, but its development can be improved by using an electron transport material as graphene or graphene oxide.

Modification of ZnO nanoparticles with graphene and graphene oxide (GO) was carried out, and the obtained hybrid photocatalyst was used for the photodegradation of TCS. The carbon material amount was evaluated to modify nano-ZnO catalyst using two different methods mechanical and photo-irradiation, and the resultant materials were characterized in order to determine their physicochemical and photocatalytic properties. Regarding the photocatalytic evaluation, the results of the photodegradation process for TCS showed that carbon materials act as a trap of electrons improving the performance of ZnO even at low TCS concentration (8 $mg.L^{-1}$) under visible and UV radiation. The graphene base-modified photocatalysts with the highest concentration (0.5% w/w) showed the best photocatalytic performance under visible light degrading up to 47% of TCS and showed a reaction rate constant two times higher than pure ZnO in contrast with the 95% of the TCS degraded under UV light. In addition, the hybrid nano-ZnO/GO photocatalyst was immobilized in a polymer matrix (PVA hydrogel), as an alternative to support photocatalyst in real WWTPs obtaining a TCS degradation of 32% under visible radiation. This research contributes to the understanding how to enhance the efficiency of hybrid photocatalysts and the photoactive polymer material under natural light radiation (solar light) in APOs.

Keywords: Endocrine Disrupting Compounds, Triclosan, photocatalysis, photocatalyst, nano-ZnO/Graphene, nano-ZnO/GO, UV light, Visible light, PVA, hydrogel.

Acknowledgements

The results, of this doctoral thesis, are mainly based on the research projects developed during the period 2014–2018 at the Laboratory of Advanced Polymers in Instituto Potosino de Investigacion Cientifica y Tecnologica A.C. (IPICYT), Mexico and the Laboratory of Green Chemistry at Lappeenranta University of Technology, Finland. These projects were supported by the Consejo Nacional de Ciencia y Tecnologia (CONACYT, Mexico) and the Government of Finland.

I wish to express my deepest gratitude to the supervisor of this work, Dr. Vladimir Alonso Escobar Barrios, for his precious comments on the thesis and for the encouragement for my research work. My warm thanks to all the co-workers at the Laboratory of Advanced Polymers, who established a great working atmosphere and supported my research work. In particular, my thanks to Dr. Monserrat Bizarro Sordo and Dr. Luis Felipe Cházaro Ruíz for their effort to evaluate this doctoral project, their comments and corrections to improve it.

Special thanks are due to Professor Mika Sillanpää for his support and professional help in the revision of the projects developed in Finland, during my research stay. My warm thanks to all the co-workers at the Laboratory of Green Chemistry in the Lappeenranta University of Technology, who support my research work in Finland. Additionally, my acknowledgements to Beatriz Rivera for the Raman and XRD analysis, Hector Silva for the TEM analysis and Gladys Labrada for the SEM analysis and all facilities provided to use the national laboratory of LINAN at the IPICYT, México.

The financial support (scholarship #253175) provided by the Consejo Nacional de Ciencia y Tecnologia (CONACYT) and the Government of Finland by the “Finnish Government Scholarship Pool” is greatly acknowledged.

My warmest thanks go to my husband, Ivan, who have always supported me and to my parents, Mercedes and Tomas, who give me an excellent basis for life and always support me. At last, but not least, my deepest thanks, from the bottom of my heart, go to my Tomy, Nayeli, Paco, Isaac, Fernanda, Martha, Tam, Samia, Sidra, Noman and Rutely, for their love and understanding!

Nancy Ayerim Cervantes Rincón
February, 2020

- Anyone who stops learning is old, whether at twenty or eighty. Anyone who keeps learning stays young. The greatest thing in life is to keep your mind young.

- Henry Ford

Contents

Abstract **vi**

Acknowledgements **vii**

Contents **ix**

List of publications **1**

Nomenclature **2**

1 Introduction **5**
1.1 Endocrine Disrupting Compounds 5
1.2 Triclosan 5
1.3 Advanced Oxidation Processes 6
1.4 Zinc Oxide 7
1.5 Graphene and Graphene Oxide 8
1.6 Polymer composites 8
1.7 Hyphotesis 10
1.8 Objectives 10
1.9 Materials and Methods 11
1.9.1 Materials 11
1.9.2 Methods 11

2 Chapter 1. nano-ZnO/Graphene photocatalysts **18**
2.1 Characterization and properties of nano-ZnO/Graphene photocatalysts 21
2.2 Photocatalytic performance 34
2.3 Mechanistic study 39
2.4 Previous conclusions 43

3 Chapter 2. nano-ZnO/GO photocatalysts **44**
3.1 Characterization and properties of nano-ZnO/GO photocatalysts 46
3.2 Photocatalytic performance 59
3.3 Mechanistic study 67
3.4 Previous conclusions 72

4 Chapter 3. nano-ZnO/GO/PVA composites **73**
4.1 Swelling behaviour 75
4.2 Characterization and properties of nano-ZnO/GO/PVA composites 77

4.3 Photocatalytic activity 81
4.4 Previous conlusions.....82

5 Chapter 4. Conclusions 83

6 References 84

7 Appendices 93
Appendix A: Band Gap results of nano-ZnO/Graphene photocatalysts synthesized by MI method……93
Appendix B: Adsorption isotherms ..…….. 94

8 Publications 97

List of publications

This section contains material from the following publications. The rights have been granted by publishers to include the papers in dissertation.

I. Nancy Cervantes Rincón, Samia Ben Hammouda, Mika Sillanpää, Vladimir Escobar Barrios. (2018). Enhanced photocatalytic performance of zinc oxide nanoestructures via photoirradiation hybridization with graphene oxide for the degradation of triclosan under visible light: Synthesis, characterization and mechanistic study. *Journal of Environmental Chemical Engineering*, 6 (5), pp. 6554-6567.

II. Vladimir A. Escobar Barrios, Dalia Verónica Sánchez Rodríguez, Nancy Ayerim Cervantes Rincón, Alma Berenice Jasso-Salcedo. (2018). Modified Metallic Oxides for Efficient Photocatalysis. *Photocatalysts – Applications and Attributes*, IntechOpen, Chapter 4.

Author's contribution

I am the first author and main investigator in paper I. In paper II, Dr. Vladimir A. Escobar Barrios was the corresponding author and I conducted the experiments and post processed the experimental data corresponding to the ZnO/Graphene and ZnO/GO hybrid catalysts.

Nomenclature

In the present work, variables and constants are denoted using *slanted style* and abbreviations are denoted using regular style.

Latin alphabet

k_{app}	apparent reaction rate constant	min^{-1}
t	time	min

Greek alphabet

θ	(theta), angular degrees
λ	(lambda), wavelenght

Chemical symbols

$^{\bullet}OH$	hydroxyl radical
TiO_2	titanium dioxide
ZnO	zinc oxide
H_2SO_4	sulfuric acid
NaOH	sodium hydroxide
DMPO	5.5´-dimethyl-1-pirrolidone-N-oxide
N_2	nitrogen gas

Units

$ng.L^{-1}$	nanograms per liter
$\mu g.L^{-1}$	micrograms per liter
$mg.L^{-1}$	miligrams per liter
$g.L^{-1}$	grams per liter
W	watts
nm	nanometer
µm	micrometer
mm	milimeter
cm	centimeter
µl	microliter

m	meter
ml	mililiter
$mV.cm^{-2}$	milivolts per square centimeter
$ml.min^{-1}$	mililiter per minute
ºC	degrees Celsius
Å	amstrong
eV	electron volts
e^-	electron
h^+	hole

Abbreviations

EDC	endocrine disrupting compounds
WWTPs	wastewater treatment plants
GAC	granulated activated carbon
AOPs	advanced oxidation processes
UV	ultra violet
GO	graphene oxide
PVA	poly(vinyl alcohol)
MI	mechanical impregnation
PI	photoirradiation
M_w	molecular weight
C	Concentration
C_0	initial concentration
ln	natural logarithm
M	molar concentration
SEM	scanning electron microscopy
TEM	transmission electron microscopy
FTIR	Fourier transform infrared spectroscopy
HPLC	high performance liquid chromatography
ESR	electron espin resonance
XRD	X-ray difraction
EDS	energy dispersive X-ray spectroscopy
ATR	attenuated total reflection
BET	Brunauer Emmett Teller
2D	two dimensional

BJH	Barret Joyner Halenda
ICDD	International Centre for Diffraction Data
DSC	Differential Scanning Calorimetry
TGA	Thermo-Gravimetric Analysis
T_g	transition temperature
T_m	melting temperature
T_c	crystallization temperature

1 Introduction

1.1 Endocrine Disrupting Compounds.

In recent years, a growing problem with water treatment has arisen due to the presence of endocrine-disrupting compounds (EDC), which persist in surface, waste, and drinking water. The endocrine-disrupting compounds term defines a diverse and heterogeneous group of chemicals that alter the hormonal balance [1], i.e., they interfere in the normal functions of the hormonal processes of living beings. Such chemical compounds can mimic hormones, because their similar chemical structure, but they do not act as hormones and are responsible for the homeostasis, reproduction, and non-adequate developmental process in living beings [2, 3]. The ways of exposure to EDCs occur through drinking contaminated water, breathing contaminated air, ingesting food, or being in contact with contaminated soil and by using commercial products.

1.2 Triclosan.

A significant example of EDC is triclosan (TCS, 5−chloro−2−(2,4−dichloro phenoxy) phenol), an antimicrobial agent, widely applied in popular personal care products such as soaps, deodorants, toothpaste, cosmetics and laundry detergents [4]. Unfortunately, due to the high levels of TCS consumption, the overloading residues, from personal−care products, are transported from domestic sewage to wastewater treatment plants (WWTPs) and, eventually, from wastewater effluents into the aquatic environment [5]. As a consequence, the residue of TCS as an emerging contaminant was globally detected in surface waters at levels from ng L^{-1} to μg L^{-1} [6]. Recent studies have reported that TCS, at trace level, is acutely toxic to aquatic organisms, and subsequently poses a harmful effect on mammalian via the food chain [7]. The well−documented TCS toxicity in mammalians models that include irritation of eyes and skins, allergies, detrimental effects on development and reproduction, weakening of the immune system, inhibition of muscle function and genotoxicity, arouses great attention and public concerns [8]. More seriously, high levels of TCS have been detected in several human tissues, which present very harmful effects on human health [9].

The growing awareness about the environmental damages, by TCS, urged that over−the−counter antibacterial soaps and body washed containing TCS were banned by the U.S. Food and Drug Administration [10]. Meanwhile, the European Commission (2016/110/EU) adopted the decision to disapprove TCS for use in human hygiene biocidal products (product−type 1). For the prevention of deleterious effects of triclosan on the aquatic environment, it is of great importance to explore selective, efficient, and recyclable sorbents for TCS removal and determination from aqueous matrices.

Conventional wastewater treatment, like the sewage adsorption is the most common technique, which could achieve removal efficiencies of TCS in the range of 58–99% [11]. However, approximately 50% of sludge−adsorbed TCS, persisted in the biosolids, mostly was backed to land and resulted in secondary pollution. Other methods, like granulated activated carbon (GAC) and ozonation, also displayed their limitations, due to the absence of separation and recovering from aqueous solutions and the interference of adsorption by humic acids and surfactants [12, 13]. In particular, it is easy to make large amounts of wasteful adsorbents or oxidants because of their non-specificity [14]. Moreover, biological treatment, which is an environment−friendly method, was hardly carried out in realistic applications, because microorganisms were lethally impacted by traces of TCS, and preferentially metabolized other substances with higher concentrations [15]. Hence, it is urgent to develop a new and specific method with fast separation, and convenient recycling to considerably enhance the efficiency of TCS removal, at trace concentration, from the aquatic environment.

1.3 **Advanced Oxidation Processes.**

Advanced Oxidation Processes (AOPs) is one of the most effective methods due to the high oxidizing power of free radicals, generated during such processes, like hydroxyl radical ($^{\bullet}$OH) that can mineralize compounds that cannot be oxidized by oxidizing agents such as oxygen, ozone, and chlorine [16]. Among the methodologies to generate hydroxyl free radicals, we can find the heterogeneous photocatalysis, which is usually carried out under ultraviolet radiation to activate the semiconductor and thereby to trigger reduction and oxidation reactions that are responsible for degrading and mineralizing organic compounds, such as triclosan.

Generally, the semiconductors used for this purpose are cheap, non-toxic, and can be regenerated without losing their photocatalytic activity [17, 18]. Examples of the most used semiconductors in heterogeneous photocatalysis for organic compounds are titanium dioxide, zinc oxide, tellurium cadmium, and zinc selenide, although the titanium dioxide is the material that has gained much attention and we can find extensive literature regarding this compound. However, in the case of TiO_2, its oxidative degradation, by the effect of high recombination of electrons, limits its use at the industrial scale.

1.4 **Zinc Oxide.**

ZnO has attracted much attention in the degradation of various pollutants due to its high photosensitivity. The ZnO has wide bandgap (3.37 eV), large excitation binding energy (60 MeV) and low threshold power for optical pumping and is thus considered a low-cost alternative photocatalyst to TiO_2 for the degradation of organic compounds in aqueous solution [19, 20]. In addition, ZnO absorbs a greater fraction of the radiation spectrum for the photocatalytic process and, therefore, it has been used in the manufacture of solar panels and for optoelectronic applications. This characteristic of ZnO to absorb a larger fraction of the radiation spectrum if it is modified and its chemical resistance opens the possibility to use this material in water treatment to degrade EDC, such as triclosan.

Despite the advantages of ZnO and its promising application in photocatalytic degradation using UV, visible and sunlight, there are questions to be answered regarding the degradation of EDC, such as triclosan, because the main problem that affects the photocatalytic efficiency of semiconductors as ZnO is the recombination of excited electrons, which decreases the formation of hydroxyl free radicals and, hence, there is a decrement of the efficiency of pollutant degradation. Moreover, it has been stated that when irradiated by UV light, triclosan (in its anionic form) is involved in an efficient ring closure. It leads to the formation of highly toxic compounds like chlorodioxins [16].

Thus, some strategies have been focused to reduce the recombination of excited electrons and to avoid toxic compounds like chlorodioxins, such as the modification of ZnO nanoparticles with metal, thereby forming hetero-structure. The obtained results by other researchers show the relevance of modifying the ZnO with gold [21],

silver [22] and platinum [23] nanoparticles for the photodegradation of different organic pollutants as dyes [24, 25], considering that they are good electron conductors, property that imparts to the ZnO a delayed recombination of excited electrons.

1.5 Graphene and Graphene Oxide.

However, metals are not the only materials that exhibit good electrical properties to retard the electron recombination process occurring in photocatalysts. Recently, graphene and graphene oxide (GO) has been used for the development of new materials, due to their properties and chemical surface properties (functional groups), which promote the interactions between GO and several types of material [26].

Furthermore, the graphene may exceed the electron-transport property, a key characteristic of metals. In the case of GO, this property depends on the number of functional groups present on its surface [27]. Studies show excellent chemical properties of GO to form compounds with other materials due to its surface chemistry and its delocalized π–π conjugated structures that reduce the recombination rate of charge carriers as well as its ability to be reduced to graphene using ultraviolet radiation. Indeed, specific features to achieve high efficiency, like high surface area and the reduced recombination rate of charge carriers, both improve the response to visible light [28, 29]. Thus, it is possible to obtain compounds of ZnO/GO or ZnO/Graphene with high thermal and electrical conductivity (higher than the pure semiconductor or metal), which delay the recombination process. These important chemical and electrical characteristics do impart, to these materials, certain attractiveness for potential applications such as photocatalysts.

1.6 Polymer composites.

Despite the excellent efficiency of photocatalysts to degrade EDCs, as triclosan, at trace concentration, different materials have been supported in order to be used in common water treatment systems, mainly polymers have been used for this purpose. However, when polymeric composites are packed in carrier or column usually clogging and back-pressure problems arise [30]. Therefore, a major challenge is the development of polymeric composites that contains active

photocatalysts with adequate capacity of photodegradation, convenient recycling, quick and easy separation. Membrane support technology has harvested highlighted attention, since its application provided a simple way to degrade organic pollutants from sample matrices [31], especially using non-toxic, low cost and mechanically resistant polymers.

1.7 Hypothesis.

Nano-ZnO photocatalyst are able to be modified with graphene oxide (GO) and graphene by mechanical and photoirradiation methods due to their surface chemistry and their delocalized π–π conjugated structures. Therefore, the recombination rate of charge carriers of the nano-ZnO photocatalyst is reduced since graphene or GO can acts as an electron tramp, retaining the excited electrons on the nano-ZnO surface.

Thus, the degradation percentage of triclosan is increased under UV and visible light due to the capacity of nano-ZnO/Graphene or nano-ZnO/GO composites to increase the amount of free radicals, which are responsible for degrading triclosan.

Finally, the poli(vinyl alcohol) composites can be synthesized by esterification reaction allowing the dispersion of nano-ZnO hybrid photocatalysts in the polymeric matrix.

1.8 Objectives.

The thesis aims to modify ZnO with graphene or graphene oxide to increase its potential as photocatalyst for water treatment contaminated with triclosan, an endocrine-disrupting compound, and evaluate the photocatalytic activity once they are immobilization in poly(vinyl alcohol) matrix.

The specific objectives are:

I. The study of the influence of the method modification of nano-ZnO photocatalyst on the degradation of triclosan, under visible light.
II. The study of the influence of graphene's and GO's concentration in the modified nano-ZnO on the degradation of triclosan under UV and visible light.
III. Establish the reaction rates for the degradation of triclosan.
IV. Immobilization of nano-ZnO hybrid photocatalysts into poly(vinyl alcohol) matrix and their physicochemical characterization.
V. Evaluation of the polymeric composites for the photodegradation of triclosan.

1.9 Materials and Methods.

1.9.1 Materials.

Nano zinc oxide was obtained from Degussa (Germany) under name VP AdNano ZnO 20, the graphene and graphene oxide HC (5 g/L) was purchased from Supermarket Company. Triclosan (≥97%), pure ethanol, 5.5´-dimethyl-1-pirrolidone-N-oxide (DMPO), poly (vinyl alcohol) (M_w 31,000-50,000, 98-99% hydrolyzed), citric acid (≥99.5%) and 2-propanol (≥99% purity) were purchased from Sigma-Aldrich. Deionized water used in the work was purified and its conductivity was 17.5 siemens.m^{-1}. All of the materials purchased were used as received, without any further purification.

1.9.2 Methods.

Preparation of nano-ZnO/Graphene and nano-ZnO/GO photocatalysts.

Nano-ZnO hybrid catalysts were prepared following the mechanical impregnation (MI) or photoirradiation (PI) methods, reported elsewhere [32]. The ZnO solutions (1% w/w) were prepared using isopropanol. Then, graphene or graphene oxide was added with different concentrations regarding the ZnO weight (Table 1) to evaluate the effect of graphene material in the overall photocatalytic process for triclosan degradation. The resulting nano-ZnO/Graphene, or nano-ZnO/GO, solutions were sonicated for one hour and then they were exposed to mechanical agitation or UV radiation (205 nm) and stirred continuously for 2 hours. Finally, the obtained materials were recovered by centrifugation (3200 rpm for 10 minutes) and oven-dried at 50°C for 12 hours and then stored for use.

Table 1. Synthesised nano-ZnO/Graphene and nano-ZnO/GO photocatalysts.

Sample	Graphene Concentration (% w/w)	Sample	GO Concentration (% w/w)
Nano-ZnO/Graphene 0.10%	0.10	Nano-ZnO/GO 0.10%	0.10
Nano-ZnO/Graphene 0.25%	0.25	Nano-ZnO/GO 0.25%	0.25
Nano-ZnO/Graphene 0.50%	0.50	Nano-ZnO/GO 0.50%	0.50

Preparation of nano-ZnO/GO/PVA composites.

Nano-ZnO/GO/PVA composites were prepared as follows: PVA and PVA composites films were produced by preparing 10 $g.L^{-1}$ PVA aqueous solution at 70 ºC in the absence, or in the presence, of citric acid at 0.5 $g.L^{-1}$. The solutions were stirred to homogenize them, for one hour, and the previous synthesized photocatalyst solution was added and stirred for one hour. The resultant solution was sonicated for 10 minutes to remove air bubbles, before casting. Crosslinking was carried out by heating the dried films at 165 ºC for 20 minutes. The resulting PVA hydrogels and PVA composites were dried at 45 ºC for 48 hours and then stored for use.

Photodegradation of triclosan

The photodegradation of TCS was conducted by batch-type experiments. The reactor system consisted of a top open glass reactor of 150 mL capacity. The lamps for irradiation (UV or visible) were put on top of the reactor at 8 cm distance. All the mixtures were stirred for homogenization. Typically, the required amount of catalyst (1 $g.L^{-1}$) was first added to 100 mL of the TCS solution, which had an initial concentration of 8 mgL^{-1} and then exposed to the light illumination source for 2 hours, UV light (254 nm with intensity of 858 $mW.cm^{-2}$) or visible radiation (150 W halogen lamp with light intensity of 308 $mW.cm^{-2}$) as it is shown in Figure 1. Samples of 1 mL were withdrawn from the reactor at set intervals and filtered immediately through a 0.22 µm filter film.

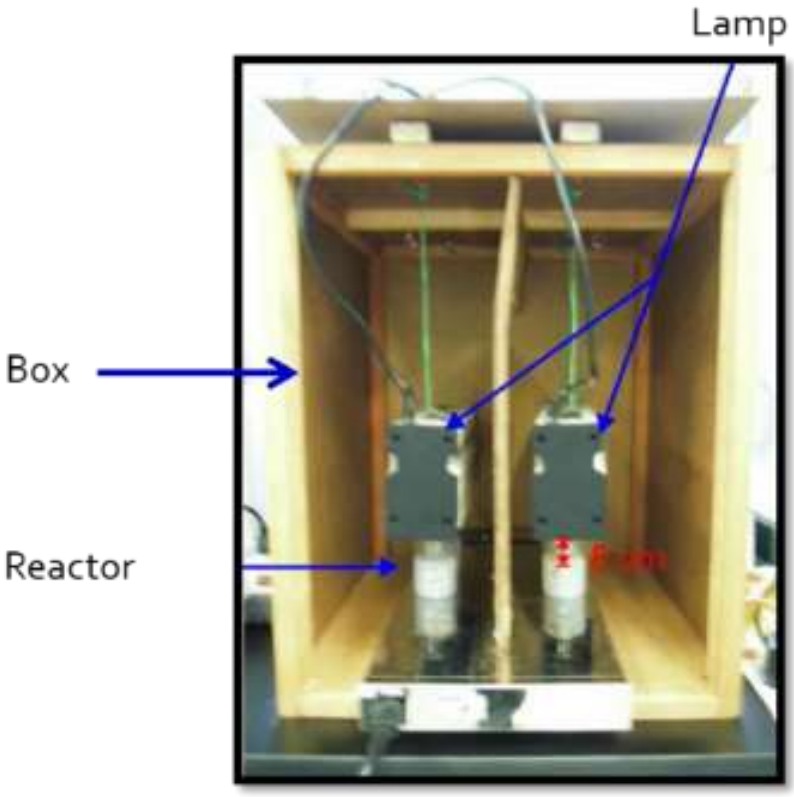

Figure 1. Photodegradation system.

The adsorption tests, for the synthesized photocatalysts, were conducted in dark conditions; such tests were carried out before photocatalysis and it was established that adsorption takes place during the first one hour of contact between triclosan solution and photocatalyst. Thus, all the photocatalytic experiments began after one hour in dark conditions.

In addition, cycling experiments were carried out to verify the photocatalyst stability. For this purpose, after each run, the catalyst was recovered, washed and reused in the subsequent run. The recovered catalysts were collected and dried to evaluate weight loss.

As it has been reported by other researchers [33] the photocatalytic process using heterogeneous catalyst can be described using the Langmuir-Hinshelwood model, which was simplified to the pseudo-first order, as shown in Eq. 1, and it was adopted to describe the photocatalytic kinetic behaviors of triclosan through the as-prepared materials.

$$ln\frac{C}{C_0} = -k_{app}t \quad (1)$$

where C (mg.L^{-1}) is the triclosan concentration at certain time t during photodegradation, Co (mg.L^{-1}) is the initial triclosan concentration, t (min) is the degradation time, and k_{app} (min^{-1}) is the apparent reaction rate constant.

Swelling behavior

The swelling behavior was determined gravimetrically, as follows. The dried PVA and PVA composites were immersed in water (pH=7) until the swelling equilibrium was reached. The swollen samples were taken out, wiped with tissue paper to remove the excess of water on the surface, and weighed immediately. The equilibrium swelling (%) was calculated using equation 2:

$$Swelling\ (\%) = \frac{W_s - W_d}{W_d} \quad (2)$$

Where W_d and W_s are the weights of dried and swollen samples, respectively.

Characterization Techniques

Scanning Electron Microscopy (SEM)

Scanning Electron Microscopy (SEM) was used to characterize the morphology and chemical composition of the nano-ZnO hybrid photocatalysts. To carry out the analysis, the samples were directly deposited on carbon membrane grids. A microscope FEI-FIB Dual Beam Helios Nanolab 600 was used for this purpose.

Transmission Electron Microscopy (TEM)

Transmission Electron Microscopy (TEM) was used to determine the structure and morphology of the hybrid nano-ZnO/Graphene and nano-ZnO/GO compounds. For this study, a TEM Tecnai (300 keV) type FEG model (FEI Company) microscope was used with a resolution of 1.8Å, point to point, in HRTEM and 3Å in contrast Z, while the resolution of EDS analysis in the bright field is 20 nm and 1nm in contrast Z. The samples were supported on copper grids with carbon membrane.

Fourier Transform Infrared Spectroscopy (FTIR)

The equipment model Nicolet iS10 (Thermo Scientific) was used for this characterization with measurements in the wavenumber range 400 to 4000 cm^{-1}. All the analyzed samples were powdered and analyzed using the ATR mode.

Raman Spectroscopy

Raman spectroscopy was used to provide an overview of the potential interaction between the pristine nano-ZnO and Graphene and GO materials in the investigated hybrid photocatalysts (nano-ZnO/Graphene and nano-ZnO/GO). The equipment InVia Microraman-Renishaw was used for this purpose using a green laser (532 nm wavelength).

Zeta Potential

This analysis was carried out using a Zetasizer Nanoseries (Malvern) to obtain the surface zeta potential and the average size of the synthesized samples. Solutions of H_2SO_4 (0.1 M) and NaOH (0.1 M) were used for this analysis.

X-Ray Diffraction (XRD)

Determination of crystal structure of the synthesized hybrid materials and the pure nano-ZnO, graphene and GO, was carried out using the X-ray diffractometer D8 Advance model (Bruker). The conditions were at 2θ angular intervals from 10 to 90 using a step size of 0.02°.

UV-Vis Spectroscopy

This technique was used to determine the bandgap based on the absorption spectra of the nano-ZnO and nano-ZnO/Graphene and nano-ZnO/GO photocatalysts. The equipment Cary 5000 UV-Vis-NIR with high resolution (<0.047 nm) was used in a wavelength range of 190 - 3300 nm.

Nitrogen Physisorption

For this analysis, a Micromeritics TriStar II Plus analyzer was used to obtain the pore dimension and surface area of the nano-ZnO/Graphene and nano-ZnO/GO hybrid catalysts and the pristine materials, nano-ZnO, graphene and GO. All the studied materials were pre-degassed by vacuum at 120ºC for 5 hours. The specific surface area was determined using the classical BET model.

Thermic Evaluations

Differential Scanning Calorimetry (DSC) and Thermo-Gravimetric Analysis (TGA) were used to determine the thermal properties of the synthesized polymeric composites. For DSC a TA Instruments Q-2000 equipment was used with a heat flow of 10ºC/minute. For TGA a TA Instruments Q-500 was used in a temperature range of 30ºC-900ºC under nitrogen atmosphere.

High Performance Liquid Chromatography (HPLC)

The concentration of triclosan was quantified by a Shimadzu liquid chromatograph equipped with a UV detector. The column used was a Kinetex 5µm EVO C18 100Å, LC Column 150x4.6 mm (Phenomenex). The mobile phase consisted of 70% acetonitrile and 30% water, which was pumped with a flow of 1 $mL.min^{-1}$. The detector SPD-20AV UV wavelength was set at 254 nm. The sample was injected through an autosampler and the injection volume was 50 µL.

Electron Spin Resonance (ESR)

The ESR signals for radicals spin-trapped were examined using an ADANI CMS Model 8400 spectrometer, using as spin-trap reagent the 5,5´-dimethyl-1-pyrrolidone-N-oxide (DMPO). To minimize experimental errors, the same type of quartz capillary tube was used for all the ESR measurements. The magnetic parameters of the radicals detected were obtained from direct measurements of the magnetic field and microwave frequency.

2 Chapter 1
nano-ZnO/Graphene photocatalysts

ZnO is one of the most promising photocatalysts that has been attracted much attention due to its wide bandgap energy, low cost, non-toxicity, and high photosensitivity [34]. However, ZnO is only active in the ultraviolet region and is characterized by its quick recombination of photoinduced charge carriers, then its practical application in visible-light conditions are limited. Therefore, expanding its optical absorption from UV to visible-light region and reduction of recombination, of the photoexcited electron-hole pairs, are the main challenges and extensive research has been devoted to overcoming such limitations.

One strategy to improve its visible-light photocatalytic efficiency is to prepare various composites by modifying ZnO particles with metals, non-metals, rare-earth elements, and carbon-based material, like graphene oxide. It has shown the enhanced visible-light photocatalytic efficiency due to the increase of electron-transfer between ZnO and the dopant material. So far, numerous methods have been used to design and synthesize ZnO hybrid photocatalysts with various morphologies, however, many processes inevitably lead to a higher operating cost or long reaction time.

Graphene, a two-dimensional (2D) single sheet of carbon atoms arranged in a hexagonal network, is one of the most promising materials in nanoscience and nanotechnology. Owing to its remarkable chemical, physical and mechanical properties, such as large surface area, excellent electrical and thermal conductivity, high mechanical strength, flexibility, and efficient wide range of light adsorption, graphene-based materials are popular in a broad range of environmental applications as absorption, transformation, and detection [35]. Hence, many efforts have been devoted to utilizing graphene to enhance the photocatalytic activity of semiconductors to degrade organic compounds [36-39]. Most of the literature has reported the preparation of graphene-based photocatalysts using graphene oxide (GO) as initial material that is reduced by methods as chemical reduction [40, 41] or hydrothermal [42-43] to eliminate chemical oxygen groups, impurities, which negatively affect the electronic and catalytic properties of graphene-based photocatalysts [44].

Thus, to solve the issues in the preparations of graphene-based semiconductors are crucial for potential applications, and to the best of our knowledge, however, graphene sheets already synthesized have rarely been used as the base material to prepare hybrid photocatalysts.

This study proposes the synthesis of ZnO/Graphene semiconductors by developing a facile, cheap, environmentally and high reproducibility approach to obtain an efficient material to degrade organic pollutants like triclosan. For instance, it has been demonstrated that using the inductive irradiation method is possible to synthesize ZnO composites due to its polarity [45].

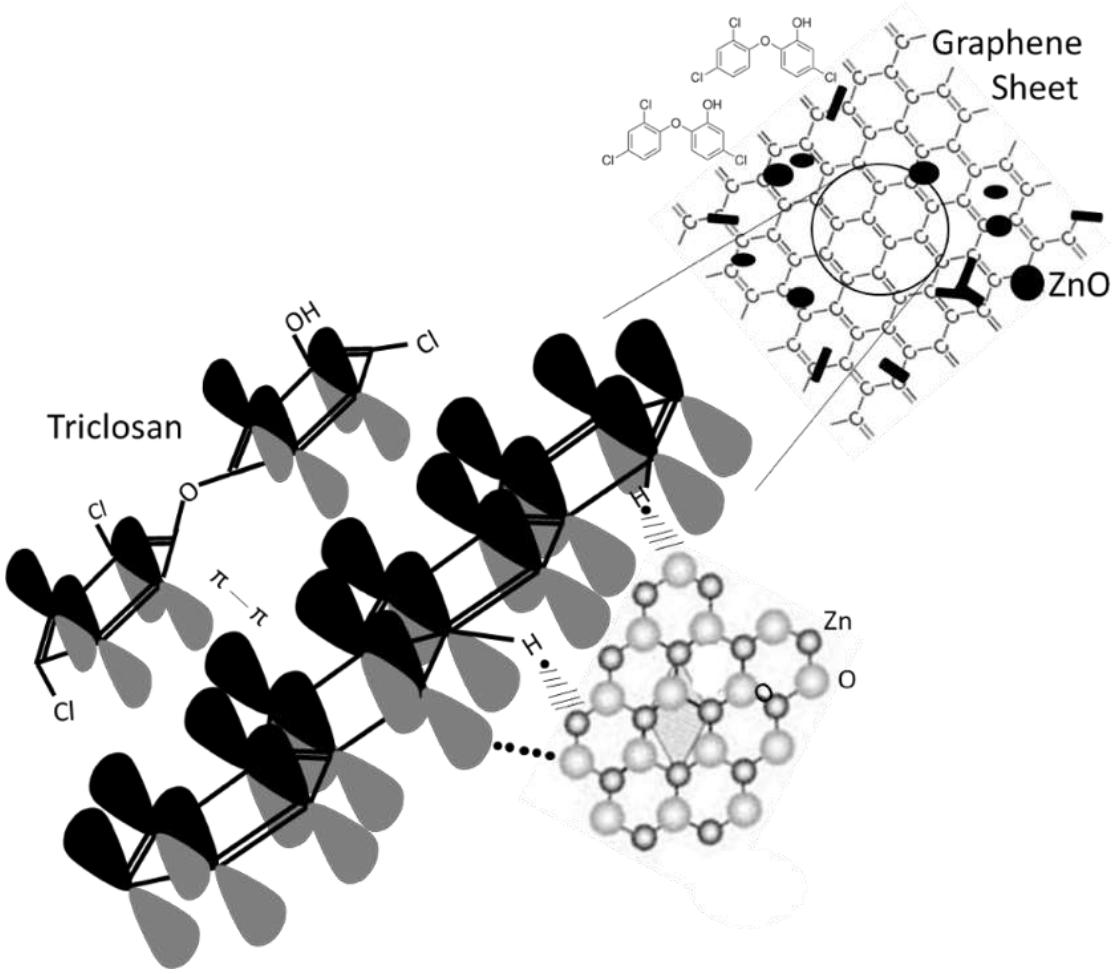

Scheme 1. Schematic drawing of the proposed interaction between ZnO nanoparticles, graphene sheets, and triclosan.

In particular, graphene is a significant material because of its high surface area (2600 m^2/g) high electronic conductivity, high surface to volume ratio and high mechanical properties [46]. Graphene can accept, efficiently, electrons due to the absence of oxygen chemical groups on its surface, which prevents the recombination and provides a favorable surface area for triclosan interaction through π-π conjugation, between TCS and aromatic rings of graphene as well as between ZnO (Scheme 1). The trapped electrons on graphene react with the dissolved oxygen and water to form reactive oxygen and hydroxyl radicals, which further oxidizes triclosan.

In this chapter, the results of nano-ZnO/Graphene hybrid photocatalysts are presented. Two modification methods (MI and PI) were studied for the degradation of triclosan, under visible light.

2.1 **Characterization and properties of nano-ZnO/Graphene photocatalysts.**

Figure 2 shows the SEM micrographs of pristine nano-zinc oxide and graphene sheets along with the corresponding size distribution of ZnO particles obtained by zeta potential. Figure 2-a shows different morphologies of the nano-ZnO particles, including prisms, spheroids and tetrapods, besides other irregular geometries.

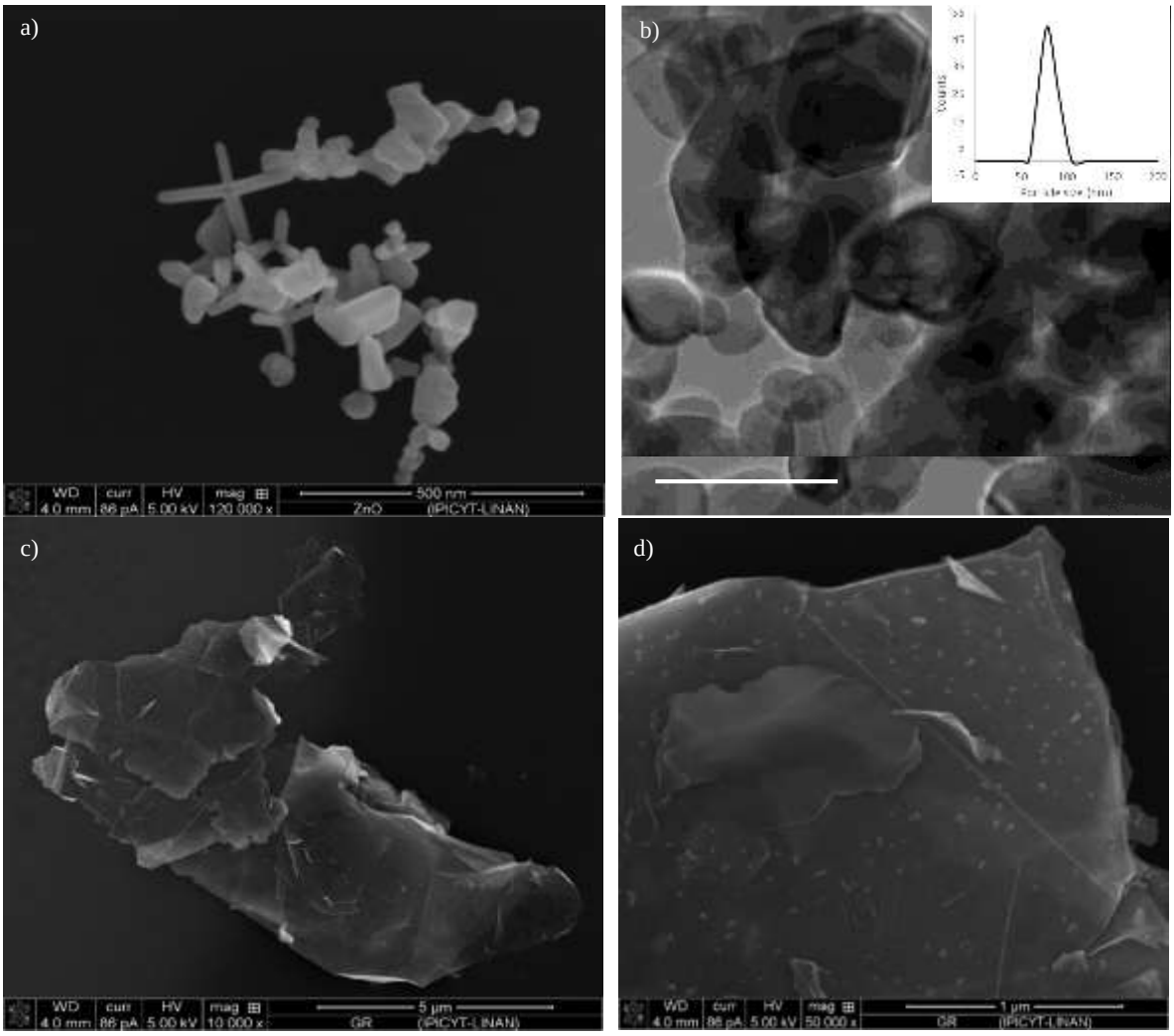

Figure 2. SEM micrographs of a) pristine nano-zinc oxide (120000 x), b) TEM micrograph of ZnO nanoparticles (insert size distribution of pure ZnO nanoparticles obtained by zeta potential). SEM micrographs of c) pure graphene agglomerate sheets (10000 x) and d) zoom of surface (50000 x).

Furthermore, the topology of nano-ZnO particles was observed by TEM (Figure 2-b) and it was detected a hexagonal morphology. Moreover, different particle sizes were determined, which ranged from 30 to 130 nm, as it was confirmed by zeta potential (insert Figure 2-b). Also, the small agglomerates of ZnO nanoparticles, with sizes up to 500 nm, were observed.

Figures 2-c and 2-d show the micrographs obtained by SEM for the graphene sheets, which have greater dimensions (3-4 μm) than the ZnO particles shown in Figures 2-a and 2-b, and such graphene sheets are stacked with even larger dimensions (> 11 μm).

The observed graphene sheets are transparent with a flat topology. Based on these observations, it is suggested that the obtained nano-ZnO/Graphene hybrid photocatalysts in this research are graphene sheets covered by ZnO nanoparticles and/or their agglomerates.

The following micrographs (Figure 3) correspond to nano-ZnO/Graphene hybrid photocatalyst prepared by MI (Figures 3-a and 3-b) and the PI (Figures 3-c and 3-d), loaded with 0.5% w/w of graphene.Figure 3-d reveals the decoration on the surface of graphene sheets with zinc oxide nanoparticles, which are homogeneously distributed. Zinc oxide particles exhibited the same shapes as those observed in the pure material (Figure 2-a). However, this homogenous distribution of zinc oxide nanoparticles indicates the reduction of their agglomeration and enabled a well-wrapped morphology of nano-ZnO particles by graphene sheets.

It is important to note that the homogenous distribution of ZnO nanoparticles on the surface of graphene sheets is probably ascribed to the photoirradiation method. This distribution could be attributed to the energy used during the synthesis of hybrid photocatalysts, which promotes the interaction between zinc oxide nanoparticles and graphene sheets due to a polarity effect of the ZnO catalyst, as it has been reported by Nikolai Kislov et al. in 2009 and other authors [45, 47, 48]. This polarity favors the homogeneous distribution of ZnO nanoparticles to decorate graphene sheets and promotes the contact and interaction between both materials rather well, characteristically playing an important role in a photocatalytic process. In particular, using the MI method, the used energy (mechanical stirring) during the nano-ZnO/Graphene photocatalysts synthesis is not enough to distribute ZnO nanoparticles on graphene sheets.

The particle size of the nano-ZnO/Graphene hybrids, synthesized in this work, was between 1.3 and 3 μm independent of graphene sheets concentration (0.1% w/w, 0.25% w/w or 0.5% w/w). This result was confirmed by zeta potential (insert Figure 3-b and 3-d). The size reduction of the graphene sheets after the synthesis of the ZnO/Graphene photocatalysts is a result of the sonication process, used during their preparation, as it was mentioned in section 1.9.

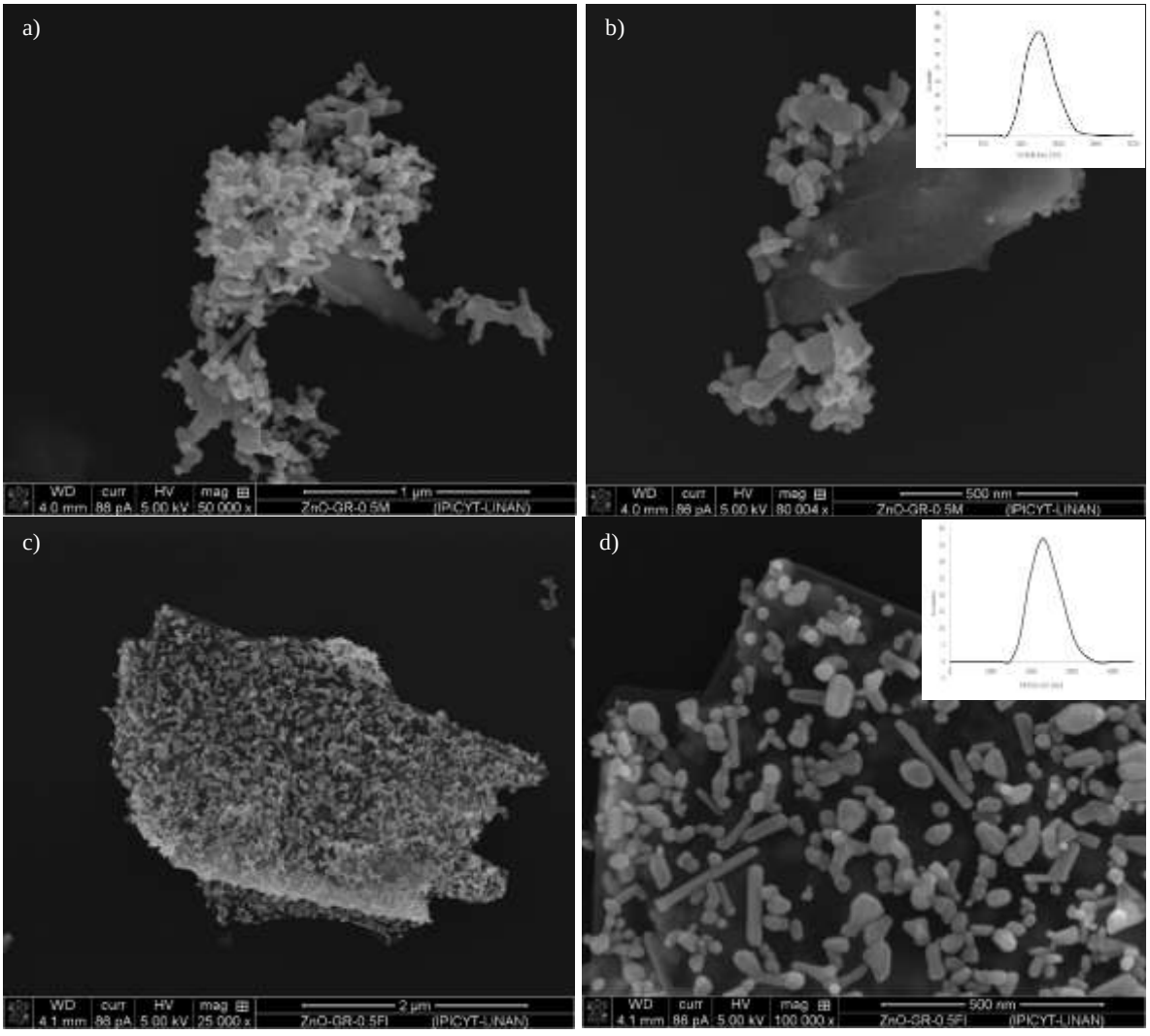

Figure 3. a) SEM micrographs of nano-ZnO/Graphene hybrid material (0.5% w/w) synthesized by MI method and the photoirradiation 3-c and 3-d. Magnification 25000 x. d) zoom of surface (100000 x). Inserts in Figures 3-b and 3-d of the size distribution of nano-ZnO/Graphene photocatalysts, obtained by zeta potential.

Figure 4 shows the TEM micrographs of pristine graphene sheets and nano-ZnO/Graphene hybrid photocatalyst. In Figure 4-a, a flat topology is observed on the surface of graphene, also transparent and thin stacked sheets (monolayers) were observed in this sample.

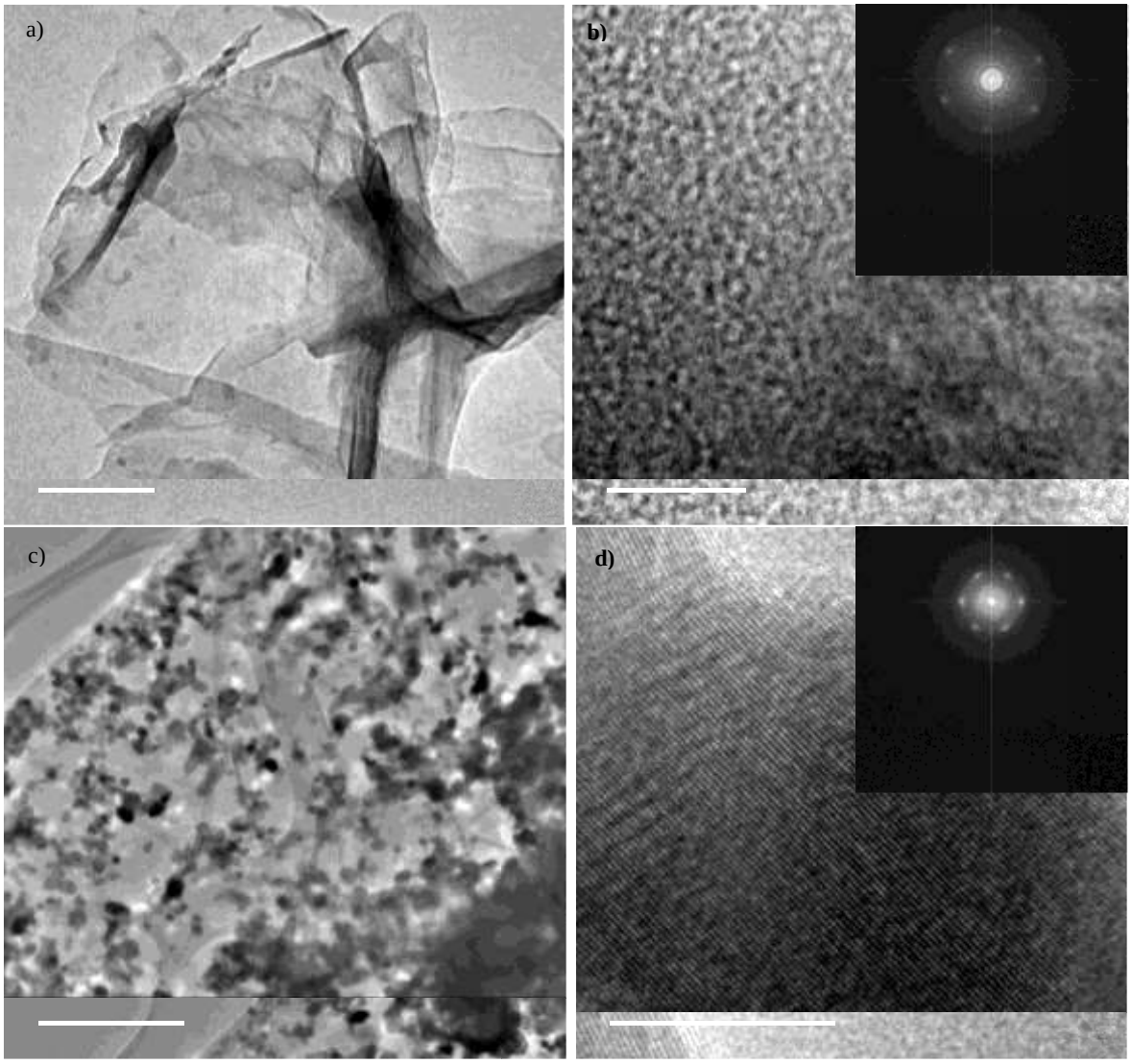

Figure 4. TEM micrographs of a) pristine graphene sheets and b) zoom of graphene sheets surface (insert hexagonal crystalline structure by diffraction pattern), c) nano-ZnO/Graphene photocatalyst (0.5% w/w) synthesised by the photoirradiation method with magnification of 500 nm and d) zoom on the surface of nano-ZnO/Graphene hybrid catalyst (insert hexagonal crystalline structure by diffraction pattern).

Furthermore, TEM revealed the structural ordering of atoms in a hexagonal arrangement characteristic of graphene (Figure 4-b) obtained by electron diffraction patterns. This pattern also provides the interlayer separation of the graphene sheets, studied in the present research, which corresponds to 0.085-0.091nm.

Figures 4-c and 4-d display the TEM micrographs of the final nano-ZnO/Graphene hybrid photocatalyst synthesized with the highest concentration of graphene sheets (0.5% w/w). These images confirm the dimensions of these compounds as determined by SEM (between 1.3 and 3 μm), in addition to the information related to zinc oxide nanoparticles distribution on the graphene sheets and their crystalline structure stability. It was corroborated the effect of the photoirradiation method on the homogenous distribution of ZnO nanoparticles onto the graphene sheets.

The resultant interlayer separation value of the nano-ZnO/Graphene (0.5% w/w) photocatalyst was 0.063-0.065 nm, 25% lower than the calculated value for pristine graphene sheets. This result suggests the reduction of the interlayer distance between graphene sheets stacked in the analyzed sample due to their interaction with ZnO nanoparticles, which have a partial positive surface charge due to their polarity as it was mentioned above, this charge interacts with the electronic cloud of graphene and reduces the interlayer separation of their sheets.

The specific area of pristine ZnO nanoparticles, graphene and nano-ZnO/Graphene hybrid photocatalysts was determined via N_2 adsorption isotherms using the Brunauer Emmett Teller (BET) method. Table 2 summarizes the BET results of the surface area, pore diameter, and pore volume for pristine nano-ZnO, graphene sheets and their corresponding hybrid photocatalysts. The values of average, pore diameter and pore volume were determined using the Barrett-Joyner-Halenda (BJH) method.

The results revealed that the graphene monolayers showed the highest surface area for the analyzed pristine materials. Among the three investigated composites, the photocatalyst loaded with 0.5% w/w of graphene has the highest surface area, followed by nano-ZnO/Graphene 0.25% w/w and nano-ZnO/Graphene 0.1% w/w catalysts as it is shown in table 2. Thus, the addition of graphene sheets increases the surface area of hybrid catalysts up to 69% of the initial area of zinc oxide because of good dispersion of such nanoparticles, indicating that graphene is an excellent material to support ZnO nanoparticles due to its high surface area.

Table 2. Surface area, pore diameter and pore volume of pristine nano-ZnO and Graphene materials, and nano-ZnO/Graphene hybrid photocatalysts.

Sample	BET Area (m2/g)	Pore Diameter (Å)	Pore Volume (cm3/g)
ZnO	10.8	183.4	0.024
Graphene	44.2	398.2	0.015
nano-ZnO/Graphene 0.10% - MI	13.3	368.6	0.060
nano-ZnO/Graphene 0.25% - MI	14.0	333.1	0.096
nano-ZnO/Graphene 0.50% - MI	18.3	236.1	0.160

Besides, the pore diameter values were obtained for the hybrid catalysts with values between those of the base materials, ZnO (183.4 Å) and graphene sheets (398.2 Å), and increasing up to 2.17 times compared with ZnO nanoparticles when is added a small amount of graphene sheets (0.1% w/w). As the graphene content increases, the pore diameter reduces, possibly this result describes the obstruction of ZnO nanoparticles on the graphene surface due to their interaction. Following the last results, the pore volume varies and depends on the quantity of graphene, being the highest value for nano-ZnO/Graphene 0.5%, then nano-ZnO/Graphene 0.25% and finally ZnO/GO 0.1%, all of them present higher values than the pristine materials.

X-ray diffraction was used to confirm the presence of graphene sheets in nano-ZnO/Graphene hybrid photocatalysts and to verify if the crystalline structure of graphene is modified by the UV radiation, used in the synthesis method (PI). Figure 5 shows the XRD patterns of pristine materials; ZnO and graphene sheets, and ZnO/Graphene composites synthesized in this work.

In Figure 5, it is concluded that there are no changes in the geometry observed in the diffraction directions, which are related to the size and shape of the crystal unit cell of the characterized pristine materials, this result provides information on the studied crystalline system. The ZnO pattern is identified by the characteristic peaks of the crystalline phases of hexagonal wurtzite type structure, corresponding to (100), (002), (101), (102), (110), (103), (112) and (201) planes (ICDD). However, no characteristic peaks of graphene are observed in the nano-ZnO/Graphene photocatalyst patterns in the corresponding region, which may arise from the content of the graphene that is low, and possibly undetectable.

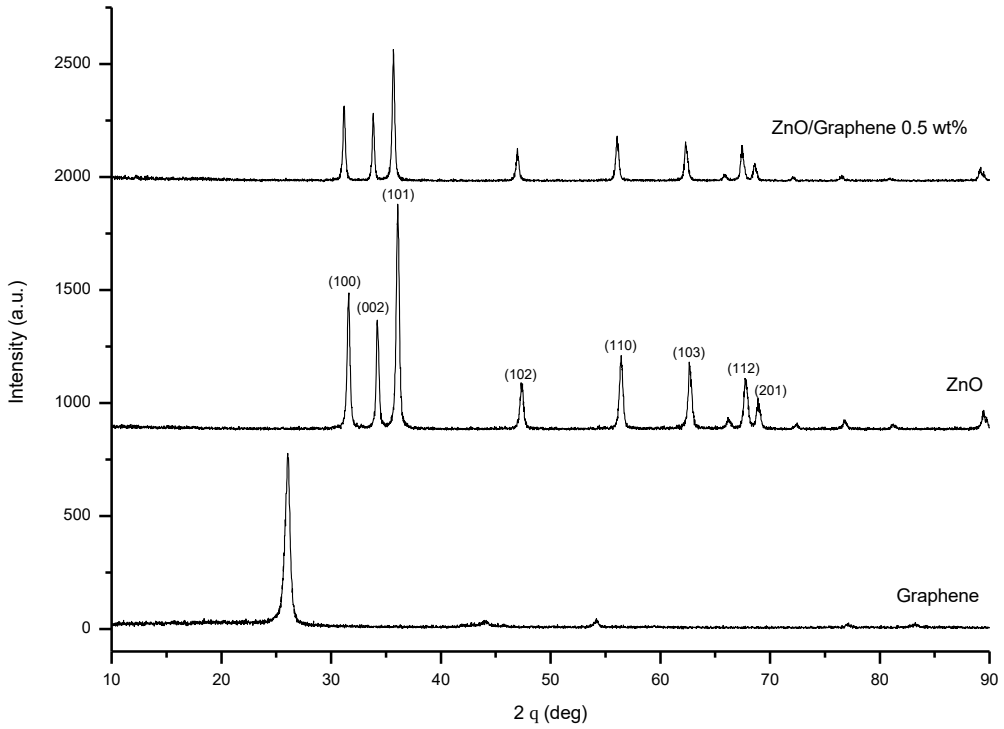

Figure 5. XRD patterns of pristine ZnO and graphene; and the as-prepared ZnO/Graphene hybrid photocatalyst loaded with 0.5 wt%.

Furthermore, the diffraction peaks of the nano-ZnO/Graphene hybrid catalyst are unchanged compared with those pristine ZnO nanoparticles, which indicates that the lattice constants or the ZnO have unchanged due to the hybridization surface of the carbonaceous material [50]. The results of the peak intensities for each analyzed sample are reported in Table 3.

As can be observed, from Table 3 and Figure 5, there are slight intensity changes between the patterns of the nano-ZnO/Graphene hybrid photocatalysts and ZnO, which are not representative and suggest a different position of the surface atoms of the crystal lattice of the ZnO due to its interaction with graphene sheets.

Table 3. Peaks intensities corresponding to the XRD patterns of pristine ZnO nanoparticles, graphene sheets and nano-ZnO/Graphene hybrid photocatalysts synthesized by the photoirradiation method.

Graphene		ZnO		Nano-ZnO/Graphene 0.1% w/w		Nano-ZnO/Graphene 0.25% w/w		ZnO/Graphene 0.5% w/w	
2θ (deg)	Intensity (u.a.)	2θ (deg)	Intensity (u.a.)	2θ (deg)	Intensity (u.a.)	2θ (deg)	Intensity (u.a.)	2θ (deg)	Intensity (u.a.)
26.01	792.56	31.66	598.39	37.10	2038.2	37.06	1825.1	31.17	337.59
43.82	26.82	34.26	495.62	40.25	1684.6	40.19	1624.8	33.92	305.01
54.23	72.01	36.01	991.98	42.42	3171.2	42.37	2757.2	35.74	586.28
77.70	37.75	47.31	221.20	55.88	921.1	55.79	769.9	46.93	147.89
83.32	49.41	56.42	341.47	66.84	1148.8	66.77	975.3	56.09	202.38
		62.93	307.58	74.54	978.5	74.49	887.1	62.32	176.16
		66.34	61.28	79.03	562.5	78.96	521.2	65.98	34.40
		68.14	238.70	80.91	893.3	80.90	863.3	67.46	69.48
		69.44	118.44	82.44	699.2	82.35	657.8	68.74	82.54

The FTIR spectra of pristine ZnO nanoparticles and graphene, and nano-ZnO/Graphene hybrid materials (0.5% w/w) are presented in Figure 6. Two FTIR peaks are observed at 883 and 672 cm^{-1} for pristine ZnO, attributed to the Zn-O stretching modes. For the nano-ZnO/Graphene hybrid photocatalysts, three new characteristic adsorption bands appearing at 1559, 1512, 1386 and 826 cm^{-1} indicating strong chemical interactions between graphene and zinc oxide molecules, due to the energy applied during the PI method.

The peak located at 1559 $cm^{-1}$is ascribed to the vibration of the C-O bonds formed between graphene and ZnO, such a hybridization interaction between ZnO and graphene sheets with a π-conjugative 2D system that could reduce the activation of surface oxygen atoms of ZnO, thus the photo-corrosion of zinc oxide could be significantly inhibited. This phenomenon has been described in previous research on C_{60}-ZnO composites [51]. The spectra of the mechanically synthesized nano-ZnO/Graphene, show a decrement in the band located at 1000 cm^{-1} that suggests secondary interactions, between ZnO nanoparticles and graphene sheets.

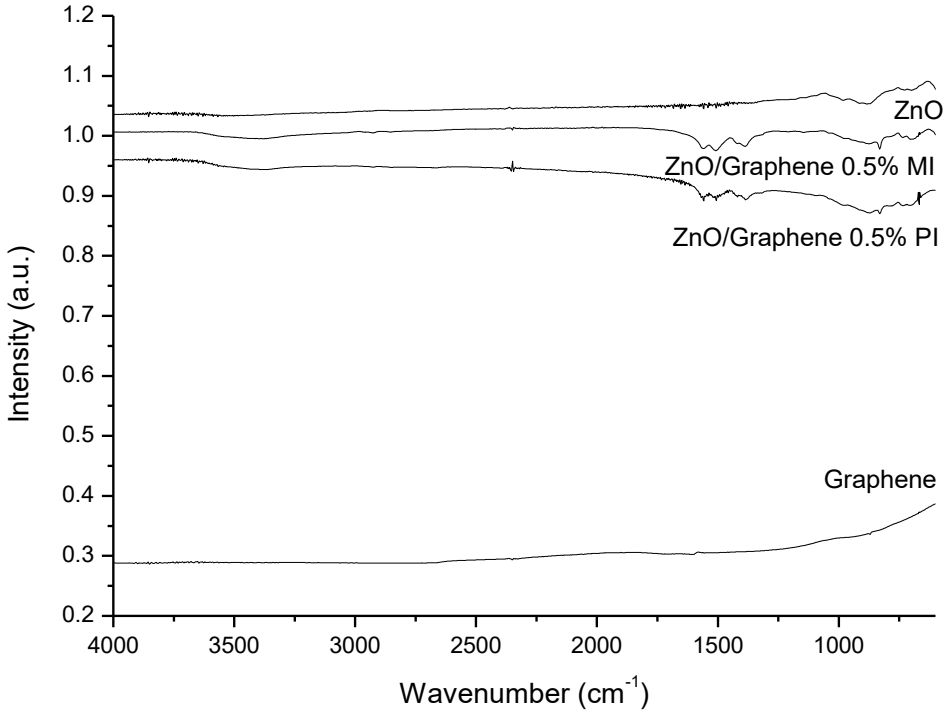

Figure 6. IR spectra of pure ZnO, pristine graphene and nano-ZnO/Graphene 0.5% w/w synthesized by MI and PI methods.

The Raman spectra of zinc oxide, graphene sheets, and ZnO/Graphene photocatalysts are shown in Figure 7. The Raman mode of ZnO located at 439 cm^{-1} is attributed to the optical E_2 high scattering mode of wurtzite ZnO [52]. The D and G bands at 1338 and 1578 cm^{-1}, respectively, are the characteristic peaks for the disordered and graphitic portions of graphene. The G peak arises from the stretching of the C-C bond of graphite materials and is highly sensitive to strain effects in the sp^2 system. The D peak is caused by the disordered structure of graphene. The 2D band of graphene is observed at 2675 cm^{-1} that corresponds to the second-order two-phonon processes, which appear usually due to multilayer structured graphene.

The intensity of the 2D band reflects the number of graphene layers. A simple layer of graphene usually shows a sharp and intense 2D peak [53]. The 2D band in Figure 7 suggests the presence of a single layer of graphene.

The integrated intensity ratio of the D to G bands, ID/IG, for the composite is 1.04 (higher than ID/IG for graphene, 0.36) indicating the presence of more defects in the graphene lattice, which implies a decrease in the size of the in-plane sp^2 domains and formation of the defects and disorders in the graphene sheets.

The above results are consistent with the FTIR characterization results, revealing the reestablishment of the conjugated graphene network (sp^2 carbon) [54] in the nano-ZnO/Graphene photocatalyst due to the hybridization of graphene via photoirradiation method. In contrast, the spectrum of nano-ZnO/Graphene photocatalyst, synthesized by the MI method, does not show changes compared with the pristine material.

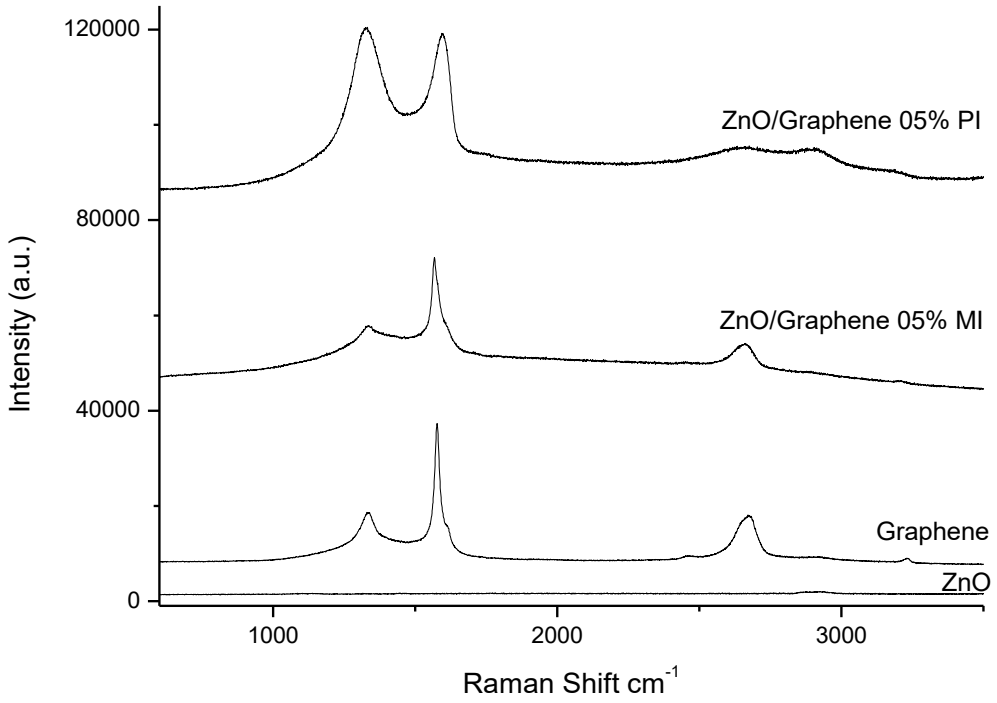

Figure 7. Raman spectra of pristine ZnO and graphene sheets, and ZnO/Graphene hybrid photocatalysts with 0.5% w/w of graphene and synthesized by the mechanical impregnation and photoirradiation methods for 2 hours.

The light absorption range plays an important role in photocatalysis. Figure 8 shows the UV-vis diffuse reflectance spectroscopy of the studied samples. The bandgap values of the different synthesized photocatalysts were estimated using UV Spectroscopy based on the absorption spectra collected in a wavelength range from 200 to 800 nm. The results provide information related to the interaction between light and the surface of the analyzed samples that defines their photocatalytic performance. In Figure 8, the peak at 360 nm corresponds to the absorbance of ZnO nanocatalyst due to the optical transition of electrons from its valence to the conduction band. The bandgap (Eg) values were estimated using the wavelength (nm) of the intersection between the slope of each curve and the Y-axis, using equation 3, based on the Beer Lambert`s Law.

$$Eg = \frac{hc}{\lambda} \tag{3}$$

The bandgap value for pristine ZnO was obtained, it is 3.21 eV, and in the case of the synthesized ZnO/Graphene photocatalysts, following the PI method with 0.1% w/w, 0.25% w/w and 0.5% w/w of graphene sheets, the obtained values are 3.19 eV, 3.18 eV, and 3.15 eV, respectively (see Table 4).

A decrement of the bandgap values of ZnO hybridized materials was determined related to the bandgap value of pristine ZnO in the following order ZnO > ZnO/Graphene 0.1% > ZnO/Graphene 0.25% > ZnO/Graphene 0.5%. This result implies an increase in light absorption intensity in the visible region due to the presence of graphene sheets, which possibly enhances the anti-photo corrosion of ZnO and increases the retention time of the electrons that are promoted from the valance band to the conductive band in ZnO semiconductor.

The stronger absorption intensity in the visible region for ZnO/Graphene hybrid photocatalysts, in comparison to that of ZnO, is a key factor for the higher photocatalytic activity even at low concentrations of graphene sheets.

Therefore, it is possible to enhance the performance of ZnO/Graphene hybrid photocatalysts under visible light, resulting in an opportunity to use natural energy sources as solar radiation, which more than 50% of its spectrum is in the visible light range compared to the 5% of the UV range [35, 55].

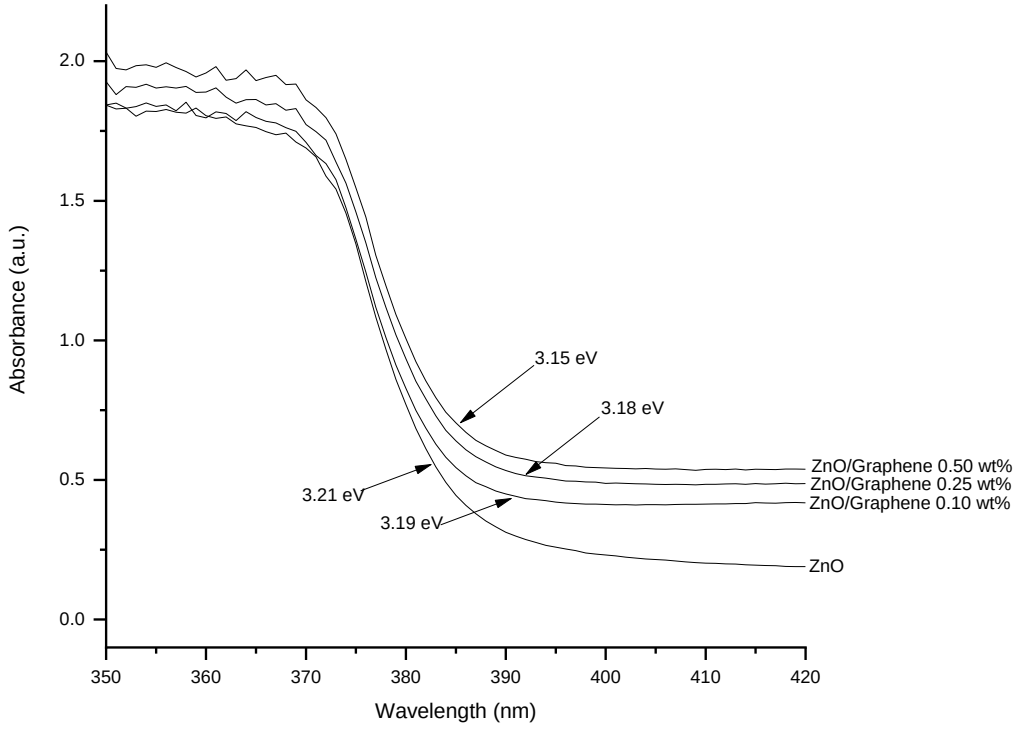

Figure 8. UV-vis spectra of ZnO and ZnO/Graphene hybrids photocatalysts with different content of graphene sheets (0.1% w/w, 0.25% w/w and 0.5% w/w) synthesized by the PI method.

It could be expected that the visible-active photocatalysts will show remarkable potential in exploring solar energy to solve the energy crisis and severe environmental problems of the world by taking advantage of stable semiconductor photocatalysts sensitive to visible light in APO´s systems.

In appendix A, the bandgap results are presented for the nano-ZnO/Graphene hybrid photocatalysts synthesized by mechanical impregnation. In the present research, we concluded that there is not an important and significant change in the corresponding estimated values of their bandgap, obtained by UV-vis spectroscopy. This result correlates with previous results obtained by SEM, TEM, FTIR, and Raman. The ZnO

nanoparticles are not homogeneously distributed on the graphene surface, an effect that not allows the improvement of ZnO photocatalytic properties.

Table 4. Bandgap of pristine ZnO photocatalyst and ZnO/Graphene hybrid materials with different content of graphene sheets (0.10%, 0.25% and 0.50% w/w), obtained by UV-vis spectrophotometry.

Photocatalyst	Band Gap (eV)
ZnO	3.21
ZnO/Graphene 0.10%	3.19
ZnO/Graphene 0.25%	3.18
ZnO/Graphene 0.50%	3.15

2.2 Photocatalytic performance using visible light.

To reveal the photocatalytic performance of nano-ZnO/Graphene photocatalysts, triclosan degradation experiments were conducted in batch systems, using visible light radiation (Halogen lamp, 150 W). The catalyst adsorption capacity for all the photocatalysts was determined previously in dark conditions, and it was determined that the adsorption phenomena for all the different materials takes place in one hour. Thus, after this time it is feasible to evaluate the photocatalytic performance for the TCS degradation, excluding the effect of adsorption, of the pristine ZnO and hybrid photocatalysts.

The photocatalytic activity of the nano-ZnO/Graphene hybrid photocatalysts, with different contents of graphene sheets, is shown in Figure 9, including the photolysis experiment (degradation in the absence of catalyst). It is clearly noticed that all the nano-ZnO/Graphene photocatalysts exhibit much higher photocatalytic activity than photolysis and the pristine ZnO sample, which degraded 10% and 32% of the initial concentration of TCS, respectively. The nano-ZnO/Graphene 0.5% w/w exhibits the maximum degradation of triclosan (41%), while the photocatalyst nano-ZnO/Graphene 0.25% w/w degraded 36% of the initial TCS. The photocatalyst synthesized with the lowest amount of graphene (0.1% w/w) exhibited degradation percentage of 34%.

The enhanced performance of nano-ZnO/Graphene hybrid photocatalysts, to degrade triclosan under visible light, is attributed to the facile charge transportation and separation from ZnO to graphene, which is a large π-π network [56]. The enhancement is related to the increase of graphene sheets content in the hybrid photocatalysts. The optimal graphene amount loaded in the hybrid photocatalysts was 0.5% w/w, much lower quantity than those reported (up to 5%) for synthesized graphene-based photocatalysts, mainly synthesized from reducing graphene oxide (that implies longer and more expensive procedures) [57, 58]. This result is an important approximation to achieve a good photocatalyst to be used under visible light synthesized by the photoirradiation method, a promising, facile and friendly technique to synthesize active photocatalysts under visible and solar radiation.

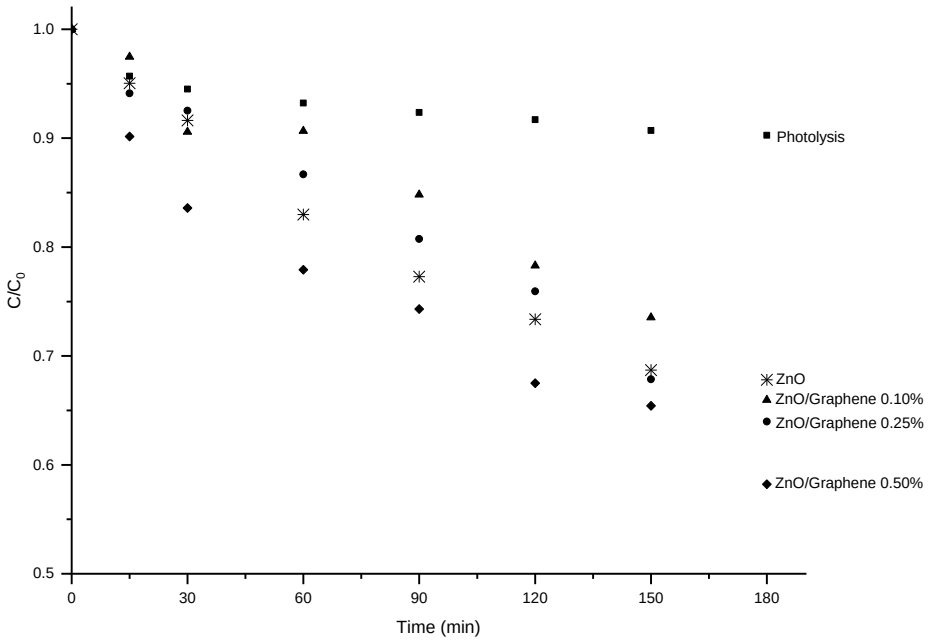

Figure 9. TCS degradation profiles under visible radiation (Halogen lamp 150 W), for photolysis and using pristine ZnO and nano-ZnO/Graphene hybrid photocatalyst modified with 0.1% w/w, 0.25% w/w and 0.5% w/w of graphene sheets. Conditions: pH=7, T=23°C.

Figure 10 shows the TCS photodegradation reaction rate constants k_{app} for nano-ZnO/Graphene hybrid photocatalysts under visible light radiation. The degradation kinetic data were fitted using a pseudo-first-order equation. The photocatalytic activity trends to follows the order nano-ZnO/Graphene 0.5% > nano-ZnO/Graphene 0.25% > nano-ZnO/Graphene 0.1% > ZnO. The values of the calculated reaction rate constants are 0.0027 min^{-1} for nano-ZnO/Graphene 0.5% followed by nano-/Graphene loaded with 0.25% of graphene sheets, 0.0024 min^{-1}. Less content of graphene decreases the photocatalytic activity up to 0.0021 min^{-1} corresponding to nano-ZnO/Graphene 0.1% hybrid photocatalyst, similar rate constant value was calculated for pristine ZnO (0.0020 min^{-1}).

The graphene sheets enhance the photocatalytic activity and efficiency of ZnO nanoparticles. Hence, the increase of surface area, as well as the excellent interaction between graphene sheets and ZnO nanocatalyst, are important factors to improve the photocatalytic performance of nano-ZnO/Graphene photocatalysts. Graphene is characterized by its electronic cloud, which could act as an electron trap to retain the electrons promoted from the valance to conductive band in ZnO increasing the number of radicals, species responsible for efficiently degrading organic molecules such as TCS.

Thus, the proposed photoirradiation method and developed in the current research allows synthesizing hybrid graphene-sheets base photocatalysts conserving graphene properties as crystallinity structure, high surface area, morphology, and excellent electron transfer charge. This result contributes to the development of new active photocatalysts under visible light as it has been reported in several studies that demonstrate the photodegradation of triclosan up to 47% using photocatalysts based on rare-earth elements such as Ceria (47%) [59], metals such as Au (10% after 5 h) [60], silver [61] and Cu [62]; and oxides like MgO, WO_3, TiO_2, ZnO or GO [63].

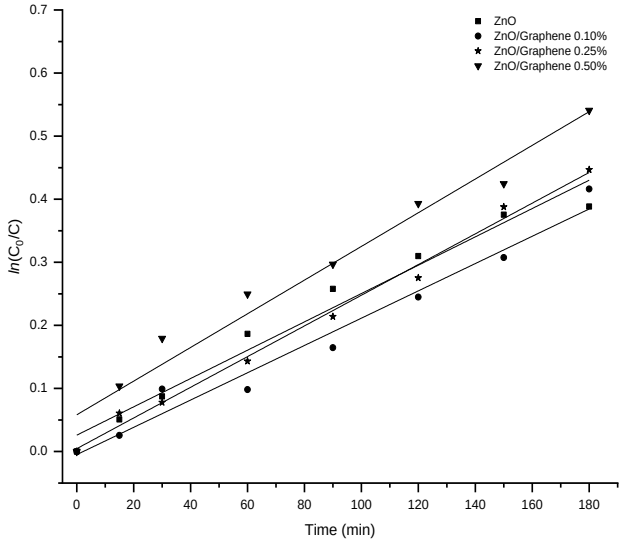

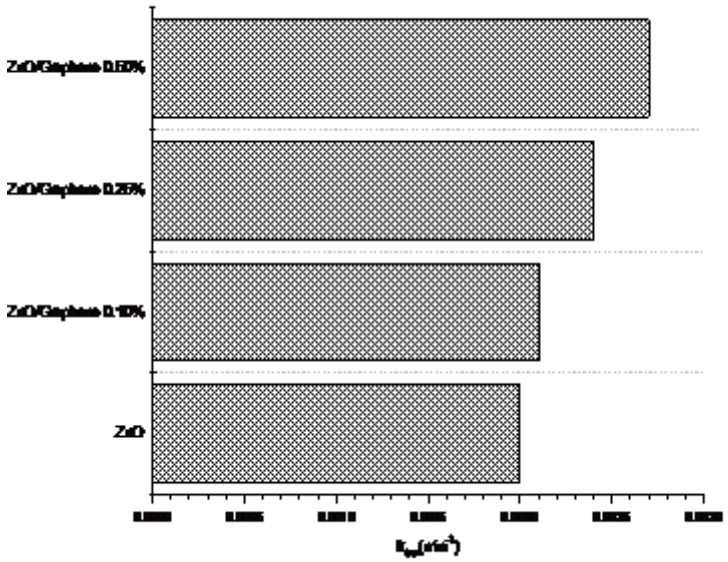

Figure 10. The pseudo-first-order reaction rate constants (k_{app}) for triclosan degradation under visible light with as-prepared samples nano-ZnO/Graphene photocatalysts 0.5% w/w, 0.25% w/w and 0.1% w/w% and pristine ZnO.

The reusability for the best hybrid photocatalyst (nano-ZnO/Graphene 0.5%) was determined using visible radiation. Therefore, four degradative cycles were carried out. After each cycle, the photocatalyst was filtered and dried thoroughly, and then a fresh TCS solution was added. The results are displayed in Figure 11, and it is seen a slight decrement of photoactivity during the four cycles test. Thus, nano-ZnO/Graphene 0.5% exhibited excellent recycling stability and its photocatalytic degradation rate of triclosan remained unchanged after the fourth cycle degradation.

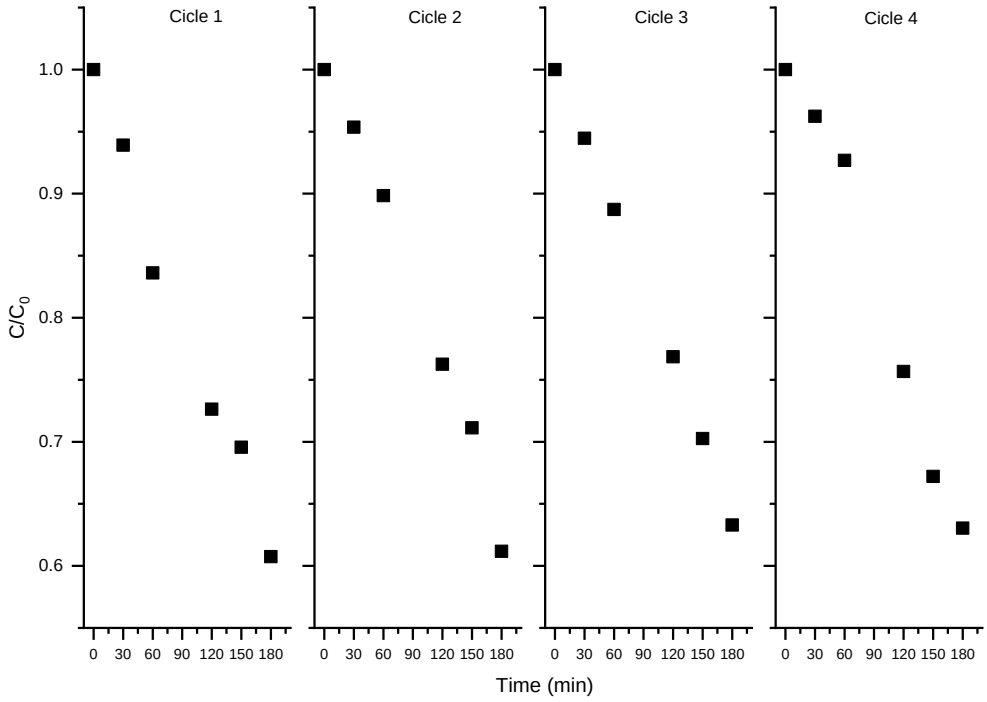

Figure 11. Cycling experiment for the photocatalytic degradation of triclosan by the as-prepared nano-ZnO/Graphene 0.5% w/wt photocatalyst under visible light. Conditions: pH=7 and T=23°C.

2.3 **Mechanistic study**

Surface area, phase structure, crystallinity and separation efficiency of photogenerated charges are crucial factors for photocatalytic activity [64]. Therefore, in the as-prepared nano-ZnO/Graphene hybrid samples, the enhancement of their photocatalytic activity is attributed mainly to the effective separation of the photogenerated electron-hole pairs. To confirm the mechanism, the ESR technique and trapping experiments of radicals were performed. ESR spin-trap technique (with DMPO) was used to monitor the reactive oxygen species generated during the light irradiation step, the results are shown in Figure 12. Both signals, DMPO-•OH and DMPO-O_2•$^-$, are observed when pristine ZnO and nano-ZnO/Graphene were exposed under visible radiation. Therefore, a dual mechanism involving both hydroxyl radicals and superoxide radicals is expected during the photocatalytic process.

However, the signals for nano-ZnO/Graphene hybrid photocatalysts are stronger than the signals in pristine ZnO, thus accounting for the higher and stable photocatalytic performance of hybrid photocatalysts than bare ZnO toward the degradation of triclosan, especially the nano-ZnO/Graphene 0.5%, as it was demonstrated in section 2.2. The hydroxyl radicals trapped by DMPO (DMPO-•OH) and superoxide radicals (DMPO-O_2•$^-$) for ZnO and nano-ZnO/Graphene hybrid photocatalyst were characterized by detecting four characteristic signals in water, and six signals in ethanol for DMPO-•OH and DMPO-O_2•$^-$, respectively. Thus, the enhanced photocatalytic activity of nano-ZnO/Graphene photocatalysts, at any composition, but especially 0.5%, compared to pristine ZnO is due to the introduction of graphene sheets, which promotes an increment in the charge separation to the effective utilization of electrons that produce more •OH and O_2•$^-$ radicals. In this case, the signals of O_2•$^-$ (Figure 12-b) radicals are higher than those for •OH (Figure 12-a), which suggest the predominance of hole oxidation and O_2•$^-$ oxidation reactions, which mainly govern the photocatalytic process to degrade triclosan. Furthermore, ZnO photocatalyst exhibits photocatalytic activity under visible light but generate higher signals light after graphene hybridization, showing that graphene is responsible for the visible light performance due to the electronic interaction between ZnO and graphene.

a)

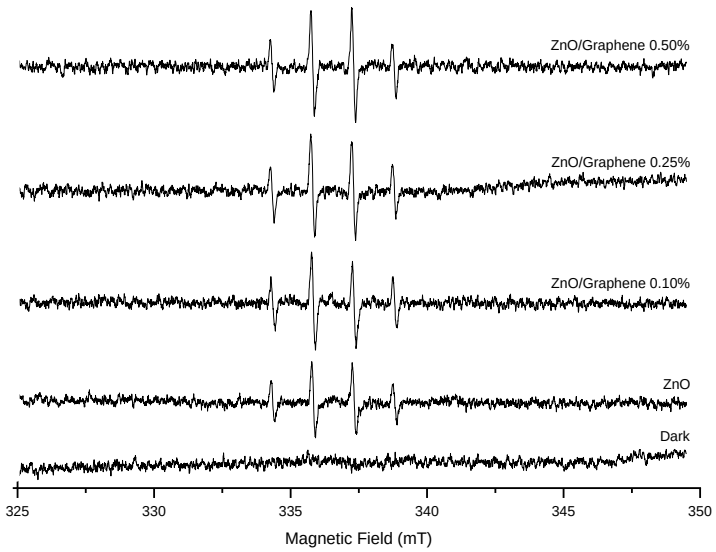

b)

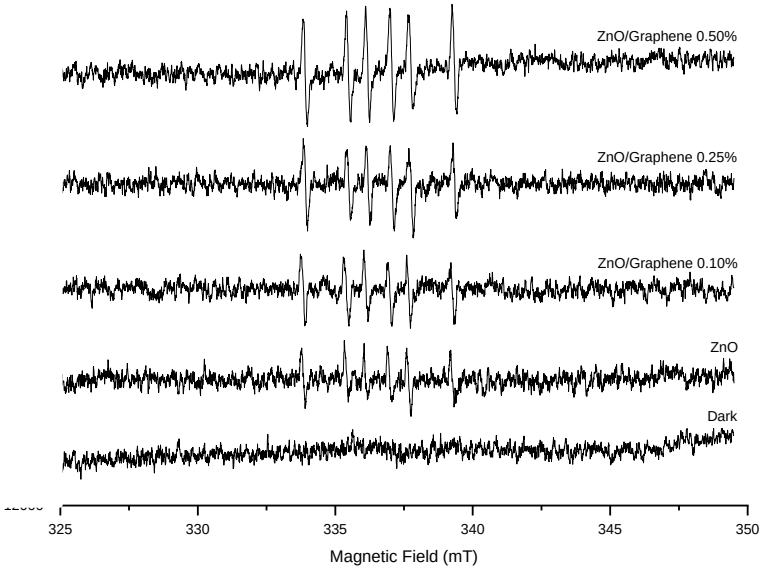

Figure 12. ESR analysis in dark conditions and visible light radiation of pristine ZnO and nano-ZnO/Graphene hybrid photocatalysts in a) water and b) ethanol. DMPO was used as the radical trapper.

The enhancement of the photocatalytic activity of ZnO, after graphene hybridization, could be attributed to the higher separation efficiency of electron-hole pairs caused by the rapid photo-induced charge separation and the inhibition of the recombination of electron-hole pairs, increasing the number of holes participated in the photo-oxidation process. Because the graphene has a delocalized conjugated π structure and superior electrical conductivity, the photo-generated electrons are transferred from the conductive band of ZnO to graphene sheets, thus graphene sheets acts as an electron trap and dramatically improving the visible light activity in the nano-ZnO/Graphene photocatalysts, thus the possibility of the recombination of the e^-/h^+ pairs decreases. The photo-generated electrons in the nano-ZnO/Graphene photocatalysts could easily migrate from the inner region to the surface to react with O_2, adsorbed on the surface [65]. The schematic illustration of the mechanism of the enhancement of the photocatalytic activity of nano-ZnO/Graphene photocatalysts by the separation efficiency of their photoinduced electron-hole pairs is shown in Scheme 2. The following reactions, 1 to 7, describe the proposed reaction mechanism.

$ZnO + hv \rightarrow ZnO + e^- h^+$ Reaction (1)

$ZnO (e^-) + Graphene \rightarrow ZnO (h^+) + Graphene (e^-)$ Reaction (2)

$ZnO (h^+) + Graphene (e) + H_2O \rightarrow ZnO + Graphene + \bullet OH + H^+$ Reaction (3)

$ZnO (h^+) + Graphene (e) + {}^-OH \rightarrow ZnO + Graphene + \bullet OH$ Reaction (4)

$ZnO + Graphene + \bullet OH + R \rightarrow ZnO + Graphene + H_2O + R\bullet$ Reaction (5)

$ZnO + Graphene + R\bullet + O_2 \rightarrow ZnO + Graphene + ROO\bullet$ Reaction (6)

$ZnO + Graphene + ROO\bullet + O_2 \rightarrow ZnO + Graphene + CO_2 + H_2O$ Reaction (7)

Such reactions describe the transportation of electron-hole pairs between ZnO and graphene sheets. Thus, the photocatalytic degradation of triclosan is enhanced.

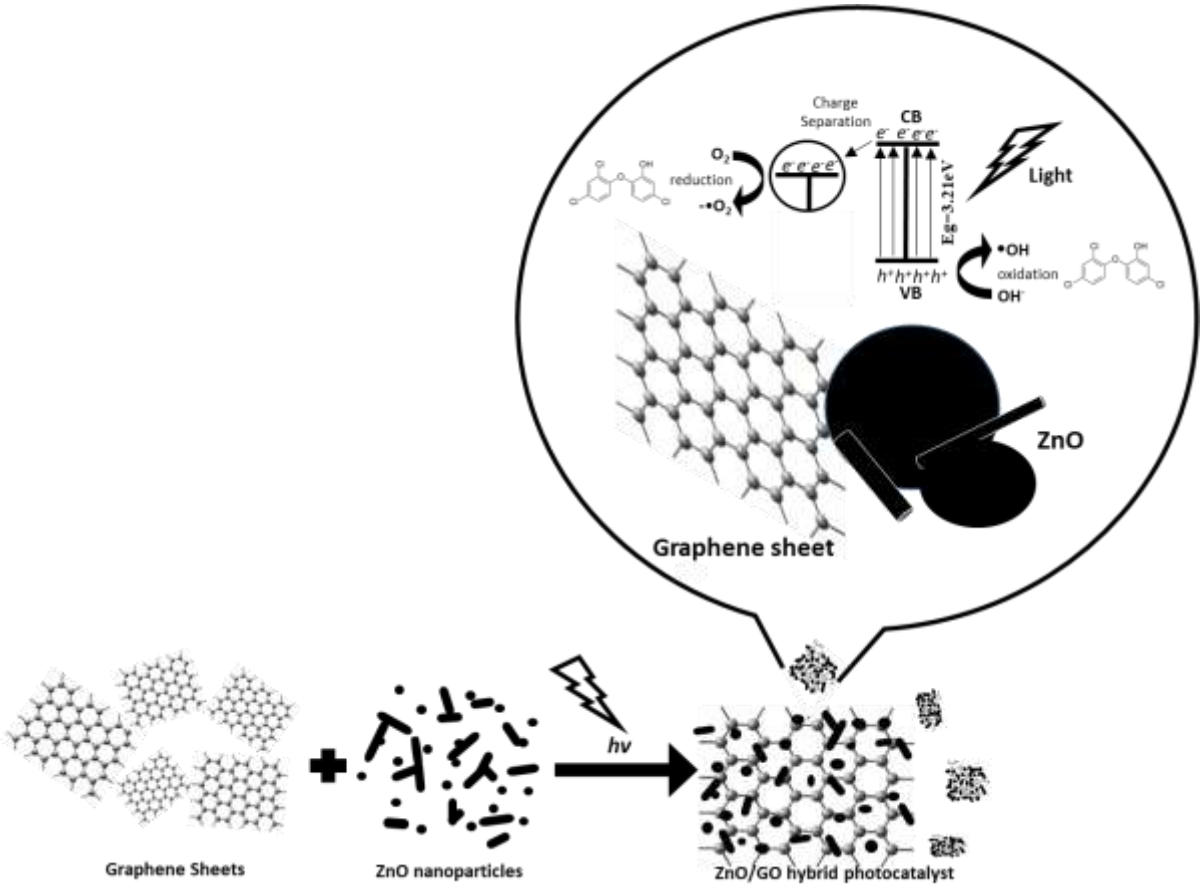

Scheme 2. Photocatalytic mechanism of nano-ZnO/Graphene hybrid photocatalysts in the degradation of a model disrupting endocrine molecule, namely triclosan.

2.4 **Previous conclusions.**

The photoirradiation method allows a homogeneous distribution of the ZnO particles on the graphene sheets and promotes an excellent charge interaction between those materials. It was demonstrated that surface area, crystallinity structure and separation efficiency of photogenerated charges are crucial factors to enhance photocatalytic activity of the as-prepared nano-ZnO/Graphene materials, which can degrade up to 41% of the initial concentration of triclosan (8 ppm) under visible light radiation using nano-ZnO/Graphene hybrid photocatalyst even at low concentrations, as 0.5% w/w.

The results indicate that graphene sheets act as electron scavenger reducing the recombination process and promotes the charge separation between the valance and conductive bands in the ZnO semiconductor, increasing the amount of $^{\bullet}OH$ and $O^{2\bullet-}$ radicals and resulting in the increase of the apparent constant reaction rate up to 45% in nano-ZnO/Graphene hybrid photocatalyst compared to the apparent reaction rate constant of pristine ZnO. The ZnO/Graphene hybrid photocatalyst can be used in four cycles (cyclic way) without a significant reduction of its efficiency to degrade triclosan.

3 Chapter 2
nano-ZnO/GO photocatalysts

Nowadays, solar energy is the most abundant clean energy available source. Thus, research studies and the development of materials that can efficiently harvest solar irradiation and used it for green environmental pollution management are essential. Photocatalysis, which could use renewable solar energy to activate the chemical reactions via oxidation and reduction, as occur in Advanced Oxidation Processes (AOPs), is a sustainable technology to provide a solution for environmental issues. These photocatalytic systems have attracted great interest from the scientific community as the most promising way to solve the environmental problems, especially getting rid of residual pollutants from the wastewater stream.

In the field of photocatalysis, ZnO has emerged as the leading candidate for green environmental management systems due to its wideband energy. Nevertheless, the recombination of the photogenerated hole and electron is the major disadvantage in semiconductor photocatalysis like ZnO. This recombination step reduces the quantum yield and causes energy wasting.

Therefore, the e−/h+ recombination process should be inhibited to ensure efficient photocatalysis. Metal doping could counter the recombination problem with efficient charge separation between electrons and holes in ZnO photocatalyst [66]. Furthermore, the generation of hydroxyl radicals and active oxygen species will greatly increase resulted from enhancement in the charge separation efficiency [67].

Semiconductors like graphene can improve the visible-light photocatalytic efficiency of ZnO due to its remarkable chemical, physical and mechanical properties, as it has been demonstrated and discussed in the previous Chapter 1. The photo-deposition method is a successful process to prepare ZnO/Graphene hybrid photocatalysts with enhanced photocatalytic activity under visible light radiation.

On the other hand, the graphene oxide (GO) has been used for the development of new materials due to its chemical surface properties (functional groups), which promote the interactions between GO and other materials. Studies show excellent chemical properties of GO to generate compounds as well as having the ability to be reduced to graphene using ultraviolet radiation [68].

Thus, it is possible to obtain stable photocatalysts based on ZnO/GO due to interactions between pristine materials, able to delay the recombination process during photocatalysis and improving the degradation of TCS.

In the present chapter three different concentrations (0.10% w/w, 0.25% w/w and 0.50% w/w) of GO were used to modify nano-ZnO by the photoirradiation method and the resultant photocatalysts were characterized to determine their physicochemical and photocatalytic properties. This research contributes to the understanding of the efficiency enhancement of nano-ZnO/GO hybrids, and contributes to obtaining a photoactive material, under natural light radiation, in an Advance Oxidation Process to eliminate endocrine-disrupting compounds, like triclosan.

3.1 Characterization and properties of nano-ZnO/GO photocatalysts

Figure 13 shows SEM images of pristine graphene oxide along with the corresponding size distribution of photocatalyst particles obtained by zeta potential (0.5 µm – 2.5 µm). These images show a semi-transparent continuous surface that has slight folds on it, probably as a consequence of sheet stacking.

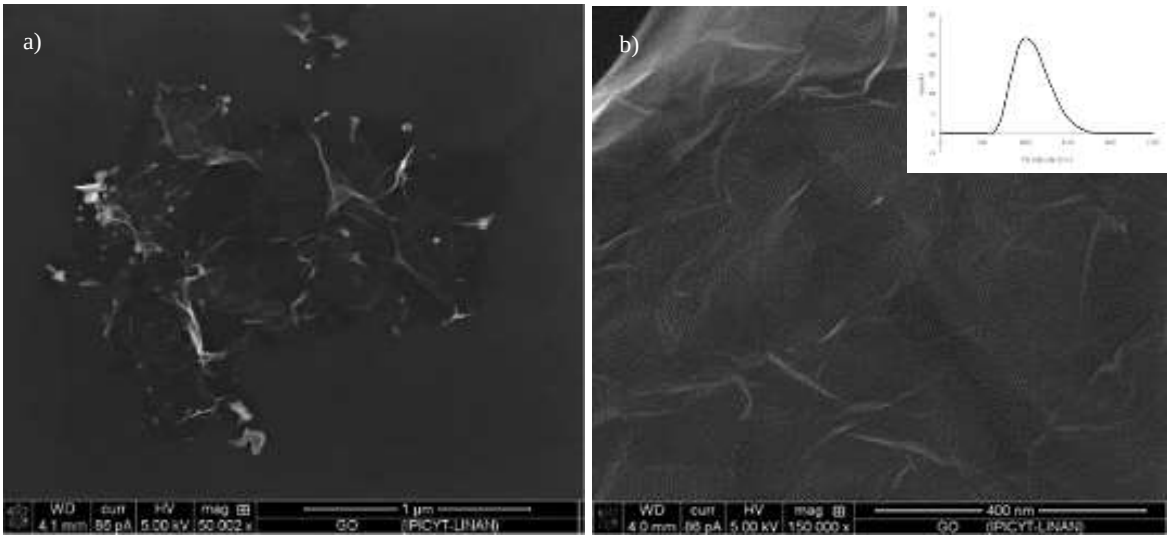

Figure 13. SEM images of pure graphene oxide (50000 x) and d) zoom of surface (150000 x).

Based on the size observations of GO, it is suggested that obtained nano-/GO hybrid photocatalysts are GO sheets covered by ZnO nanoparticles and/or their agglomerates.The following image (Figure 14-a) corresponds to nano-ZnO/GO hybrid photocatalyst prepared by the photoirradiation method loaded with 0.25% w/w of graphene oxide.

Figure 14-a reveals the decoration of the surface of graphene oxide sheets with zinc oxide nanoparticles, which are homogeneously distributed. Zinc oxide nanoparticles exhibited the same shapes as those observed in the pure material (Figure 13-a). It must be pointed out that the complete distribution of zinc oxide nanoparticles enabled a well-wrapped morphology of graphene oxide sheets by ZnO nanoparticles.

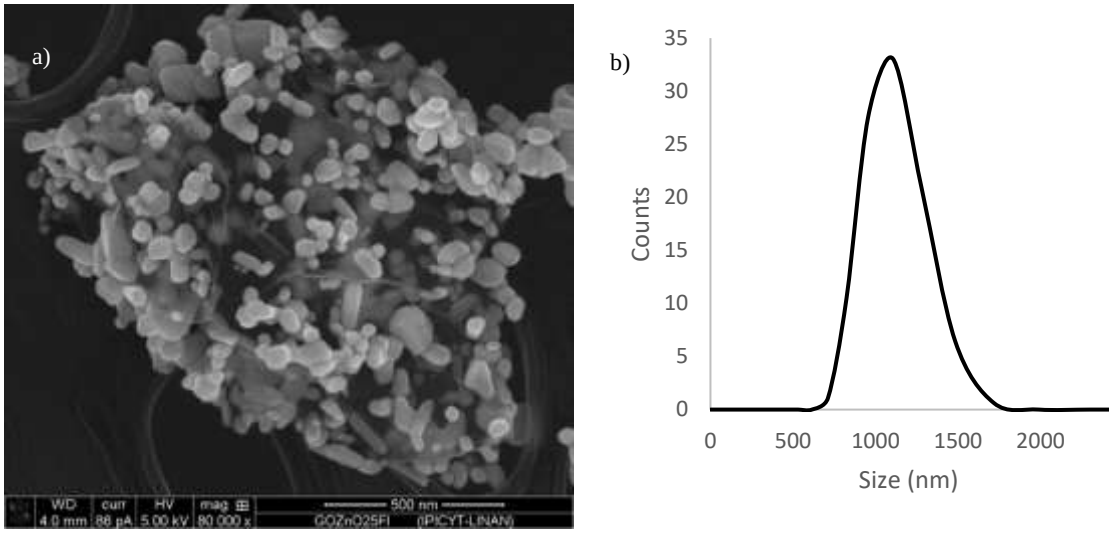

Figure 14. a) SEM images of nano-Zn/GO hybrid material (0.25% w/w) synthesized by photoirradiation method. Magnification 80000x. b) Size distribution of nano-ZnO/GO particles.

The homogeneous distribution of ZnO nanoparticles on the surface of GO is probably ascribed to the photoirradiation method since the energy used during the synthesis of hybrid photocatalysts would induce a polarity effect to ZnO, as it was described in chapter 2. Thus, the polarization favors the homogeneous distribution of ZnO nanoparticles to decorate graphene oxide sheets and promotes the contact and interaction between both materials playing an important role in the photocatalytic process.

The particle size of the synthesized nano-ZnO/GO hybrids was between 1 and 2 µm, independently of the GO concentrations (0.1% w/w, 0.25% w/w or 0.5% w/w). This result was confirmed with the size distribution obtained by zeta potential (Figure 14-b).

Figure 15 shows the TEM images for pristine GO and the nano-ZnO/GO 0.5 %w/w photocatalyst. Images 15-a and 15-b show a thin, transparent and rugose surface of GO that contain more than one layer of GO. In the insert image is presented the EDS result that confirms the elemental composition of GO (N, C and O).

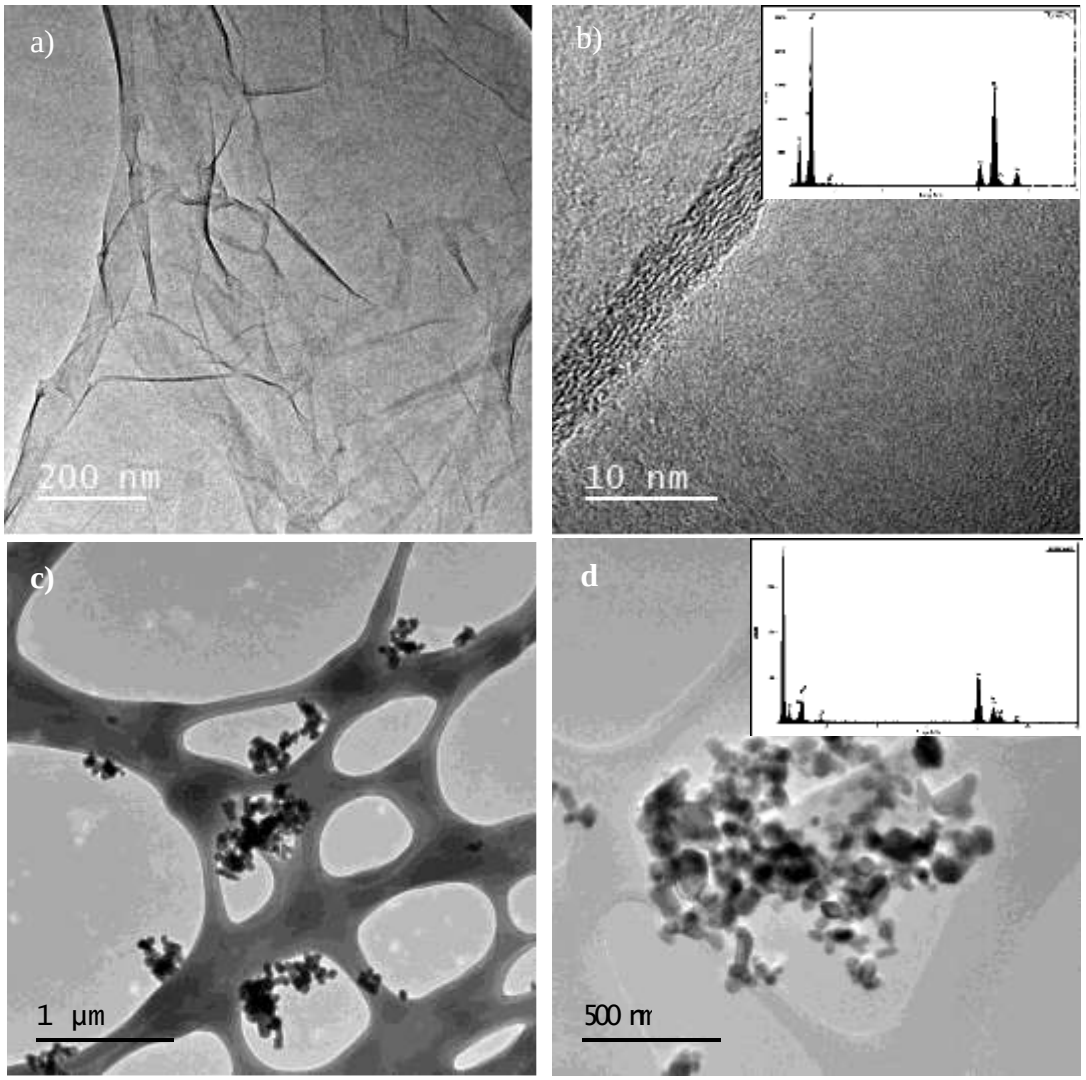

Figure 15. TEM images of a) pristine graphene oxide and b) graphene layers in GO sample c) nano-Zn/GO photocatalysts (0.5% w/w) synthesized by the photoirradiation method and d) zoom of nano-ZnO/GO photocatalyst (insert scale of 290 nm).

Figures 15-c and 15-d display the sample TEM images of the final nano-ZnO/GO hybrid photocatalyst with the highest concentration of graphene oxide (0.5% w/w). These images confirm the dimensions of these compounds, as determined by SEM (between 1µm and 2 µm), in addition to the information related to zinc oxide nanoparticles distribution on the graphene oxide sheets.

It was corroborated that the photoirradiation method promotes the homogenous distribution of ZnO nanoparticles on the graphene oxide surface. It is noteworthy that the dimensions of pure GO are higher than those present in the hybrid nano-ZnO/GO photocatalysts, due to the ultrasonication that was carried out during their synthesis.

The specific area of ZnO, graphene oxide and nano-ZnO/GO hybrid photocatalysts was determined via N_2 adsorption isotherms using the Brunauer Emmett Teller (BET) method. Table 5 summarizes the BET results of the surface area, pore diameter and pore volume for such samples. The values of average pore diameter and pore volume were determined using the Barrett-Joyner-Halenda (BJH) method.

Table 5. Surface area, pore diameter and pore volume of pristine ZnO and GO materials and nano-ZnO/GO hybrid photocatalysts.

Sample	BET Area (m2/g)	Pore Diameter (Å)	Pore Volume (cm3/g)
ZnO	10.8	183.4	0.024
GO	46.81	682.8	0.012
nano-ZnO/GO 0.1% w/w-PI	13.3	398.6	0.060
nano-ZnO/GO 0.25% w/w-PI	15.8	306.5	0.073
nano-ZnO/GO 0.5% w/w-PI	17.0	219.9	0.089

The results revealed that the graphene oxide showed the highest surface area for pristine materials. Among the three investigated hybrid photocatalysts, the material loaded with 0.5% w/w of GO had the highest surface area, followed by nano-ZnO/GO 0.25% and finally the nano-ZnO/GO 0.1% catalysts. Thus, the addition of GO increases the surface area of hybrid nano-ZnO/GO catalysts up to 57% of the initial area of zinc oxide as a consequence of good dispersion of such nanoparticles, indicating that graphene oxide has excellent surface chemistry to support ZnO nanoparticles. The increase in surface area is one of the most important properties of a photocatalyst to improve its efficiency.

The pore diameter values for the photocatalysts had values between those of base materials, ZnO (183.4 Å) and GO (682.8 Å), increasing up to 2.17 times compared with ZnO when adding a small amount of GO (0.1% w/w) and then as the GO content increases the pore diameter is reduced, which might be ascribed to the obstruction of ZnO nanoparticles surface when they interact with GO.

Following the last results, the pore volume varies and depends on the quantity of GO being the highest value for nano-ZnO/GO 0.5%, then nano-ZnO/GO 0.25% and finally nano-ZnO/GO 0.1%, all of them exhibit higher values than the pristine materials ZnO and GO. Such dimensions are indicative of the interaction between the ZnO and graphene oxide.

As can be seen from Figures presented in Appendix 2, the isotherms are type II with an H3-type hysteresis loop, which corresponds to a microstructure containing macropores or micrometric cavities in the case of nano-ZnO/GO samples. Also, it is noted that the quantity adsorbed was increased when GO was added, therefore it contributes to such quantity more than the ZnO.

The X-ray diffraction characterization was used to confirm the presence of graphene oxide in the nano-ZnO/GO hybrid photocatalysts and also to verify the possible reduction of graphene oxide during the synthesis of nano-ZnO/GO photocatalysts due to the high energy (UV radiation) as previously has been reported [69-71]. Figure 16 shows the XRD patterns of pristine materials; ZnO and graphene oxide, and nano-ZnO/GO composites synthesized in this work.

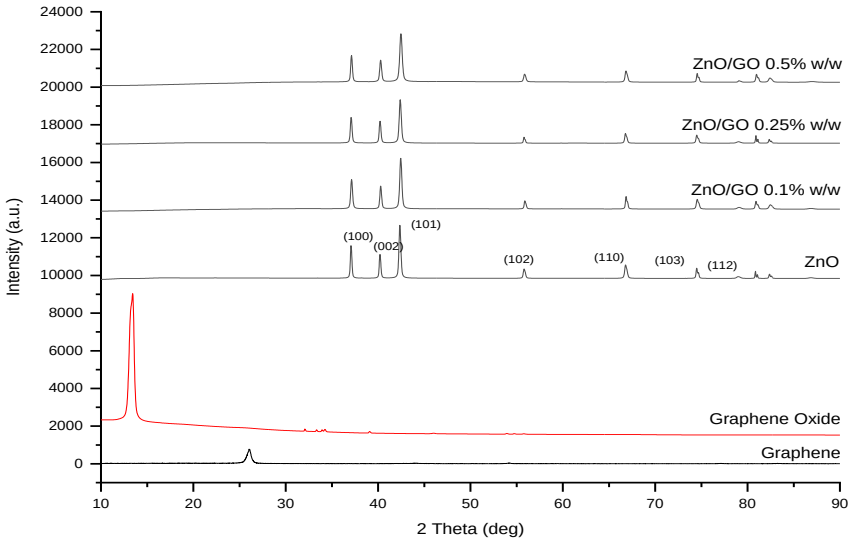

Figure 16. XRD patterns of pristine ZnO and graphene oxide; and the as-prepared nano-ZnO/GO hybrid photocatalysts with 0.1% w/w, 0.25% w/w and 0.5% w/w of GO.

From Figure 20 it is concluded that there are no changes in the geometry observed in the diffraction directions, which are related to the size and shape of the crystal unit cell of the characterized samples. The ZnO pattern is identified by the characteristic peaks of the crystalline phases of hexagonal wurtzite type structure, corresponding to (100), (002), (101), (102) and (103) planes [32]. The results of the peak intensities for each analyzed sample are reported in Table 6.

Table 6. Peak intensities for the XRD patterns of pristine ZnO and graphene oxide, and nano-ZnO/GO photocatalysts synthesized by the photoirradiation method for two hours.

Graphene		Graphene Oxide		ZnO	
2θ (deg)	Intensity (a. u.)	2θ (deg)	Intensity (a. u.)	2θ (deg)	Intensity (a. u.)
26.01	792.6	13.46	7577.1	37.05	2219.9
43.82	26.8	32.06	403.12	40.18	1749.8
54.23	72.1	33.33	372.4	42.33	3318.1
77.70	37.8	34.22	359.2	55.79	986.8
83.32	49.4	39.06	280.4	66.77	1201.1
		45.98	188.5	74.49	1035.6
		53.91	171.1	78.95	571.9
		54.71	162.6	80.85	864.4
		55.75	153.6	82.37	718.3
				86.79	517.8
ZnO/GO 0.1% w/w		ZnO/GO 0.25% w/w		ZnO/GO 0.5% w/w	
2θ (deg)	Intensity (a.u)	2θ (deg)	Intensity (a.u)	2θ (deg)	Intensity (a.u)
37.10	2038.2	37.06	1825.1	37.10	1912.4
40.25	1684.6	40.19	1624.8	40.25	1690.6
42.42	3171.2	42.37	2757.2	42.44	3080.1
55.88	921.1	55.79	769.9	55.84	938.9
66.84	1148.8	66.77	975.3	66.82	1103.2
74.54	978.5	74.49	887.1	74.50	966.6
79.03	562.5	78.96	521.2	79.06	916.1
80.91	893.3	80.90	863.3	80.96	574.4
82.44	699.2	82.35	657.8	82.40	921.05
86.80	506.1			86.91	528.8

As can be observed from Table 5 and Figure 20, there are slight intensity changes between the patterns of the nano-ZnO/GO hybrid photocatalysts and ZnO, in the region between 70 and 85 degrees, that probably suggests a different position of the atoms on the surface of the crystal lattice of the ZnO because the interactions with graphene oxide.

Regarding the diffraction pattern of GO, and based on bibliographic information referring to characteristic diffraction peaks of three crystal planes of this material, the first peak corresponds to 001plane at 13°, the second peak located at 32° corresponds to the 002 plane and the third peak located at 45° is attributed to the 100 plane [72, 73]. The ZnO and nano-ZnO/GO hybrid photocatalysts exhibit the typical XRD diffraction related to the wurtzite structure. However, no characteristic peak of graphene oxide is observed for none nano-ZnO/GO photocatalyst, which may arise by the low content of GO. Furthermore, the diffraction peaks of the hybrid composites are mostly unchanged compared to that of pure ZnO, which indicates that the lattice constants of ZnO have unchanged because of surface hybridization of the carbonaceous material

The FTIR spectra of pristine ZnO and GO, and nano-ZnO/GO hybrid material (0.5% w/w) are shown in Figure 17 that shows the typical fingerprint groups of graphene oxide, including the hydroxyl, carboxyl and alkoxy groups. The band located around 3400 cm^{-1} corresponds to the stretching vibrations of the –OH group.

The band at 1711 cm^{-1} corresponds to the C=O bond of carbonyls while the band located at 1612 cm^{-1} is attributed to the vibration of the C=C bond and, finally, the characteristic vibration band associated with alkoxy C-O stretches bond is located at 1031 cm^{-1}.

The band located at 699 cm^{-1}, corresponding to the Zn-O bond, is preserved in the spectrum of the nano-ZnO/GO photocatalyst. It is also noted that vibrations corresponding to the epoxy, carbonyl and carboxyl bonds of the GO drastically decrease or disappear; this might to two possibilities a) low concentration of GO in nano-ZnO/GO samples or b) indicating the reduction of GO during the synthesis of these materials.

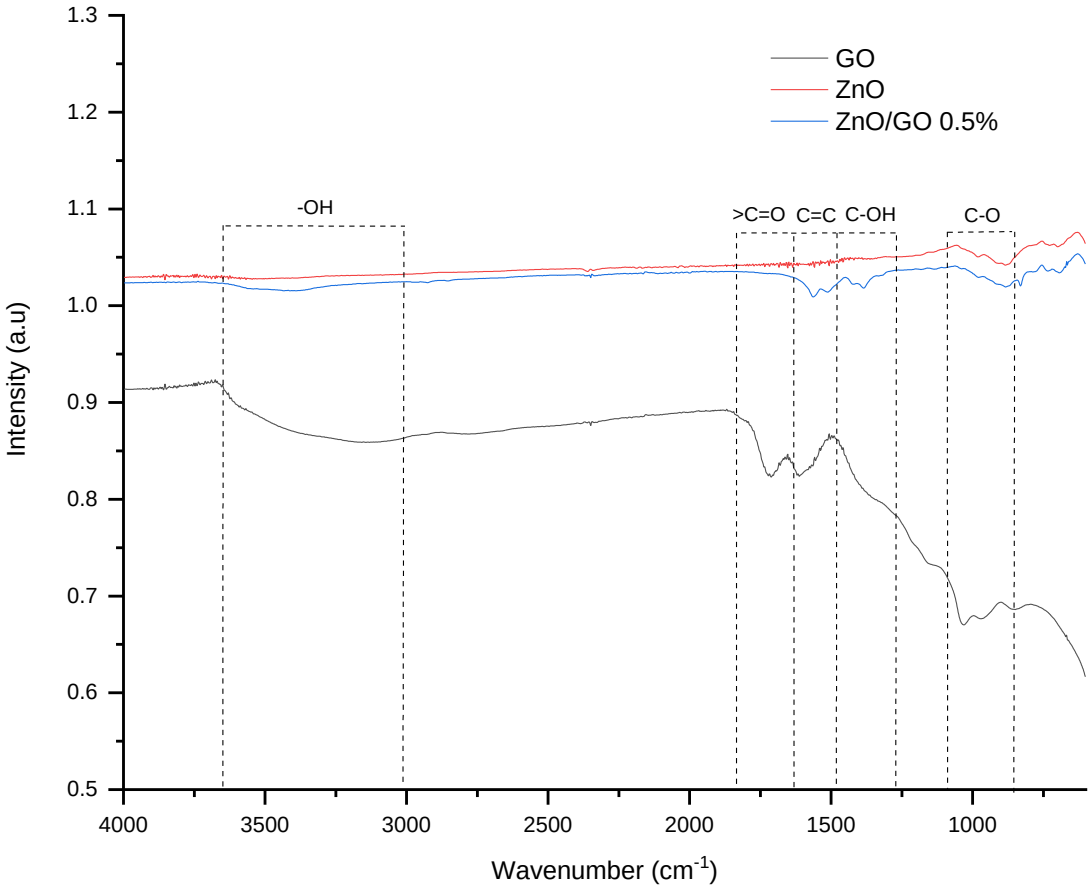

Figure 17. IR spectra of pure ZnO, pure GO and nano-ZnO/GO photocatalyst (0.5% w/w) synthesized by the photoirradiation method.

In particular, it should be noticed that a specific adsorption band appearing at 1386 cm^{-1}, which is observed only in the nano-ZnO/GO hybrid photocatalyst. This peak could be ascribed to the vibration of the C-O bonds formed between GO and ZnO, such a hybridization interaction between ZnO with a π-conjugative 2D system that could reduce the activation of surface oxygen atoms of ZnO, by which the photo-corrosion of zinc oxide could be significantly inhibited. This phenomenon has been described in previous research on C_{60}-ZnO composites photocatalysts. Moreover, there is a shift in the C=O band located at 1711 cm^{-1} that implies the hybridization of ZnO/GO photocatalysts [74].

The Raman spectra of zinc oxide, graphene oxide, and nano-ZnO/GO photocatalyst are shown in Figure 18, from which it can be seen that the pristine zinc oxide shows an intense peak at 438 cm^{-1} corresponding to E_2 crystal mode of the wurtzite structure. The D and G bands of graphene oxide were identified at 1350 cm^{-1} and l593 cm^{-1}, respectively. The Raman-reactive G mode at 1593 cm^{-1} is attributed to all sp^2 carbon-type structures and provides information on the in-plane vibration of sp^2 bonded carbon atoms while D band suggests the presence of sp^3 defects in the hexagonal graphitic layers [75].

The G band has been identified within the nano-ZnO/GO samples and is related to carbon-hybridized bonds in these photocatalysts. A slightly blue shift by 9 cm^{-1} in the D band of hybrid photocatalyst compared with D band of graphene oxide and a redshift in the G band of 8 cm^{-1} was observed. These shifts in the Raman peak could be attributed to the chemical interaction between ZnO and graphene oxide as it was suggested by FTIR results.

Besides, the D/G intensities ratio is a measure of the defects in the structure of graphitic materials. Regarding the sp^3 and sp^2 hybridizations ID/IG value, in the case of pure graphene oxide is 0.93, indicating that the intensity of the G band is slightly higher than D band which results in a lower amount of sp^3 defects and less structural disorder in this material.

Compared with graphene oxide (0.93), the reduction ID/IG intensity ratio for nano-ZnO/GO 0.5% hybrid photocatalyst (ID/IG=0.91) is observed, implying a reduction of sp^3 defects compared with pure graphene oxide. This fact confirms the interaction between ZnO and GO given by sp^3 defects. The results given hereinabove are consistent with the results in FTIR characterization, revealing the reestablishment of the conjugated graphene oxide network.

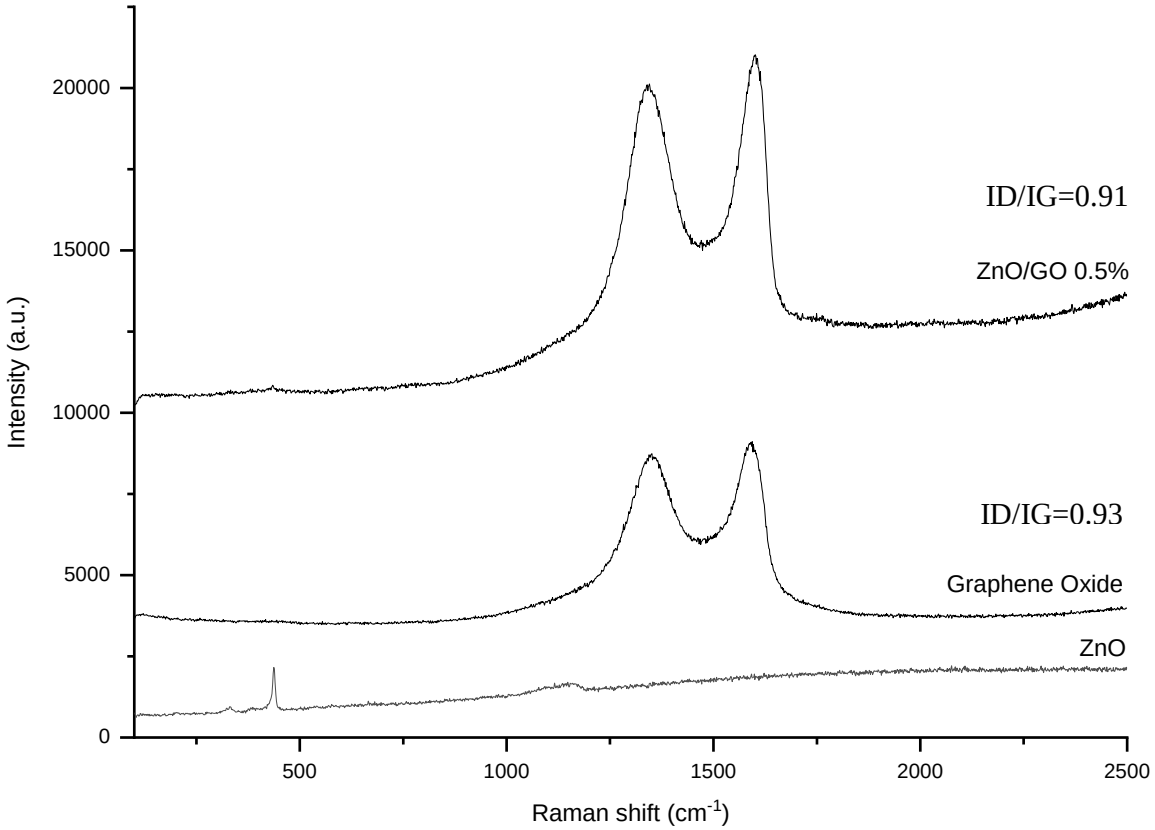

Figure 18. Raman spectra of pure ZnO, pure graphene oxide and nano-ZnO/GO photocatalyst loaded with 0.5% w/w of graphene oxide and synthesized by the photoirradiation method.

The light absorption range plays an important role in photocatalysis. Figure 19 shows the UV-vis diffuse reflectance spectroscopy of the samples. The bandgap values of the different synthesized photocatalysts were estimated using UV Spectroscopy, based on the absorption spectra collected in a wavelength range from 200 to 800 nm. The interaction between light and the surface of the samples analyzed defines their photocatalytic performance. In Figure 23, the peak at 360 nm corresponds to the absorbance of ZnO due to the optical transition of electrons from the valence to the conduction band. The bandgap (Eg) values were estimated using the wavelength (nm) of the intersection between the slope of each curve and the Y-axis according to equation 2.

Based on this calculation, the bandgap value for pristine ZnO was obtained, it is 3.21 eV, and for the nano-ZnO/GO photocatalysts, with 0.1%, 0.25% and 0.5% of GO, the obtained values are 3.20 eV, 3.17 eV, and 3.12 eV, respectively (see Table 7).

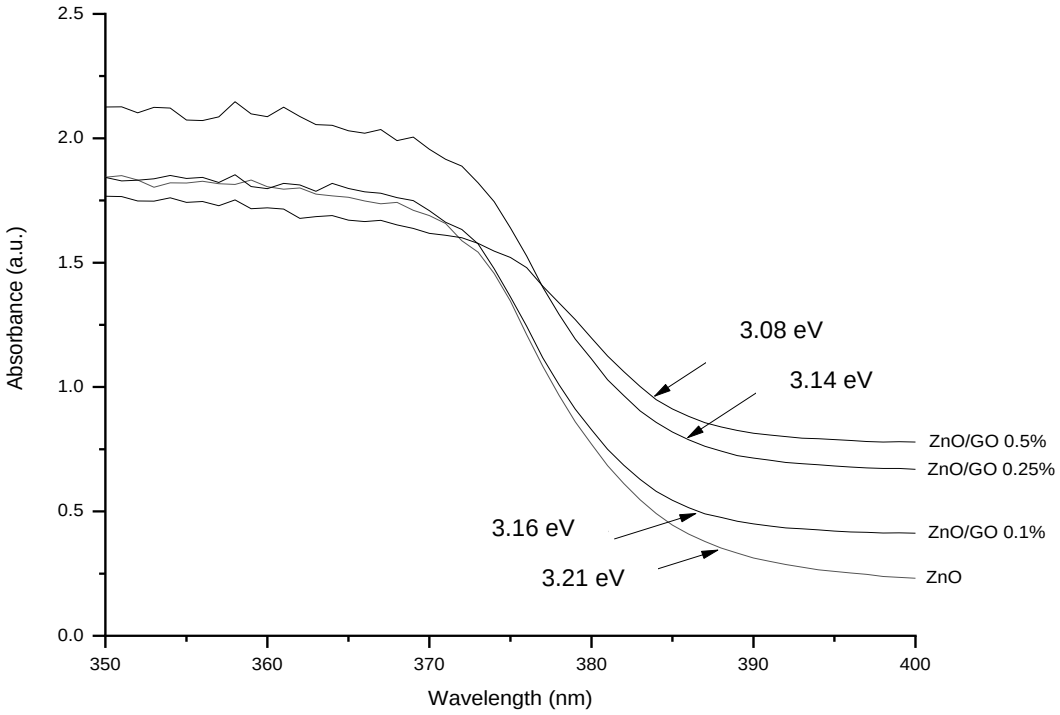

Figure19. UV-vis spectra of ZnO and nano-ZnO/GO hybrids compounds with different content of GO 0.1% w/w, 0.25% w/w and 0.5% w/w.

A decrement of the band gap values of ZnO hybridized materials, regarding the pristine ZnO catalyst, has the following order ZnO > nano-ZnO/GO 0.1% > nano-ZnO/GO 0.25% > nano-ZnO/GO 0.5% (see Table 7). The obtained Eg values imply an increment in light absorption intensity, in the visible region, due to the presence of GO, which possibly enhances the anti-photo-corrosion of ZnO and increases the retention time of the electrons that are promoted from the valance band to the conductive band in ZnO semiconductor.

The stronger absorption intensity in the visible region for nano-ZnO/GO hybrid photocatalysts is a key factor for higher photocatalytic activity even at low concentrations of GO. It is also observed that hybridized ZnO with graphene oxide showed an enhanced intensity of light absorption.

Table 7. Bandgap of pristine ZnO photocatalyst and nano-ZnO/GO hybrid materials with a different content of GO (0.1%, 0.25%, and 0.5%) obtained by UV-vis spectrophotometry.

Photocatalyst	Band Gap (eV)	λ (nm)
ZnO	3.21	386
ZnO/GO 0.10%	3.16	391
ZnO/GO 0.25%	3.14	393
ZnO/GO 0.5%	3.08	401

Therefore, it is possible to activate nano-ZnO/GO hybrid photocatalysts under visible light resulting in an opportunity to use these materials under such radiation, a fact that could have an impact on reducing the operating costs in water treatment systems. Regarding the method, the photoirradiation process is an easy and simple alternative to synthesize effective nano-ZnO/GO photoactive composites with a homogeneous distribution of ZnO particles.

Finally, zinc oxide and graphene oxide were evaluated by zeta potential technique, before and after they were photo-irradiated with UV light as they were irradiated during the synthesis of the nano-ZnO/GO photocatalysts. This experiment was carried out to determine and elucidate about polarisation effect during the photoirradiation method as it has been reported [76]. It is important to mention that both samples, previously to be evaluated, were thoroughly distillate-water washed and there was no control on pH during evaluation. It is important to have in mind that zeta potential for ZnO and GO were evaluated in water solution, as they were photo-irradiated using UV light, and just polarisation is focused on.

The results of this experiment showed positive zeta potential values for ZnO particles, before and after being exposed to UV radiation. These values were 58.48 mV and 50.43 mV, respectively.

This first result means a partial negative polarisation of the zinc oxide nanoparticles when they are exposed to UV radiation for two hours since there was a reduction of zeta potential value in comparison with the initial value. On the other hand, for the graphene oxide sample, an initial (before photoirradiation process) negative value of zeta potential (-40.61 mV) was obtained. Then, the GO sample was irradiated, and a positive value (36.35 mV) was determined. With this result, it is inferred that the carbon material is chemically reduced when it is subjected to UV radiation, as it has been suggested by XRD and FTIR.

Based on these results, it is concluded that the photoirradiation method promotes the interaction between graphene and zinc oxide by a negative polarisation of ZnO nanoparticles as we suggested by TEM and SEM observations and, further, the electrical conductivity of these hybrid catalysts is improved by the chemical reduction of GO particles. Both aspects contribute to improving the properties of nano-ZnO/GO photocatalysts synthesized by the photo-irradiation method and their performance during the degradation of TCS.

3.2 **Photocatalytic performance**

In order to evaluate the photocatalytic performance of nano-ZnO/GO photocatalysts, triclosan degradation experiments were conducted in batch systems, using visible light radiation (Halogen lamp, 150 W). The adsorption capacity for all the photocatalysts was determined previously, in dark conditions, and it was determined that the adsorption process for all the different materials take place in one hour. Thus, after this time (1 hour), it is feasible to evaluate the photocatalytic performance of ZnO and nano-ZnO/GO hybrid photocatalysts for the TCS degradation, excluding the effect of adsorption.

The considered “initial concentration of Triclosan” for the photocatalysis process, with the different photocatalysts, is reported in Table 8. Such “initial concentration” was obtained once the solution has been in dark, for 1 h, to achieve the sorption equilibrium. Also, before the sorption process takes place, the Triclosan concentration for all the solutions (with different photocatalyst type) was 8 mgL^{-1}, as it was mentioned previously.

Table 8. Initial concentration for the different photocatalyst samples.

Photocatalyst	Triclosan “initial concentration” for photocatalysis process, mgL-1	Amount of Triclosan adsorbed by photocatalyst, before photocatalysis, mg
ZnO	5.6	0.24
nano-ZnO/GO 0.10% - PI	5.4	0.26
nano-ZnO/GO 0.25% - PI	5.2	0.28
nano-ZnO/GO 0.50% - PI	5.1	0.29

The photocatalytic activities of the nano-ZnO/GO hybrid materials, with different amounts of graphene oxide, for the photodegradation of triclosan under visible light are shown in Figure 20, including that for the photolysis process (degradation in the absence of catalyst) and for the pristine nano-ZnO.

It is clearly noticed that all the nano-ZnO/GO photocatalysts exhibit much higher photocatalytic activities than photolysis (which degraded just 1% of the initial concentration of TCS) and ZnO sample.

The nano-ZnO/GO 0.5% photocatalyst exhibits the maximum degradation of triclosan (45%), while the photocatalyst nano-ZnO/GO 0.25% degraded up to 39% of the TCS. Finally, the photocatalyst synthesised with the lowest amount of GO (0.1% w/w) and the pristine ZnO catalyst exhibited degradation percentages of 35% and 32%, respectively. Thus, graphene oxide is beneficial for charge separation and increases the electrons lifetime promoted from the valance band to conductive band, reducing the recombination process in ZnO catalyst. The optimal loading amount of graphene oxide in nano-ZnO/GO hybrid photocatalysts, for the studied range, was 0.5% w/w. This percentage is much lower than those that has been reported for synthesised graphene oxide composites (mainly by solvothermal synthesis), which reach up to 5% [76, 77].

This result is an important approximation to achieve a good photocatalyst to be used under visible light, synthesized by the photoirradiation method, a promising, facile and friendly technique.

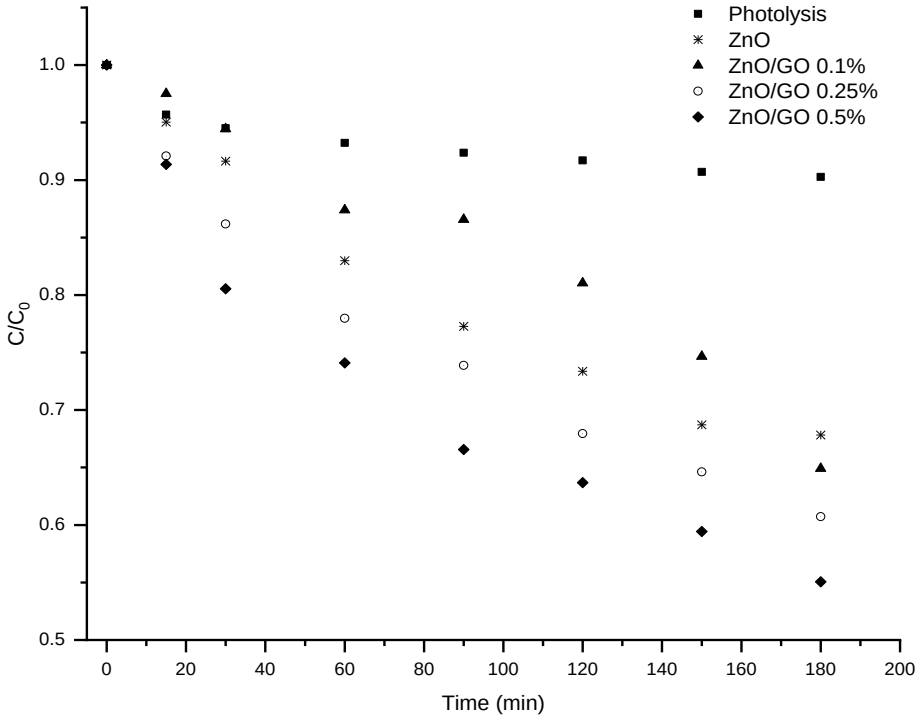

Figure 24. TCS degradation curves under visible light radiation using pristine ZnO, nano-ZnO/GO 0.1%, nano-ZnO/GO 0.25%, nano-ZnO/GO 0.5% synthesized by the photo-irradiation method. Conditions: pH=7, T=23°C.

Regarding the degradation kinetics, Figure 21 shows the TCS photodegradation apparent reaction rate constants k_{app} of nano-ZnO/GO hybrid photocatalysts, under visible light radiation. The degradation kinetic data were fitted using a pseudo-first-order equation. The introduction of graphene oxide into ZnO increased the rate constant. The photocatalytic activity follows the order nano-ZnO/GO 0.5% > nano-ZnO/GO 0.25% > nano-ZnO/GO 0.1% > ZnO, while the sample nano-ZnO/GO 0.5% shows the highest reaction rate constant of 0.0031 min^{-1} followed by nano-ZnO/GO with 0.25% w/w of graphene oxide (0.0027 min^{-1}). Lower graphene oxide content leads to a decrement of photocatalytic activity up to 0.0021 min^{-1}, corresponding to nano-ZnO/GO 0.1% sample. Pristine ZnO showed a rate reaction constant of 0.0020 min^{-1}. The kinetic rate constants of nano-ZnO/GO 0.5% and 0.25% were 55% and 27% higher than the rate constants exhibit by ZnO, respectively.

The ZnO/GO hybrid materials are able to improve the triclosan degradation efficiency because the presence of GO that act as an electron trap retaining the electrons, promoted from the valance to conductive band, in ZnO. Thus, higher number of radicals are obtained, which are responsible for efficient degradation of TCS.

This result contributes to the development of new active photocatalysts under visible light as has been investigated and reported in several studies that have demonstrated the possibility of the photodegradation of triclosan up to 47% using photocatalysts based on rare-earth elements such as Ceria (47%) [78], metals such as Au (10% after 5 h) [79], silver [80] and Cu [81]; and others, such as MgO, WO_3, TiO_2, ZnO or GO [82].

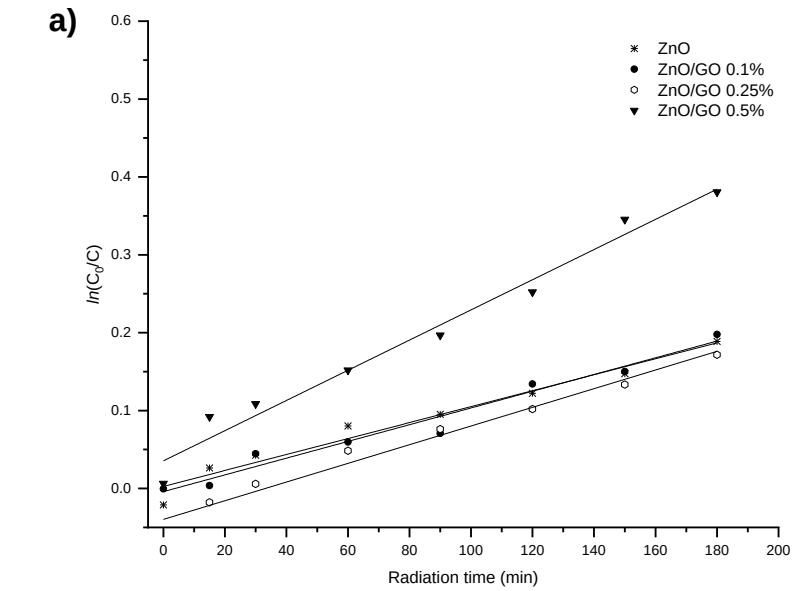

Figure 21. a) The pseudo-first-order adjustment to experimental values and b) apparent reaction rate constants (k_{app}) for triclosan degradation under visible light.

In order to compare the photoactivity of the as-prepared nano-ZnO/GO hybrid photocatalyst using higher energy irradiation, experiments were carried out under UV light (254 nm). Figure 22 shows that nano-ZnO/GO hybrids possess improved UV light photocatalytic activity versus the commercial ZnO and the photolysis. The result illustrates that the nano-ZnO/GO 0.5% hybrid photocatalyst exhibits the best performance, degrading 95% of the initial concentration of TCS, while ZnO/GO 0.25% gives 89% of degradation. Finally, the ZnO based catalyst and nano-ZnO/GO 0.1% degraded 83% and 85%, respectively, giving the lowest photocatalytic performance. The amounts of triclosan degraded by nano-ZnO/GO photocatalysts are slightly better than the degradation of TCS via photolysis and ZnO.

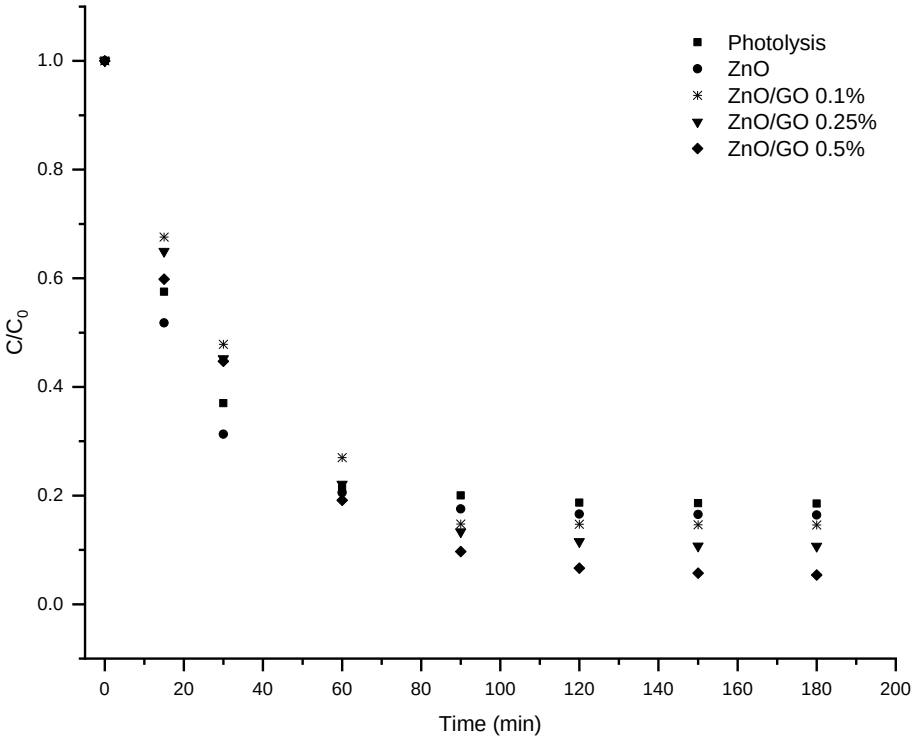

Figure 22. TCS degradation profiles under UV-radiation (254nm) using pristine ZnO, nano-ZnO/GO 0.1% w/w, nano-ZnO/GO 0.25% w/w, nano-ZnO/GO 0.5% w/w and photolysis. Conditions: pH=7, T=23°C.

It is important to mention that such values of degradation of triclosan (up to 95%) are very convenient to improve the water quality. It is very important since the conventional water treatment methods are not high efficient enough (<95%) then the residual triclosan is still able to impact the environment and affect the health of living beings.
The apparent rate constants for the degradation of triclosan under UV light were determined and the results are shown in Figure 23, which reveals a linear relationship between ln (C_0/C) and reaction time over as-prepared samples according to the pseudo-first-order kinetics plot (Figure 27-a).

The apparent reaction rate constant (k_{app}) values were enhanced by the introduction of graphene oxide in ZnO catalyst. The nano-ZnO/GO 0.5% (0.0227 min^{-1}) exhibited the highest k_{app} value among all the samples. This result suggests the improvement of the photodegradation efficiency of the ZnO semiconductor due to the presence of graphene oxide which acts as an electron trap enhancing the photodegradation performance of nano-ZnO/GO photocatalysts except for the photocatalyst with the lowest amount of GO (0.1%), which showed a slightly decrease in the slop degradation kinetic behaviour. These results are in accordance with those obtained under visible light radiation and demonstrate the enhancement of the photoactivity of ZnO due to the presence of graphene oxide.

On the other hand, the capacity of being reused is a very important feature for photocatalyst. In order to determine the photocatalytic reusability of nano-ZnO/GO 0.5% sample, using visible and UV light radiation, four degradation cycles were carried out. After each cycle, the photocatalyst was filtered and dried thoroughly, and then a fresh TCS solution was added. In Figure 24, it is seen that during four cycles the photoactivity test for the degradation of TCS, under visible radiation, with the nano-ZnO/GO 0.5% the efficiency is reduced up to 27% of the initial activity and, under UV light, for the same photocatalyst, displays a slight decrease and shows almost no deactivation. This observation could be attributed to non-degraded TCS that could be adsorbed in the surface of nano-ZnO/GO photocatalyst reducing the efficiency of this semiconductor.

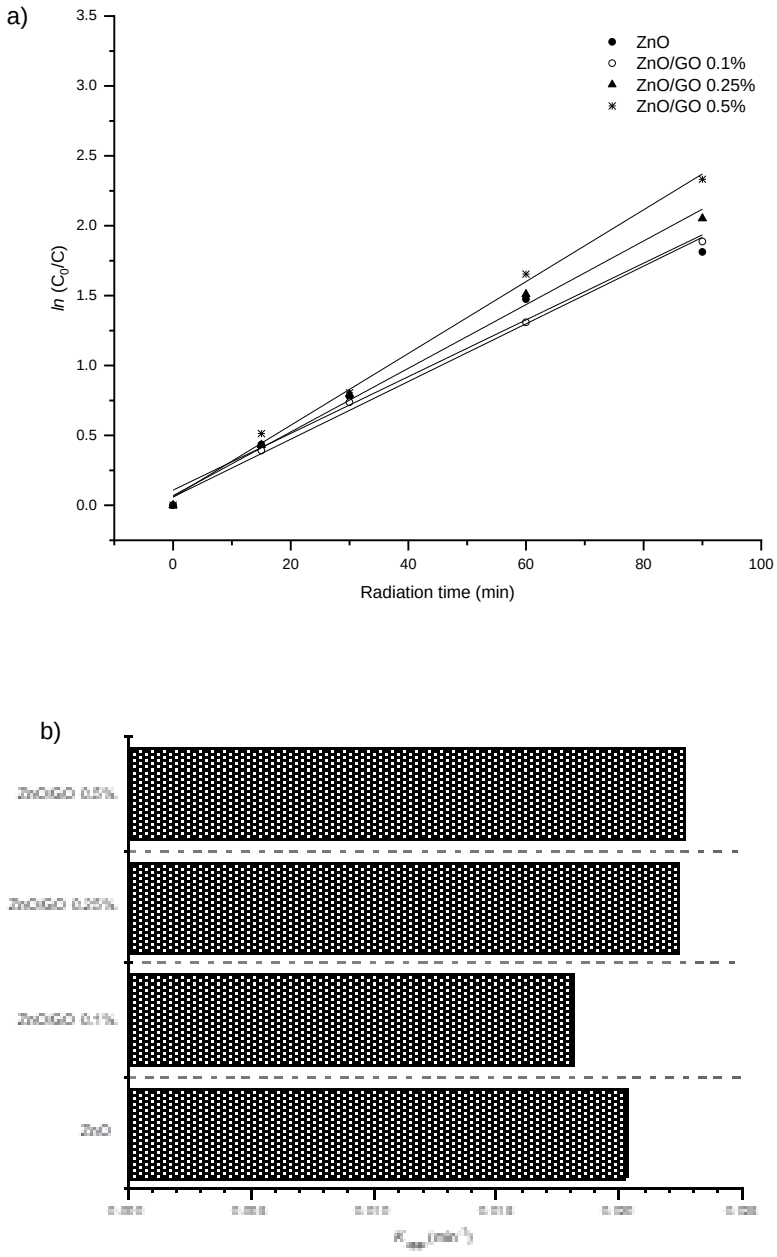

Figure 27. a) The pseudo-first-order adjustment to experimental values and b) apparent reaction rate constants (k_{app}) for triclosan degradation under UV light irradiation (254 nm) with as-prepared samples nano-ZnO/GO loaded with 0.5%, 0.25% and 0.1% of graphene oxide and pristine ZnO.

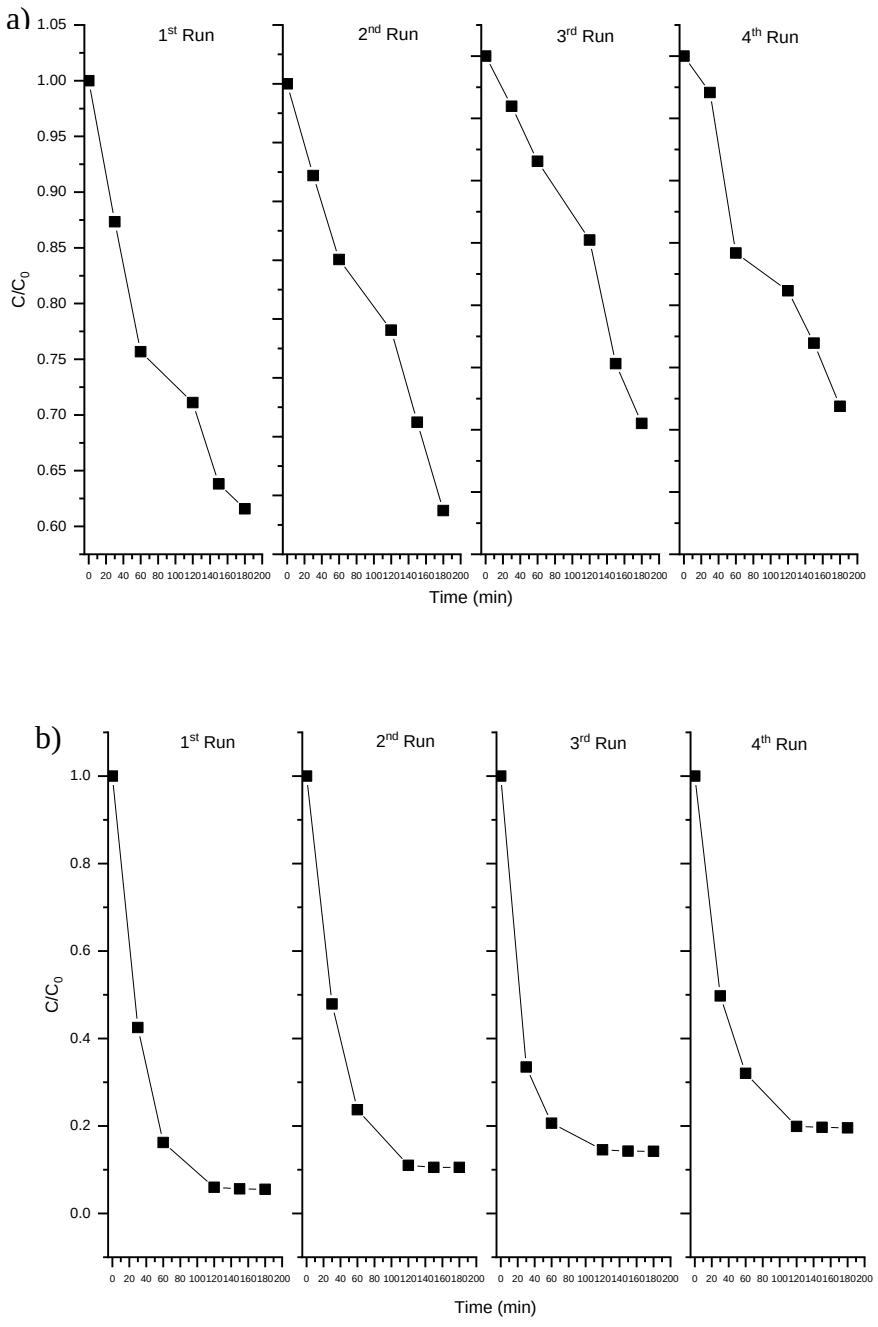

Figure 24. Reusability experiment for the photocatalytic degradation of triclosan by the prepared nano-ZnO/GO 0.5% composite under a) visible light and b) UV radiation.

3.3 **Mechanistic study.**

Surface area, phase structure, crystallinity and separation efficiency of photogenerated charges are crucial factors for photocatalytic activity. Therefore, in the as-prepared ZnO/GO hybrid samples, the enhancement of their photocatalytic activity is attributed mainly to the effective separation of the photogenerated electron-hole pairs.

In order to confirm the mechanism, the ESR technique and trapping experiments of radicals were performed. ESR results are shown in Figures 29 and 30 under visible light and UV radiation, respectively. The hydroxyl radicals (DMPO-•OH) and superoxide radicals (DMPO-O_2•$^-$) for ZnO and ZnO/GO hybrid photocatalysts in H_2O (four characteristic signals) and ethanol (six signals) using visible light are observed in Figure 29. In both cases, it is noticed that the signals for nano-ZnO/GO hybrid materials are more pronounced than those for the ZnO pristine sample, thus accounting for the higher photocatalytic performance of nano-ZnO/GO loaded with 0.5% w/w of graphene oxide than the bare ZnO photocatalyst towards the degradation of triclosan.

Thus, the enhanced photocatalytic activity of ZnO/GO, at any composition, but especially 0.5% compared with pure ZnO, is due to the introduction of graphene oxide, which promotes an increase the charge separation for the effective utilisation of electrons to stabilize the •OH and O_2•$^-$ radicals. In this case, the signals of •OH (Figure 25-a) radicals are stronger than those for O_2•$^-$ (Figure 25-b), which suggest the predominance of oxidative reactions whose holes are responsible for the degradation of triclosan. Furthermore, ZnO photocatalyst exhibits visible light photocatalytic activity but has better performance under visible light after graphene oxide hybridization, showing that graphene oxide is responsible for the injection of excited electrons from the LUMO (Lowest Unoccupied Molecular Orbit) orbit of graphene to the CB (Conduction Band) of ZnO [79].

The introduction of the graphene oxide could cause the rapid separation of electron-hole pairs during irradiation [83] prolonging the electron-hole pair lifetime and accelerating the transfer rate of electrons [84] as shown in Scheme 3.

a)

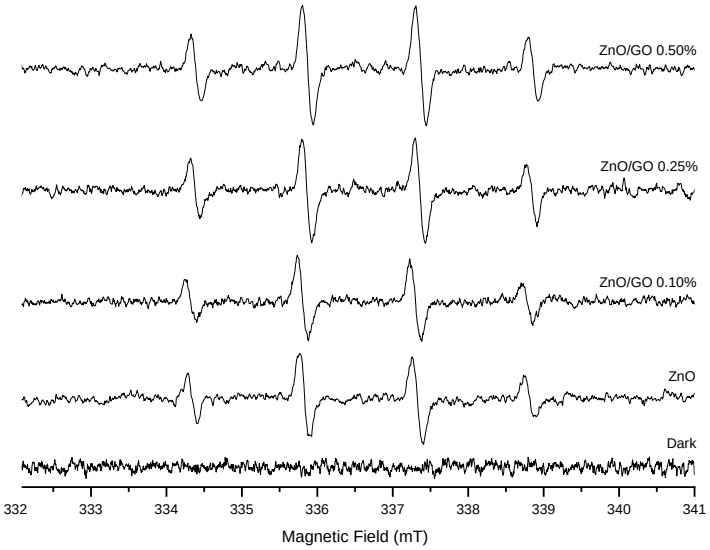

b)

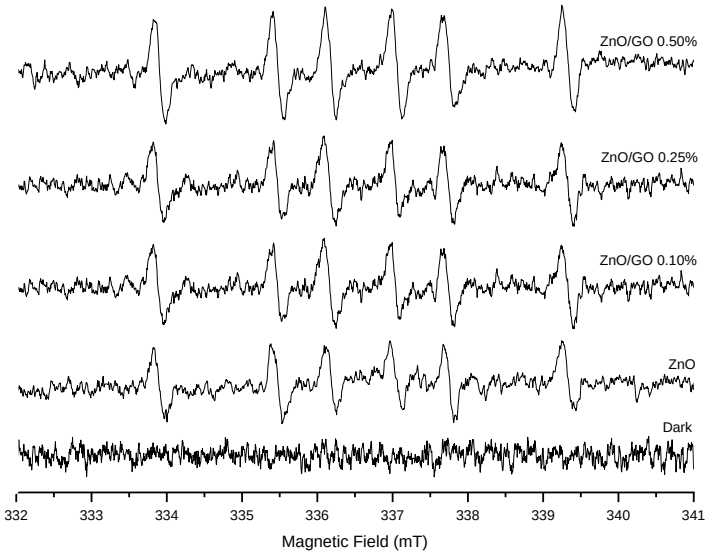

Figure 25. ESR analysis in dark conditions and visible light radiation of pristine ZnO and nano-ZnO/GO hybrid photocatalysts in a) water and b) ethanol. DMPO was used as the radical trapper.

The ESR spectra corresponding to the experiments performed in water and ethanol solvents using UV radiation are shown in Figure26. Figure 26-a corresponds to the hydroxyl radicals generated by the analysed samples and Figure 26-b shows the superoxide radicals. The same behaviour as observed under visible light radiation, higher signals of the hydroxyl radicals than superoxide radicals, occurred in the case of UV radiation.

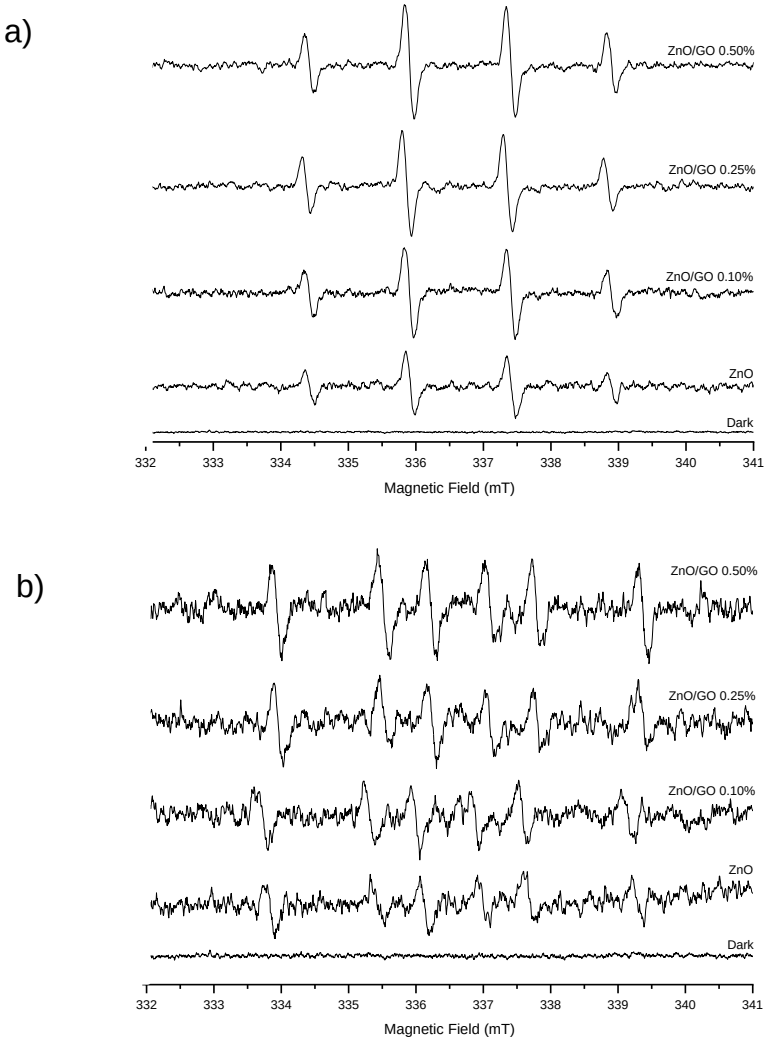

Figure 26. ESR spectra in dark conditions and UV radiation of the pure ZnO and nano-ZnO/GO hybrid photocatalysts in a) water and b) ethanol. DMPO was used as the radical trapper.

It is known that ZnO absorbs light to produce photogenerated electron-hole pairs. Since the valance band (VB) position of ZnO is lower than the HOMO (Highest Occupied Molecular Orbital) orbit of graphene, the photogenerated holes on ZnO could transfer easily to graphene oxide sheets via the well-developed interface. Meanwhile, the CB position of ZnO is lower than the LUMO orbit of graphene oxide, and the photogenerated electrons on graphene can directly inject to the CB band of ZnO, giving a more efficient charge separation and reducing the probability of recombination, and consequently, enhancing the photocatalytic activity.

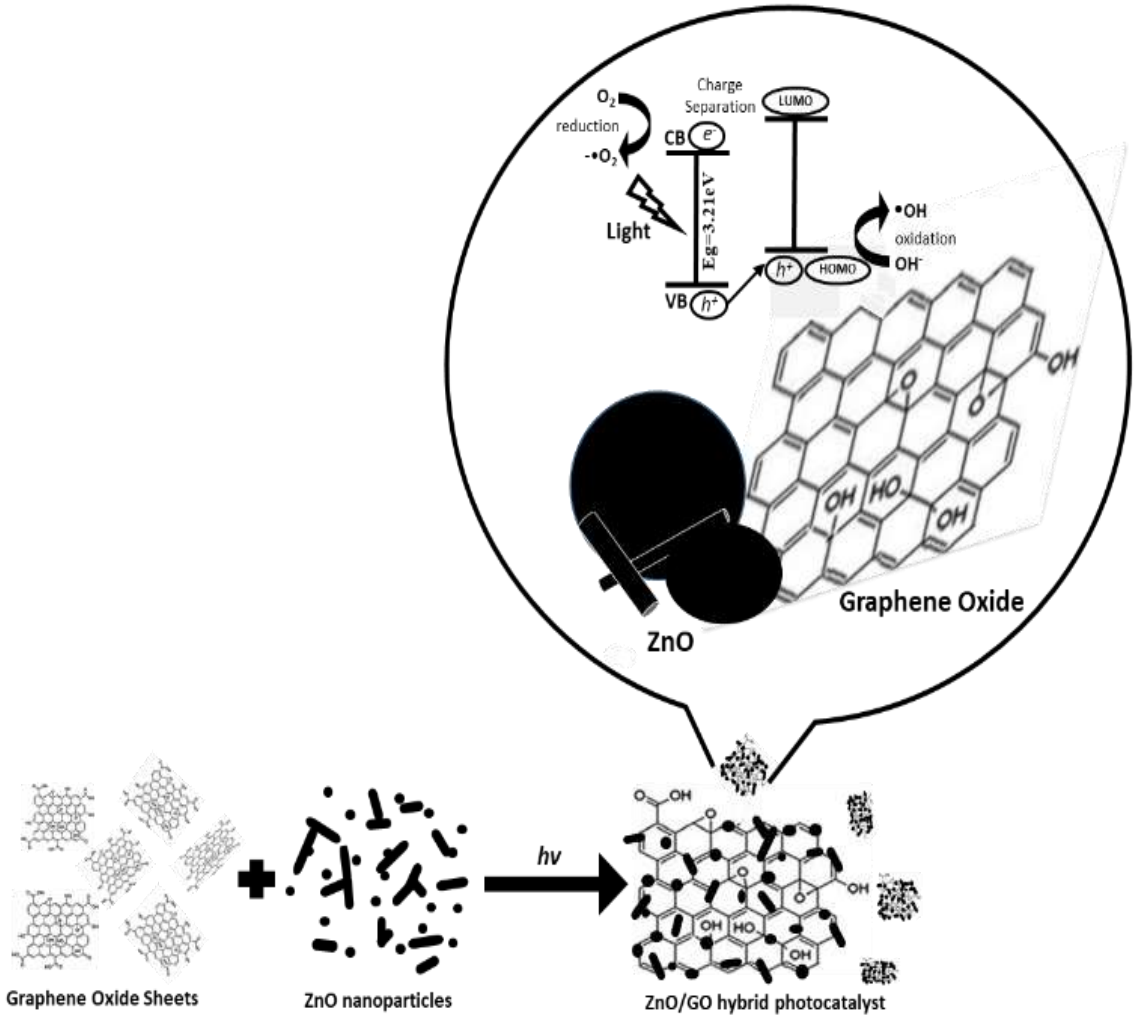

Scheme 3. Interaction of nano-ZnO/GO hybrid photocatalyst during photocatalysis process.

As shown in Scheme 3, the high separation efficiency of photoinduced electron-hole pairs is supposed to be responsible for the enhanced UV and visible light photocatalytic activity, resulting in an increase in the number of holes participating in the photo-oxidation process.

These electrons could easily migrate from the inner region to the surface to participate in oxidation and reduction reactions to generate radicals which are prolonged and enriched by the presence of functional groups of graphene oxide that acts as an electron tramp, thus dramatically improving the visible light activity.

The following reactions, 8 to 14, describe the proposed reaction mechanism.

$ZnO + h\nu \rightarrow ZnO + e^- h^+$ Reaction (8)

$ZnO\ (e^-) + GO \rightarrow ZnO\ (h^+) + GO\ (e^-)$ Reaction (9)

$ZnO\ (h^+) + GO\ (e) + H_2O \rightarrow ZnO + GO + \bullet OH + H^+$ Reaction (10)

$ZnO\ (h^+) + GO\ (e) + {}^-OH \rightarrow ZnO + GO + \bullet OH$ Reaction (11)

$ZnO + GO + \bullet OH + RH \rightarrow ZnO + GO + H_2O + R\bullet$ Reaction (12)

$ZnO + GO + R\bullet + O_2 \rightarrow ZnO + GO + ROO\bullet$ Reaction (13)

$ZnO + GO + ROO\bullet + O_2 \rightarrow ZnO + GO + CO_2 + H_2O$ Reaction (14)

Such reactions describe the transportation of electron-hole pairs between ZnO and graphene oxide sheets. Thus, the photocatalytic degradation of triclosan is enhanced.

3.4 **Previous conclusions.**

The photoirradiation method allows a homogeneous distribution of the ZnO particles on the graphene sheets surface due to the surface polarisation of ZnO nanoparticles by the high energy (UV) used during the photocatalyst synthesis process. There is a good interaction between the ZnO and GO through sp^3 hybridizations of the graphene oxide that improves the photocatalytic efficiency of nano-ZnO/GO photocatalysts.

It is possible to degrade up to 45% of triclosan (3.6 $mg.L^{-1}$) under visible light radiation using nano-ZnO/GO hybrid photocatalyst even with low concentrations as 0.5% w/w. GO acts as electron scavenger reducing the recombination process and promotes the charge separation in the ZnO semiconductor between the valance and conduction bands that increases the generation of •OH radicals, resulting in the increase of the apparent constant rate up to 55% in nano-ZnO/GO hybrid photocatalyst compared to the apparent rate constant of pristine ZnO.

The nano-ZnO/GO hybrid photocatalyst can be used in a cyclic way without a significant reduction of its efficiency to degrade triclosan.

4 Chapter 3
nano-ZnO/GO/PVA composites

The continuously increasing number of environmentally risky chemicals, strongly demands the developments of new procedures, which can be successfully deployed against a wide range of man-made contaminants. Heterogeneous photocatalysis as one of the AOPs satisfies this requirement. It has been demonstrated in Chapters 2 and 3 that nano-ZnO graphene-based photocatalysts are photoactive semiconductors for the photodegradation of TCS under visible and UV light. However, one of the main drawbacks of this method is the photocatalyst implementation is in a suspended phase and in real water treatment system its separation after the treatment results very difficult and expensive. One alternative to solve this challenge is the use of polymeric materials that lead supported photocatalysts to recover and use them again. Polymeric composites have been developed and packed in carrier or column to be used in WWTPs for the degradation of toxic chemicals present in wastewater, but usually clogging and back pressure problems are presented in the process. A major challenge is the development of polymeric composites that contains active photocatalysts with adequate capacities of photodegradation, speedy separation, and convenient recycling. Polymeric support technology has harvested highlighted attention, since its application provided a simple way to degrade organic pollutants, especially using non-toxic, low cost and resistant polymers. But, unfortunately, this method is not free of disadvantages since the photocatalyst immobilization decreases the active surface area of the catalyst, diminishing its efficiency.

Is important to consider requirements in the development of polymeric composites in order to support photocatalysts: strong interaction between the surface and the catalyst to get the desired stability, the coated support should not change the activity of the catalyst, a large surface area is essential to ensure a high efficiency of degradation via easy adsorption of the pollutants, a long-term use requires the durability of immobilization, the applied carrier must withstand the photocatalytic processes, as well as the long-term radiation [85].

Among the first, Tennakone et al. used polymer surface for fixing titanium dioxide in 1995 [86]. A catalyst film was taken up to the polyethylene backing by a simple thermal treatment.

Later, a number of other polymers were used for this purpose in other laboratories, e.g. polyethylene sheets [87], PVC [88], polyethylene terephthalate bottle [85], and poly (vinyl alcohol) [89–94]. Usually, a physical contact is formed between the polymer and the catalyst [85, 87], but in some cases they are chemically bound [89]. The advantage of the polymeric fixation is that a large proportion of the materials is chemically inert and mechanically stable, commercially available and inexpensive, most of them have a high resistance to UV radiation [85]. Recently, several research teams used titanium dioxide immobilized with poly (vinyl alcohol) for photocatalytic applications. Habibi et al. (2016) created chitosan/PVA/Na-titanate/TiO2 composite with solution casting method and used it for the photodegradation of two dyes [95]. The Na-titanate improved the water-resistance but decreased the crystallinity of chitosan. The removal efficiencies were 100% and 99% in the case of methyl orange and congo red, respectively. Adb El-Rehim et al. (2012) fixed TiO_2 at the surface of PVA microgel and used for the degradation of methyl orange dye [96]. Xiuyunet al. (2015) investigated the photocatalytic activity (in the visible range) of a PVA-TiO_2 composite film produced by a sol-gel method [93]. Lei et al. (2012) immobilized P25 TiO_2 with poly (vinyl alcohol) by a casting technique with thermal treatment [89].

In the present chapter are presented the results obtained for the nano-ZnO/GO/PVA polymeric composites developed in this research. We propose an easy preparation and low cost as an alternative to synthesize polymeric support matrices for photocatalysts.

4.1 **Swelling behavior**

In Figure 27 are presented images of the nano-ZnO/GO/PVA polymeric composite synthesized by citric acid crosslinking method [97] and its surface characteristics. The hybrid photocatalyst used was the sample that sowed the highest performance in the degradation of TCS under visible and UV light (0.5% w/w).

nano-ZnO/GO/PVA

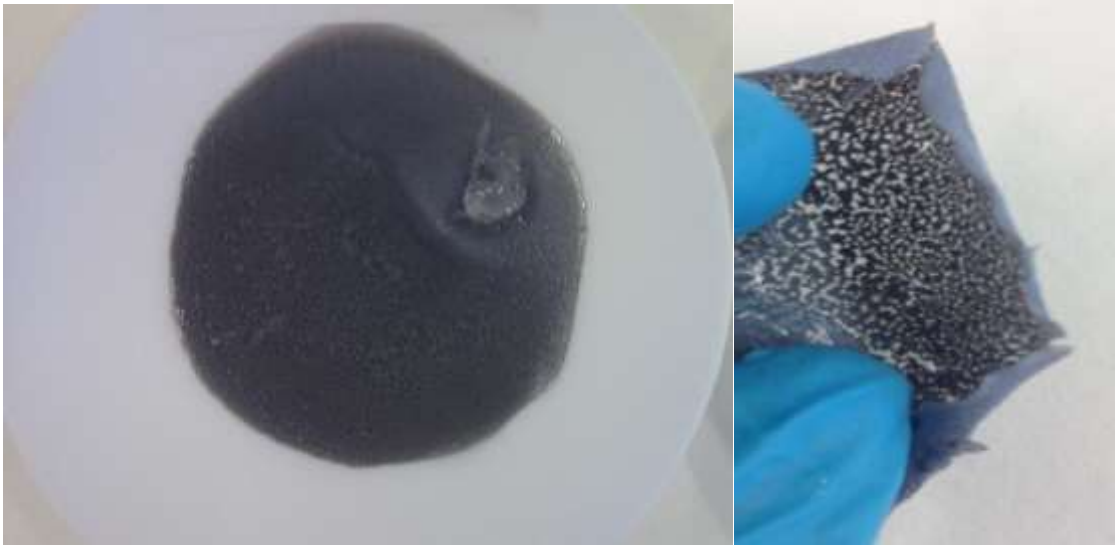

Figure 27. Images of the nano-ZnO/GO/PVA polymeric composite and its surface characteristics.

Polymeric composites were tested in water in order to determinate their swelling behaviour as was described in section 1.9.2. Results obtained are presented in Figure 28 that shows a decrement (5.5. times) in water retention of the polymeric composite compared with the swelling capacity of PVA hydrogel. This result suggests a crosslinking effect due to the presence of nano-ZnO/GO photocatalyst. Probably, free chemical groups of the hybrid photocatalyst interact with hydroxyl groups of the PVA polymer during the synthesis process.

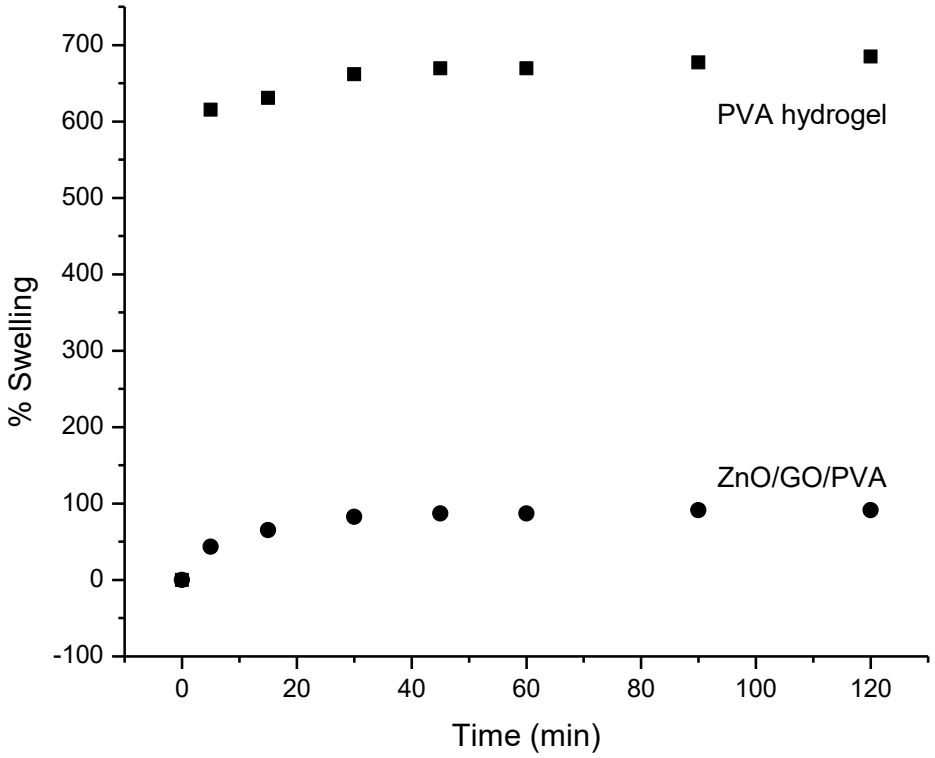

Figure 28. Swelling behavior of the PVA hydrogel and nano-ZnO/GO/PVA prepared with hybrid photocatalyst with 0.5% of GO. Conditions: pH= 7, T=23ªC.

4.2 Characterization and properties of polymer composites

FTIR studies of nano-ZnO/GO/PVA composites were carried out. Figure 29 shows the FTIR spectra of pure PVA, citric acid, PVA crosslinked with citric acid and polymeric composite. It is noticed that the polymeric composite spectra exhibits bands corresponding to the pristine ZnO, determined in section 2.1. These spectra shows slight shift at 591 cm^{-1} that suggests the interaction between the hybrid photocatalyst with PVA due hydroxyl groups interactions. Additionally, ester groups have been identified at 1240 cm^{-1} and 1570 cm^{-1} in PVA+Citric acid sample corresponding to the crosslinking process to obtain a hydrogel that it is referred in the study developed by Redy et al. (2010) [97]. This result suggests that is possible obtain a polymer with a stable structure.

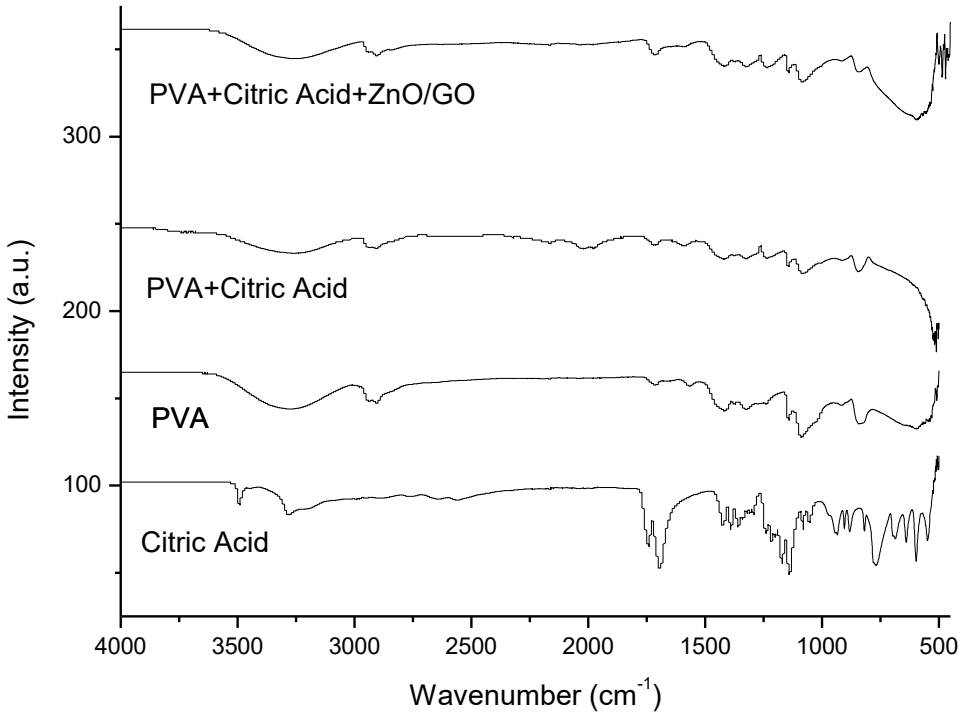

Figure 29. FTIR spectra of pure PVA, citric acid, PVA crosslinked with citric acid and polymeric composite.

Thermal properties of the polymer composites were evaluated by DSC and TGA techniques. Figure 30 shows the glass temperature (T_g), melting temperature (T_m) and crystallization temperature (T_c) obtained by DSC for pure PVA, PVA hydrogel (PVA+Citric acid) and ZnO/GO/PVA material. In Figure 30-a the pure PVA T_g increases when is cross-linked and when hybrid photocatalyst is added. In this case ZnO/GO photocatalyst acts as anchorage points into the polymer matrix. In Figure 30-b the T_m are shown, the temperatures decreases in the case of crosslinked PVA and polymeric composite respects to the Tm of pure PVA due to the presence of ZnO, GO and citric acid crystals, conferring disorder in the polymeric chains. Finally, crystallization temperatures are shown in Figure 30-c which decrease for PVA hydrogel a polymeric composite considerably due to the presence of ZnO and GO materials conferring disorder in the polymer structure.

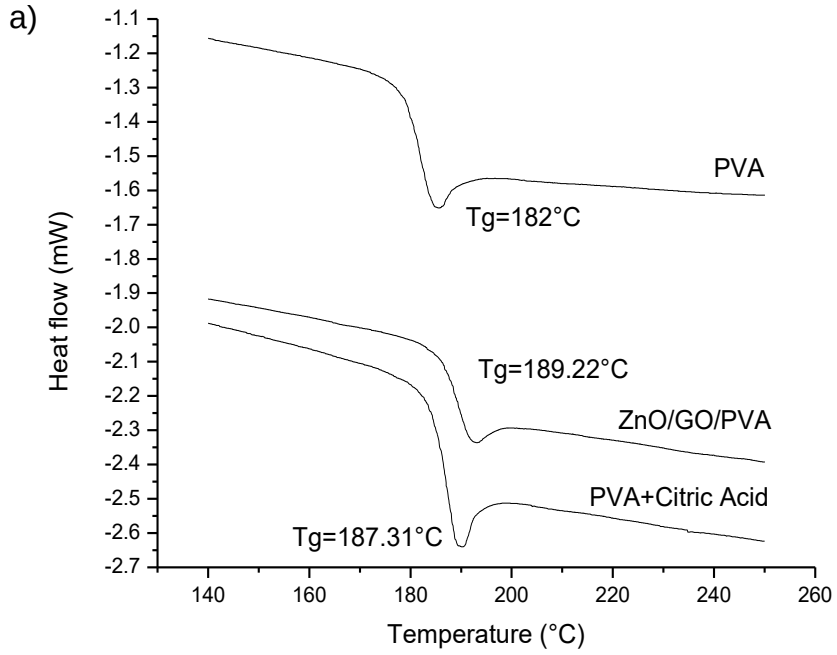

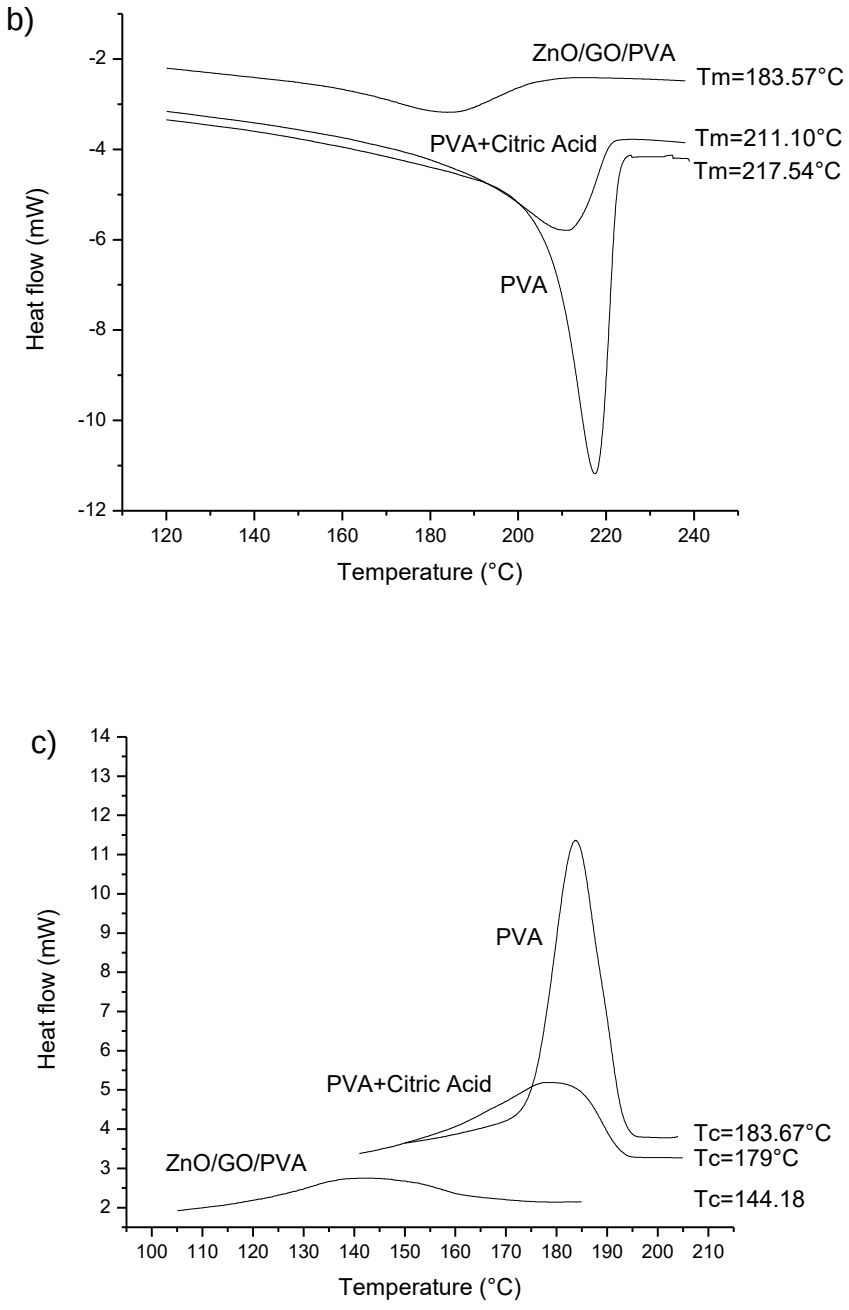

Figure 30. a) Glass transition T_g, b) melting (T_m) and c) Crystallization (T_c) temperatures for pure PVA, PVA hydrogel (PVA+ Citric acid) and ZnO/GO/PVA material.

Thermal degradation analyses are presented in Figure 31 for the same samples tested by TGA. Figure 31-a shows loss mass of 0.54% (of the total sample mass) at 600ºC corresponding to the ester chemical groups in the PVA hydrogel sample. In Figure 31-b it is observed that PVA loss hydroxyl groups (70% of the initial mass) at 200ºC. Also, it shows the zinc oxide content that corresponds to 5.1% of the total weight sample. Results that are correlated with those obtained by FTIR.

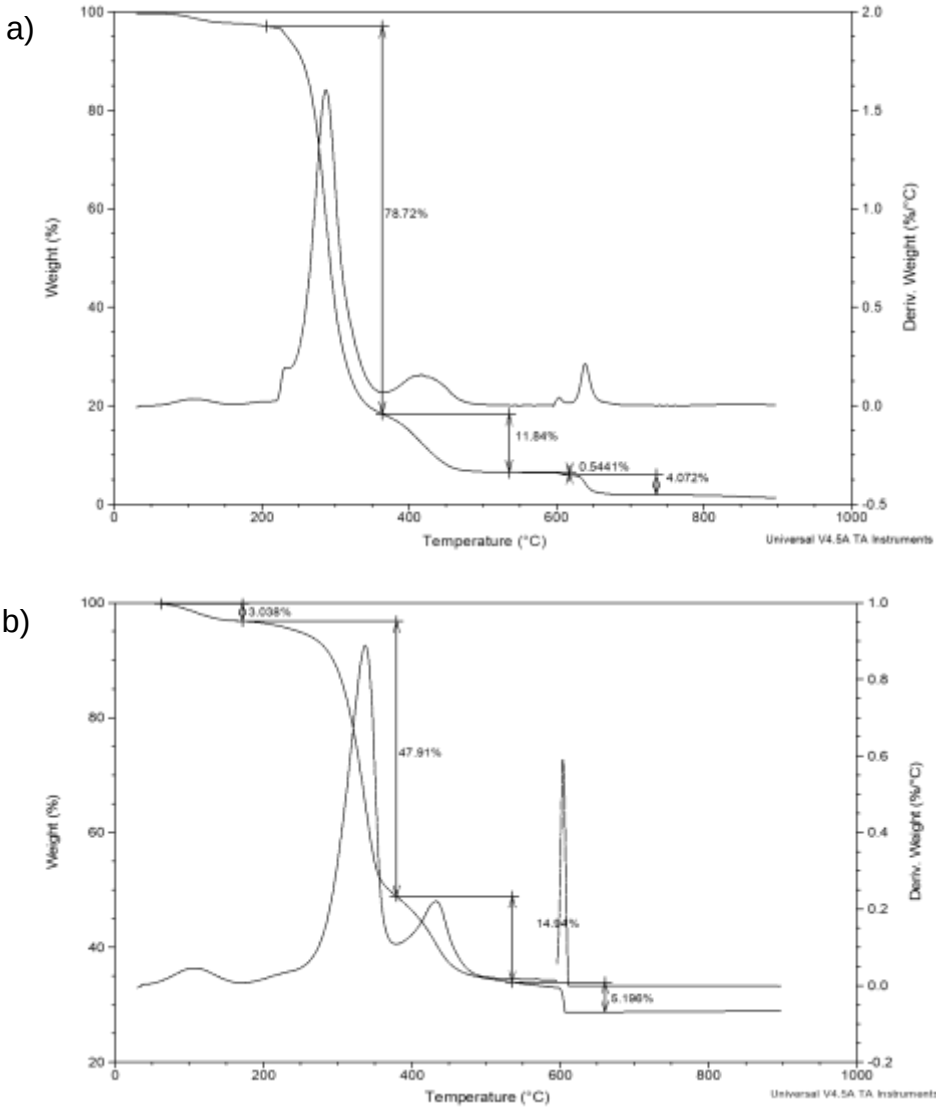

Figure 31. Thermograms of a) PVA hydrogel cross-linked with citric acid and b) nano-ZnO/GO/PVA polymer composite.

4.3 **Photocatalytic activity.**

Polymeric composite was tested for the degradation of TCS under visible light to determinate its photoactivity. The hybrid photocatalyst used to synthesise polymeric composite was nano-ZnO/GO 0.5% w/w (5 $g.L^{-1}$). Figure 32 shows a degradation of 32% of the initial concentration of TCS under visible light with the corresponding k_{app} value of 0.0028 min^{-1}. The reaction rate constant decreases compared with the result obtained in the evaluation of nano-ZnO/GO 0.5% (0.0031 min^{-1}), this effect probably is due to diffusion effects throw the polymeric matrix during the photo degradation process.

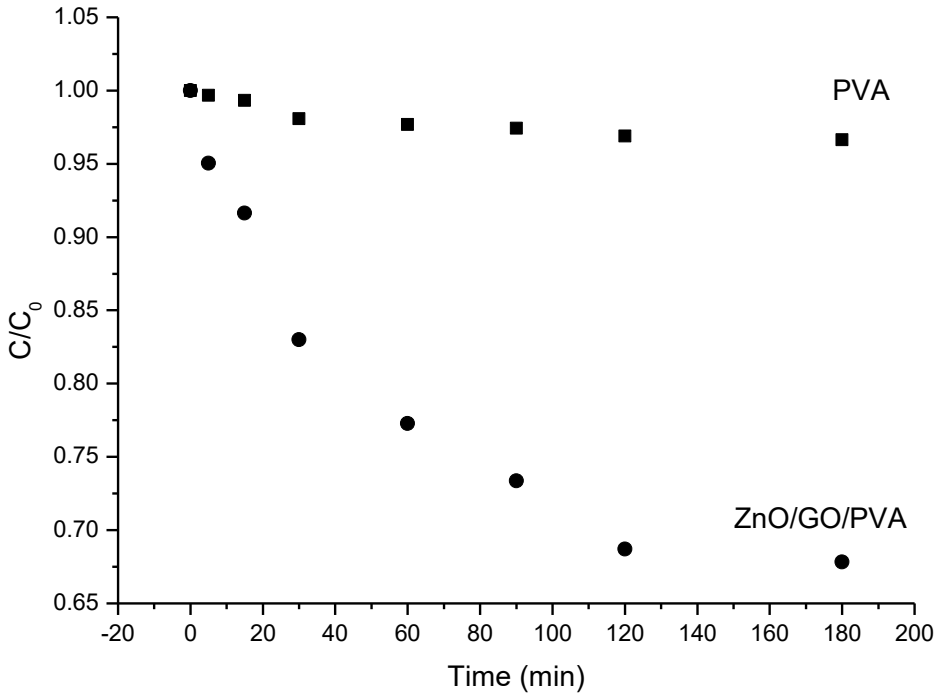

Figure 32. TCS photodegradation under visible light (lamp: 150 W) using polymeric composite loaded with nano-ZnO/GO photocatalyst (5 $g.L^{-1}$).

4.4 **Previous conclusions.**

It is possible to immobilize nano-ZnO/GO hybrid photocatalysts in poly(vinyl alcohol) by a low cost, easy and environmental friendly method. Esterification process take place into the cross-linked polymer matrix obtaining a stable and strong polymer network. In PVA hydrogel ZnO/GO photocatalyst acts as anchored points in the polymer matrix. Increasing the amount of photocatalyst in hydrogel support, it is possible to degrade up to 32% of the initial concentration of TCS under visible light, which is slightly lower than the photocatalyst noon-supported. The last is due to the loss of active area during support of photocatalyst into the polymeric matrix. However, it is a very attractive result.

5 Chapter 4
Conclusions

I. Mechanical impregnation method does not lead to homogeneous distribution of the nano-ZnO particles on the graphene or graphene oxide sheets, in contrast with the Photo-irradiation (PI) method that distributes homogeneously the ZnO nanoparticles on the graphene materials avoiding their agglomeration. PI method is an efficient and easy preparation method to synthesize hybrid photocatalysts based on nzno-ZnO and Graphene or GO materials, because a polarization effect of ZnO nanoparticles by the UV-irradation.

II. The highest content of graphene and GO used to modify nano-ZnO photocatalyst, was the concentration that degraded the highest amount of TCS under visible and UV light, 0.5% w/w. The photoactivity performance of the hybrid nano-ZnO/Graphene based materials depends on their graphene or GO concentration.

III. Hybrid photocatalysts of nano-ZnO/Graphene or nano-ZnO/GO are photoactive catalysts under UV and visible radiation due to the presence of graphene material in the sample, which acts as an electron trap retaining the electrons excited from the valance to the conduction band on the ZnO photocatalyst, improving the degradation efficiency of TCS, showed by the apparent reaction rate constants.

IV. Is possible to synthesize PVA hydrogel by esterification process by a low cost, easy and environmental alternative, which allows the immobilization of photocatalysts, obtaining photoactive polymer composites for the degradation of TCS, under visible radiation.

6 References

6.1 References

[1] T. Colborn, F.S. Vom Saal, A.M. Soto, Developmental effects of endocrine-disrupting chemicals in wildlife and humans, Environ. Health Perspect. 101 (1993) 378–384.
[2] E. Diamanti-Kandarakis, J. P. Bourguignon, L.C. Giudice, et al. Endocrine-Disrupting Chemicals: An Endocrine Society Scientific Statement. Endocr. Rev. 30 (2009) 293-342.
[3] A. Stolz, G. Schönfelder, M. R. Schneider, Endocrine Disruptors: Adverse Health Effects Mediated by EGFR?, Trends Endocrinol. Metab. 29 (2018), 69-71.
[4] Dann, A.B., Hontela, A., Triclosan: environmental exposure, toxicity and mechanisms of action, J. Appl. Toxicol. 31 (2011), 285-311.
[5] Chu, S., Metcalfe, C.D., Simultaneous determination of triclocarban and triclosan in municipal biosolids by liquid chromatography tandem mass spectrometry. J. Chromatogr. A. 1164 (2207), 212-218.
[6] Wu, J.L., Lam, N.P., Martens, D., Kettrup, A., Cai, Z., Triclosan determination in water related to wastewater treatment, Talanta, 72 (2007), 1650-1654.
[7] Chu, S., Metcalfe, C.D., Simultaneous determination of triclocarban and triclosan in municipal biosolids by liquid chromatography tandem mass spectrometry, J. Chromatogr. A, 1164 (2007), 212-218.
[8] Parenti, C.C., Ghilardi, A., Della Torre, C., Mandelli, M., Magni, S., Del Giacco, L., Binelli, A., Environmental concentrations of triclosan activate cellular defence mechanism and generate cytotoxicity on zebrafish (Danio rerio) embryos. Sci. Total Environ, 650 (2019), 1752-1758.
[9] Sola-Gutierrez, C., San Roman, M.F., Ortiz, I., Fate and hazard of the electrochemical oxidation of triclosan. Evaluation and polychlorodibenzo-p-dioxins and polychlorodibenzofurans (PCDD/Fs) formation. Sci. Total Environ, 626 (2018), 126-133.
[10] Federal Register, Volume 81, Number 172, (2016), 61099-61582 (Washington DC (USA)).
[11] Montaseri, H., Forbes, P.B., A review of monitoring methods for triclosan and its occurrence in aquatic environments. TrAC Trends Anal. Chem. (Reference Ed.) 85 (2016), 221-231.

[12] Ternes, T.A., Meisenheimer, M., McDowell, D., Sacher, F., Brauch, H.J., Haist-Gulde, B., Preuss, G., Wilme, U., Zulei-Seibert, N., Removal of pharmaceuticals during drinking water treatment, Environ. Sci. Technol. 36 (2002), 3855-3863.
[13] Fukuhara, T., Iwasaki, S., Kawashima, M., Shinohara, O., Abe, I., Adsorbability of estrone and 17β-estradiol in water onto activated carbon. Water Res. 40 (2006), 241-248.
[14] Le Noir, M., Plieva, F., Hey, T., Guieysse, B., Mattiasson, B., Macroporous molecularly imprinted polymer/cryogel composite systems for the removal of endocrine disrupting trace contaminants, J. Chromatogr. A, 1154 (2007), 158-164.
[15] Auriol, M., Filali-Meknassi, Y., Tyagi, R.D., Adams, C.D., Surampalli, R.Y., Endocrine disrupting compounds removal from wastewater, a new challenge, Process Biochem. 41 (2006), 525-539.
[16] S. Rafqah, P. Wong-Wah-Chung, S. Nelieu, J. Einhorn, M. Sarakha, Phototransformation of triclosan in the presence of TiO2 in aqueous suspension: Mechanistic approach, App. Catal. B: Environ. 66 (2006), 119-125.
[17] J.M. Poyatos, M.M. Muñio, M.C. Almecija, J.C. Torres, E. Hontoria, F. Osorio, Advanced Oxidation Processes for Wastewater Treatment: State of the Art, Water Air Soil Pollut. 205 (2010) 187–204.
[18] M. A. Fox, M. T. Dulay, Heterogeneous photocatalysis, Chem. Rev. 93 (1993), 341-357.
[19] S.K. Pardeshi, A.B. Patil, Solar photocatalytic degradation of resorcinol a model endocrine disrupter in water using zinc oxide, J. Hazard. Mat. 163 (2009), 403-409.
[20] M. Kamaraj, K.S. Ranjith, S. Rajeshwari, R.T. Rajendra, H. A. Salam, Photocatalytic degradation of endocrine disruptor Bisphenol-A in the presence of prepared CexZn1 –xO nanocomposites under irradiation of sunlight, J. Environ. Sci. 26 (2014) 2362-2368.
[21] P. Georgiev, N. Kaneva, A. Bojinova, K. Papazova, K. Mircheva, K. Balashev, Effect of gold nanoparticles on the photocatalytic efficiency of ZnO films, Colloids Surf. A Physicochem. Eng. Asp. 460 (2014) 240-247.
[22] Y. Zheng, C. Chen, Y. Zhan, X. Lin, Q. Zheng, K. Wei, J. Zhu, Photocatalytic activity of Ag/ZnO heterostructure nanocatalyst: correlation between structure and property, J. Phys. Chem. C. 112 (2008) 10773-10777.
[23] M. Hosseini-Sarvari, Z. Bazyar, Visible Light Driven Photocatalytic Cross-Coupling Reactions on Nano Pd/ZnO Photocatalyst at Room-Temperature, ChemistrySelect, 3 (2018), pp. 1898 – 1907.

[24] J. Shah, M. R. Jan, F. Khitab, Sonophotocatalytic Degradation of Textile dyes over Cu impregnated ZnO catalyst in Aqueous Solution, Process Saf. Environ. Prot. 116 (2018) 149-158.
[25] J. Wenwen, S. Yongchen, L. Gong, X. Chen, Synthesis of Al-ZnO nanocomposite and its potential application in photocatalysis and electrochemistry, Inorg. Chem. Commun. 88 (2018) 51-55.
[26] J. Park, Visible and near infrared light active photocatalysis based on conjugated polymers, J. Ind. Eng, Chem. 51 (2017) 27-43.
[27] P.T. Kurnianditia, T. Lling-Lling, W. Ong, W. S. Chang, S. Chai, Graphene oxide: Exploiting its unique properties toward visible-light-driven photocatalysis, Appl. Mater. Today, 4 (2016) 9-16.
[28] L. Xinjuan, P. Likun, Z. Qingfei, L. Tian, Z. Guang, C. Taiqiang, L. Ting, S. Zhuo, S. Changqing, UV-assisted photocatalytic synthesis of rec–reduced graphene oxide composites with enhanced photocatalytic activity in reduction of Cr (VI), Chem. Eng. J. 183 (2012) 238-243.
[29] Hanieh Fakhri, Hasan Bagheri, Highly efficient Zr-MOF@WO3/graphene oxide photocatalyst: Synthesis, characterization and photodegradation of tetracycline and malathion, Materials Science in Semiconductor Processing, 107 (2020), 104815.
[30] Le Noir, M., Plieva, F., Hey, T., Guieysse, B., Mattiasson, B., Macroporous molecularly imprinted polymer/cryogel composite systems for the removal of endocrine disrupting trace contaminants, J. Chromatogr. A, 1154 (2007), 158-164.
[31] Yi Chen Lu, Jia Hao Mao, Wen Zhang, Cheng Wang, Min Cao, Xiao Dong Wang, Kai Yin Wang, Xiao Hui Xiong, A novel strategy for selective removal and rapid collection of triclosan from aquatic environment using magnetic molecularly imprinted nano-polymers, Chemosphere, 238 (2020), 124640.
[32] A.B. Jasso-Salcedo, A.G. Palestino Escobedo, V.A. Escobar Barrios, Effect of Ag, pH, and time on the preparation of Ag-functionalized zinc oxide nanoagglomerates as photocatalysts, J. Catal. 318 (2014) 170-178.
[33] A.R. Khataee, M. Fathinia, S. Aber, Kinetic Modeling of Liquid Phase Photocatalysis on Supported TiO2 Nanoparticles in a Rectangular Flat-Plate Photoreactor, Ind. Eng. Chem. Res. 49 (2010) 12358-12364.
[34] Mahsa Pirhashemi, Aziz Habibi-Yangjeh, Shima Rahim Pouran, Review on the criteria anticipated for the fabrication of highly efficient ZnO-based visible-light-driven photocatalysts, Journal of Industrial and Engineering Chemistry, 62 (2018), 1-25.

[35] Yi Shen, Qile Fang, Baoliang Chen, Environmental Applications of Three-Dimensional Graphene-Based Macrostructures: Adsorption, Transformation, and Detection, Environmental Sciences Technology, 49 (2015), 67-84.
[36] Yi Shen, Qile Fang, Baoliang Chen, Three-dimensional graphene supported catalysts for organic dyes degradation, Environmental Science and Technology, 49 (2015), pp. 67-84.
[37] Changlong Wang, Didier Astruc, Recent developments of metallic nanoparticle-graphene nanocatalysts, Progress in Materials Science, 94 (2018), pp. 306-383.
[38] Nurhidayatullaili Muhd Julkapli, Samira Bagheri, Graphene supported heterogeneous catalysts: An overview, International Journal of Hydrogen Energy, 40 (2015), 948-979.
[39] Josep Albero, Hermenegildo Garcia, Doped graphenes in catalysis, Journal of Molecular Catalysis A: Chemical, 408 (2015), 296-309.
[40] Xiaojuan Bai, Li Wang, Yongfa Zhu, Visible Photocatalytic Activity Enhancement of ZnWO4 by Graphene Hybridization, ACS Catalysis, 2 (2012), 2769-2778.
[41] Tongguang Xu, Liwu Zhang, Hanyun Cheng, Yongfa Zhu, Significantly enhanced photocatalytic performance of ZnO via graphene hybridization and the mechanism study, Applied Catalysis B: Environmental, 101 (2011), 382–387.
[42] Xiaojuan Bai, Changpo Sun, Di Liu, Xiaohong Luo, DiLi Jun Wang, Nanxi Wang, Xiaojiao Chang, Ruilong Zong Yongfa Zhu, Photocatalytic degradation of deoxynivalenol using graphene/ZnO hybrids in aqueous suspension, Applied Catalysis B: Environmental, 204 (2017), 11-20.
[43] Stefano Lettieri, Valentina Gargiulo, Deborah Katia Pallotti, Giuseppe Vitiello, Pasqualino Maddalenad, Michela Alfè, Raffaele Marotta, Evidencing opposite charge-transfer processes at TiO2/graphene-related materials interface through a combined EPR, photoluminescence and photocatalysis assessment, Catalysis Today, 2018.
[44] Changlong Wang, Didier Astruc, Recent developments of metallic nanoparticle-graphene nanocatalysts, Progress in Materials Science, 94 (2018), 306–383.
[45] Nikolai Kislov, Jayeeta Lahiri, Himanshu Verma, D. Yogi Goswami, Elias Stefanakos, Matthias Batzill, Photocatalytic Degradation of Methyl Orange over Single Crystalline ZnO: Orientation Dependence of Photoactivity and Photostability of ZnO, Langmuir, 25 (2009), 3310-3315.
[46] Rosalin Beura, P. Thangadurai, “Structural, optical and photocatalytic properties of graphene-ZnO nanocomposites for varied compositions”, Journal of Physics and Chemistry of Solids, 102, 2017, pp. 168-177.

[47] Minh Tan Man, Ji-Hee Kim, Mun Seok Jeong, Anh-Thu Thi Do, Hong Seok Lee, “Oriented ZnO nanostructures and their application in photocatalysis”, Journal of Luminescence, 185, 2017, pp. 17-22.
[48] Kenji Matsumoto, Noriko Saito, Toshitsugu Mitate, Junichi Hojo, Miki Inada, Hajime Haneda, Surface Polarity Determination of ZnO Spherical Particles Synthesized via Solvothermal Route”, American Chemical Society-Crystal Growth and Design Communication, 9, 2009, pp. 5014-5016.
[49] Yan Chen, Hua Zhao, Bin Liu, Heqing Yang, Charge separation between wurtzite ZnO polar {001} surfaces andtheir enhanced photocatalytic activity, Applied Catalysis B: Environmental, 163 (2015), 189-197.
[50] Zhaoke Zheng, Baibiao Huang, Zeyan Wang, Meng Guo, Xiaoyan Qin, Xiaoyang Zhang, Peng Wang, Ying Dai, Crystal Faces of Cu2O and Their Stabilities in Photocatalytic Reactions, Journal of Physics and Chemistry C, 113 (2009), 14448-14453.
[51] Fangyuan Chen, Weijia An, Li Liu, Yinghua Liang, Wenquan Cui, Highly efficient removal of bisphenol A by a three-dimensionalgraphene hydrogel-AgBr-rGO exhibiting adsorption/photocatalysissynergy, Applied Catalysis B: Environmental, 217 (2017), 65-80.
[52] VD Mote, Y Purushotham, BN Dole, Williamson-Hall analysis in estimation of lattice strain in nanometer-sized ZnO particles, Journal of Theoretical and Applied Physics, 5 (2012), 1-8.
[53] Rosalin Beura, P. Thangadurai, Structural, optical and photocatalytic properties of graphene-ZnO nanocomposites for varied compositions, Journal of Physics and Chemistry of Solids, 102 (2017), 168-177.
[54] Xiaojuan Bai, Li Wang, Ruilong Zong, Yanhui Lv, Yiqing Sun, Yongfa Zhu, Performance Enhancement of ZnO Photocatalyst via Synergic Effect of Surface Oxygen Defect and Graphene Hybridization, Langmuir, 29 (2013), 3097-3105.
[55] Wenyan Zhang, Songlin Yang, Jian Li, Wei Gao, Yibing Deng, Wenping Dong, Chengjian Zhao, Gongxuan Lu, Visible-to-ultraviolet Upconvertion: Energy transfer, material matrix, and synthesis strategies, Applied Catalysis B: Environmental, 206 (2017), 89-103.
[56] Quanjun Xiang, Bei Cheng, and Jiaguo Yu, Graphene-Based Photocatalysts for Solar-Fuel Generation, Angewandte Chemie International Edition, 54 (2015), 11350-11366.

[57] Williams Graeme, Seger Brian, V. Kamat Prashant, TiO2-Graphene Nanocomposites, UV-Assisted Photocatalytic Reduction of Graphene Oxide, ACSnano, 2 (2008), 1487-149.
[58] He Kai, Chen Guiqiu, Zeng Guangming, Chen Anwei,, Huang Zhenzhen, Shi Jiangbo, Huang Tiantian, Peng Min, Hu Liang, Three-dimensional graphene supported catalysts for organic dyes, Applied Catalysis B: Environmental, 228 (2018), 19–28.
[59] Javier Santiago-Morales, María José Gómez, Sonia Herrera-López, Amadeo R. Fernández-Alba, Eloy García-Calvo, Roberto Rosal, Energy efficiency for the removal of non-polar pollutants during ultraviolet irradiation, visible light photocatalysis and ozonation of a wastewater effluent, Water Research, 47 (2013), 5546-5556.
[60] Fei Xu, Jinfan Chen, Sergii Kalytchuk, Ling Chu, Yiru Shao, Dexin Kong, Kung-Hui Chu, Patrick H.-L. Sit, Wey Yang Teoh, Supported gold clusters as effective and reusable photocatalysts for the abatement of endocrine-disrupting chemicals under visible light, Journal of Catalysis, 354 (2017), 1-12.
[61] Yunrong Dai, Lifeng Yin, Synthesis and photocatalytic activity of Ag–Ti–Si ternary modified α-Bi2O3 nanoporous spheres, Materials Letters, 142 (2015), 225-228.
[62] Junfeng Niu, Yunrong Dai, Lifeng Yin, Jianying Shang, John C. Crittenden, Photocatalytic reduction of triclosan on Au–Cu2O nanowire arrays as plasmonic photocatalysts under visible light irradiation, Phys. Chem., 17 (2015), 17421-17428.
[63] Lin Zhao, Jinghui Deng, Peizhe Sun, Jiashu Liu, Yi Ji, Norihide Nakada, Zhi Qiao, Hiroaki Tanaka, Yongkui Yang, Nanomaterials for treating emerging contaminants in water by adsorption and photocatalysis: Systematic review and bibliometric analysis, Science of the Total Environment, 627 (2018), 1253-1263.
[64] Xiaojuan Bai, Li Wang, Yongfa Zhu, Visible Photocatalytic Activity Enhancement of ZnWO4 by Graphene Hybridization, ACS Catalysis, 2 (2012), 2769-2778.
[65] Tongguang Xu, Liwu Zhang, Hanyun Cheng, Yongfa Zhu, Significantly enhanced photocatalytic performance of ZnO via graphene hybridization and the mechanism study, Applied Catalysis B: Environmental, 101 (2011), 382-387.
[66] H.Y. Hao, Y.Y. Xu, P. Liu, G.Y. Zhang, BiOCl nanostructures with different morphologies: Tunable synthesis and visible-light-driven photocatalytic properties, Chinese Chem. Lett., 26 (2015), 133–136.
[67] X. Bai, L. Wang, Y. Zhu, Visible Photocatalytic Activity Enhancement of ZnWO4 by Graphene Hybridization, ACS Catal., 2 (2012), 2769-2778.

[68] B. Xiaojuan, S. Changpo, L. Di, L. Xiaohong, W. Jun, W. Nanxi, C. Xiaojiao, Z. Ruilong, Z. Yongfa, Photocatalytic degradation of deoxynivalenol using graphene/ZnO hybrids in aqueous suspension, App. Catal. B: Environ., 204 (2017), 11–20.
[69] K. Ryong, M. Parvez, K. Chhowalla, UV-reduction of graphene oxide and its application as an interfacial layer to reduce the back-transport reactions in dye-sensitized solar cells, Chem. Phys. Lett., 483 (2009), 124–127.
[70] L. Guardia, S. Villar-Rodil, J.I. Paredes, R. Rozada, A. Martínez-Alonso, J.M.D. Tascón, UV light exposure of aqueous graphene oxide suspensions to promote their direct reduction, formation of graphene–metal nanoparticle hybrids and dye degradation, Carbon, 50 (2012), 1014–1024.
[71] J. Tianhao, H. Yongyong, S. Mei, M. Nan, The mechanism of the reaction of graphite oxide to reduced graphene oxide under ultraviolet irradiation, Carbon 54 (2013) 412–418. [72] L. Tian, P. Likun, L. Xinjuan, L. Ting, Z. Guang, S. Zhuo, Enhanced photocatalytic degradation of methylene blue by ZnO-reduced graphene oxide composite synthesized via microwave-assisted reaction, J. Alloys Compd., 509 (2011), 10086-10091.
[73] L. Benxia, L. Tongxuan, W. Yanfen, W. Zhoufeng, ZnO/graphene-oxide nanocomposite with remarkably enhanced visible-light-driven photocatalytic performance, J. Colloid Interface Sci., 377 (2012), 114-121.
[74] F. Hongbo, X. Tongguang, Z. Shengbao, Z. Yongfa, Photocorrosion Inhibition and Enhancement of Photocatalytic Activity for ZnO via Hybridization with C60, Environ. Sci. Technol., 42 (2008), 8064-8069.
[75] X. Tongguang, Z. Liwu, C. Hanyun, Z. Yongfa, Significantly enhanced photocatalytic performance of ZnO via graphene hybridization and the mechanism study, App. Catal. B: Environ., 101 (2011), 382-387.
[76] G. Williams, B. Seger, K. Prashant, TiO2-Graphene Nanocomposites. UV-Assisted Photocatalytic Reduction of Graphene Oxide, ACS Nano., 2, 7 (2008), 1487-1491.
[77] H. Kai, C. Guiqiu, Z. Guangming, C. Anwei, H. Zhenzhen, S. Jiangbo, H. Tiantian, P. Min, H. Liang, Three-dimensional graphene supported catalysts for organic dyes, App. Catal. B: Environ., 228 (2018), 19–28.
[78] J. Santiago-Morales, M.J. Gómez, S. Herrera-López, A.R. Fernández-Alba, E. García-Calvo, R. Rosal, Energy efficiency for the removal of non-polar pollutants during ultraviolet irradiation, visible light photocatalysis and ozonation of a wastewater effluent, Water Res., 47 (2013), 5546-5556.

[79] X. Fei, C. Jinfan, S. Kalytchuk, C. Ling, S. Yiru, K. Dexin, C. Kung-Hui, H.L. Sit Patrick, T. Yang, Supported gold clusters as effective and reusable photocatalysts for the abatement of endocrine-disrupting chemicals under visible light, J. Catal., 354 (2017), 1-12.
[80] D. Yunrong, Y. Lifeng, Synthesis and photocatalytic activity of Ag–Ti–Si ternary modified α-Bi2O3 nanoporous spheres, Mater. Lett., 142 (2015), 225-228.
[81] J. Niu, Y. Dai, L. Yin, J. Shang, J.C. Crittenden, Photocatalytic reduction of triclosan on Au–Cu2O nanowire arrays as plasmonic photocatalysts under visible light irradiation, Phys. Chem., 17 (2015), 17421-17428.
[82] L. Zhao, J. Deng, P. Sun, J. Liu, Y. Ji, N. Nakada, Z. Qiao, H. Tanaka, Y. Yang, Nanomaterials for treating emerging contaminants in water by adsorption and photocatalysis: Systematic review and bibliometric analysis, Sci. Total Environ., 627 (2018) 1253-1263.
[83] L.W. Zhang, H.B. Fu, Y.F. Zhu, Efficient TiO2 Photocatalysts from Surface Hybridization of TiO2 Particles with Graphite-like Carbon, Adv. Funct. Mater, 18 (2008), 2180-2189.
[84] Y. Zhang, Z. R. Tong, X. Fu, Y. J. Xu, TiO2 Graphene Nanocomposites for Gas Phase Photocatalytic Degradation of Volatile Aromatic Pollutant: Is TiO2 Graphene Truly Different from Other TiO2 Carbon Composite Materials?, ACS Nano 4, 12 (2010), 7303-7314.
[85] S. Singh, H. Mahalingam, P.K. Singh, Polymer-supported titanium dioxide photocatalysts for environmental remediation: a review, Appl. Catal. A Gen., 462-463 (2013), 178–195.
[86] K. Tennakone, C.T.K. Tilakaratne, I.R.M. Kottegoda, Photocatalytic degradation of organic contaminants in water with TiO2 supported on polythene films, J. Photochem. Photobiol. A Chem., 87 (1995), 177–179.
[87] S. Naskar, S.A. Pillay, M. Chanda, Photocatalytic degradation of organic dyes in aqueous solution with TiO2 nanoparticles immobilized on foamed polyethylene sheet, J. Photochem. Photobiol. A Chem. 113 (1998), 257–264.
[88] S. Cho, W. Choi, Solid-phase photocatalytic degradation of PVC/TiO2 polymer composites, J. Photochem. Photobiol. A Chem., 143 (2001), 221–228.
[89] P. Lei, F. Wang, X. Gao, Y. Ding, S. Zhang, J. Zhao, S. Liu, M. Yang, Immobilization of TiO2 nanoparticles in polymeric substrates by chemical bonding formulti-cycle photodegradation of organic pollutants, J. Hazard. Mater., 227-228(2012), 185–194.

[90] Y. Jumi, S. Ji, O. Aeri, J. Dong-Hwee, B. Tae-Sung, L. Young-Seak, K. Hyungil, pH-sensitive photocatalytic activities of TiO2/poly(vinyl alcohol)/poly(acrylic acid) composite hydrogels, Mater. Sci. Eng. B., 176 (2011), 276–281.
[91] B. Rajaeian, A. Heitz, M.O. Tade, S. Liu, Improved separation and antifouling performance of PVA thin film nanocomposite membranes incorporated with carboxylated TiO2 nanoparticles, J. Memb. Sci., 485 (2015), 48–59.
[92] A.M. Shehap, D.S. Akil, Structural and optical properties of TiO2 nanoparticles/PVA for different composites thin films, Int. J. Nanoelectron. Mater., 9 (2016), 17–36.
[93] L. Xiuyun, C. Qirong, L. Lizhen, F. Xiaoying, M. Xiangfu, Preparation of transparent PVA/TiO2 nanocomposite films with enhanced visible-light photocatalytic activity, Catal. Commun., 58 (2015), 30–33.
[94] J. Sonyeo, Y. Jumi, L. Young-Seak, K. Hyungil, Preparation of poly(vinylalcohol)/poly(acrylic acid)/TiO2/carbon nanotube composite nanofibers and their photobleaching properties, J. Ind. Eng. Chem., 18 (2012), 487–491.
[95] U. Habiba, S. Islam, T.A. Siddique, A.M. Afifi, B. Chin, Adsorption and photocatalytic degradation of anionic dyes on Chitosan/PVA/Na-Titanate/TiO2 composites synthesized by solution casting method, Carbohydr. Polym., 149(2016), 317–331.
[96] E.S.A. Abd El-Rehim, Photocatalytic degradation of metanil yellow dye using TiO2 immobilized into polyvinyl alcohol/acrylic acid microgels prepared byionizing radiation, React. Funct. Polym., 72 (2012), 823–831.
[97] Reddy, N., & Yang, Y. Q., Citric acid cross-linking of starch films. Food Chemistry, 118 (2010), 702–711.

7 Appendices

7.1 Appendix A: Band Gap results of nano-ZnO/Graphene photocatalists synthesized by MI method.

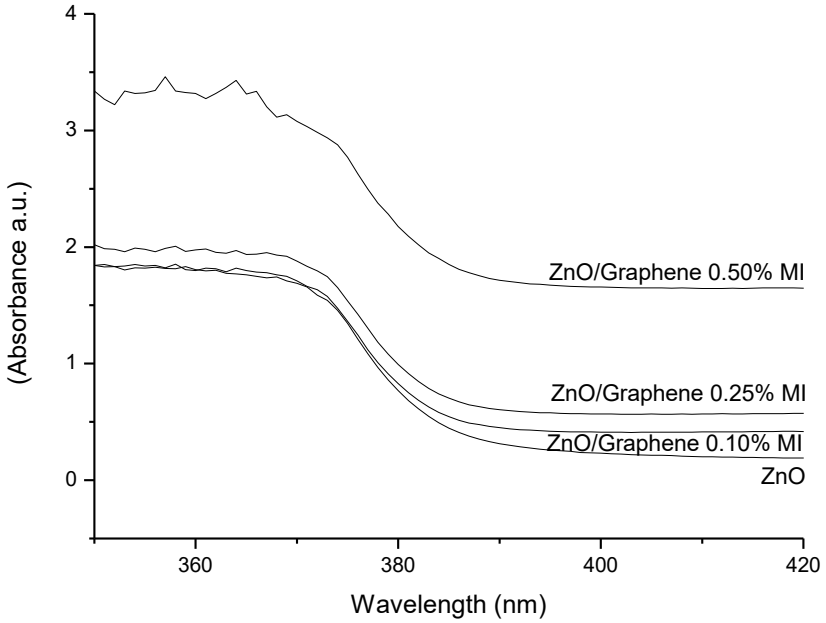

Photocatalyst	Band Gap (eV)
ZnO	3.21
ZnO/Graphene 0.10%	3.21
ZnO/Graphene 0.25%	3.20
ZnO/Graphene 0.50%	3.20

7.2 Appendix B: Adsorption isotherms.

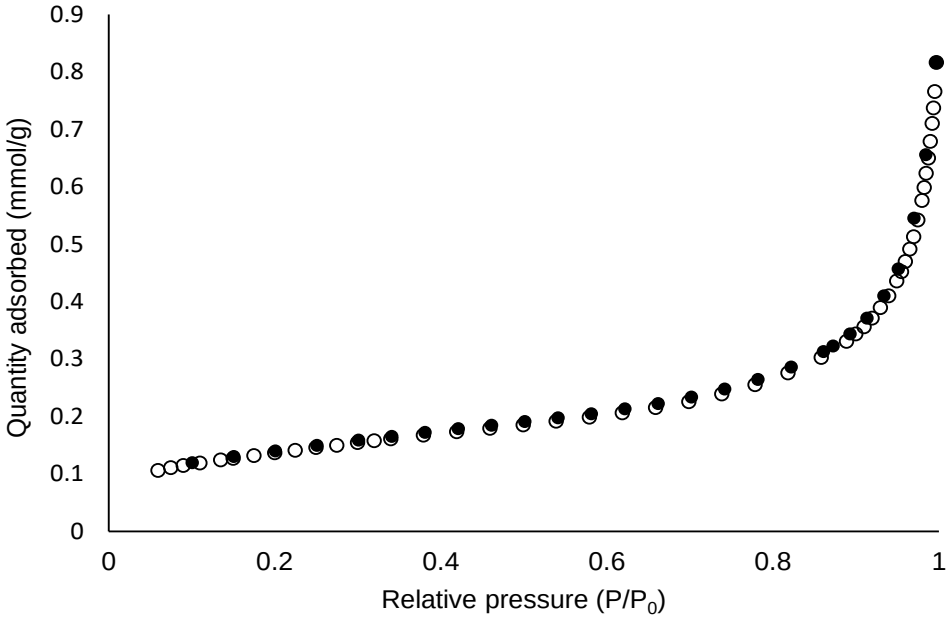

Physisorption isotherm for pristine nano-ZnO.

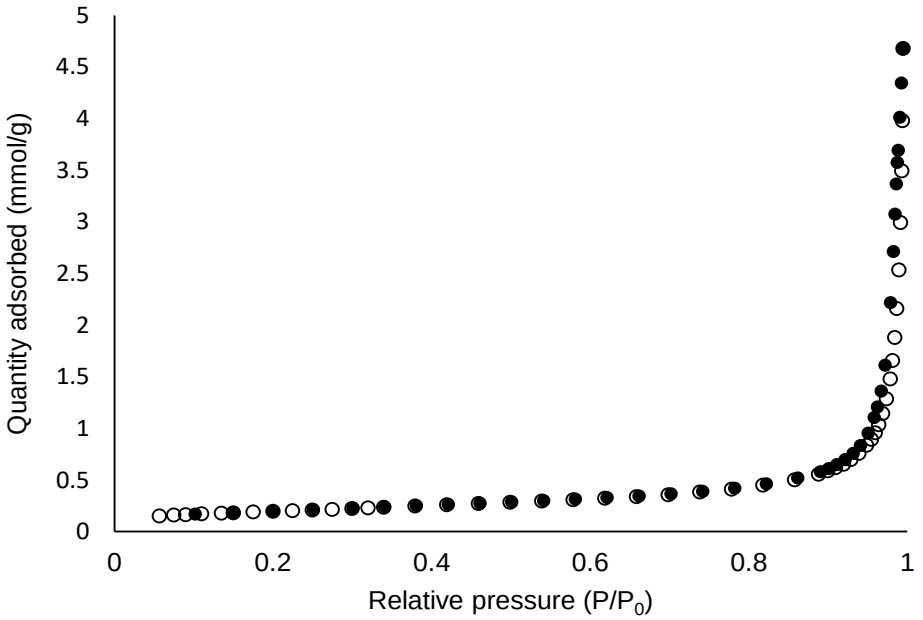

Physisorption isotherm for nano-ZnO/GO 0.1 % w/w.

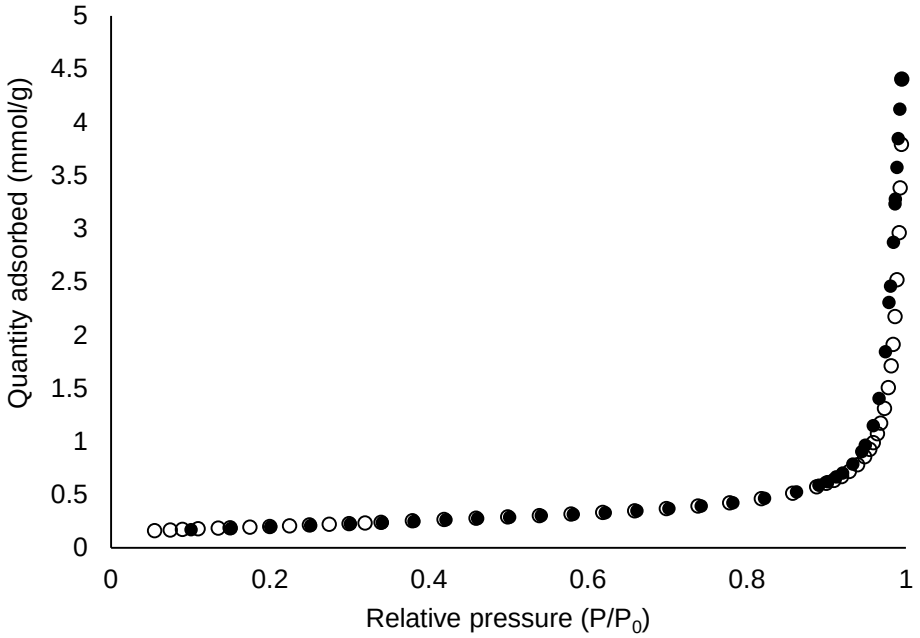

Physisorption isotherm for nano-ZnO/GO 0.25 % w/w.

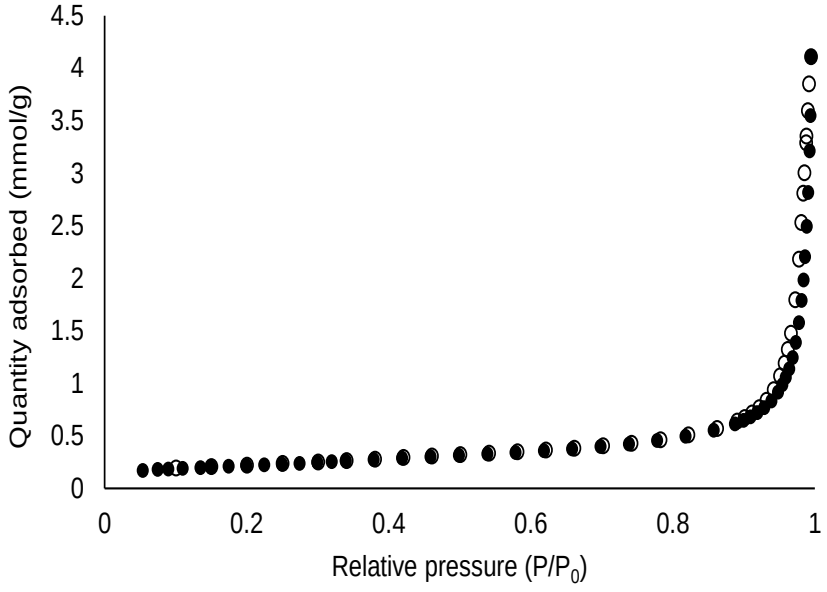

Physisorption isotherm for nano-ZnO/GO 0.5 % w/w.

8 Publications

Publication I

Nancy Cervantes Rincón, Samia Ben Hammouda, Mika Sillanpää, Vladimir Escobar Barrios.

Enhanced photocatalytic performance of zinc oxide nanoestructures via photoirradiation hybridization with graphene oxide for the degradation of triclosan under visible light: Synthesis, characterization and mechanistic study

Reprinted with permission from
Journal of Environmental Chemical Engineering
Vol. 6 (5), pp. 6554-6567, 2018

Journal of Environmental Chemical Engineering 6 (2018) 6554–6567

Contents lists available at ScienceDirect

Journal of Environmental Chemical Engineering

journal homepage: www.elsevier.com/locate/jece

Enhanced photocatalytic performance of zinc oxide nanostructures via photoirradiation hybridisation with graphene oxide for the degradation of triclosan under visible light: Synthesis, characterisation and mechanistic study

Nancy Cervantes Rincón[a,b], Samia Ben Hammouda[b], Mika Sillanpää[b], Vladimir Escobar Barrios[a,*]

[a] Instituto Potosino de Investigacion Cientifica y Tecnologica, Lomas 4a. Seccion, C.P. 78216, San Luis Potosí, S.L.P., Mexico
[b] Laboratotory of Green Chemistry, School of Engineering Science, Lappeenranta University of Technology, Sammonkatu 12, Fi-50130, Mikkeli, Finland

ARTICLE INFO

Keywords:
Nano-ZnO/GO photocatalysts
Triclosan
UV light
Visible light
Photocatalysis

ABSTRACT

Modification of ZnO nanoparticles with graphene oxide (GO) was carried out, and the obtained hybrid photocatalyst was used for the photodegradation of triclosan (TCS), which is an endocrine disrupting compound. Three different concentrations of GO were used to modify ZnO catalyst using the photoirradiation method and the resultant materials were characterised by SEM, TEM, Zeta Potential, FTIR, Raman, N_2 Physisorption, HPLC, XRD and UV–vis spectrophotometry in order to determine their physico-chemical and photocatalytic properties. Regarding the photocatalytic evaluation, the results of the photodegradation process for TCS showed that GO acts as a trap of electrons improving the performance of ZnO even at low TCS concentration (8 mg.L^{-1}) under visible light radiation. The GO-modified composite that contains the highest GO concentration (0.5% w/w) was the material that showed the best photocatalytic performance under visible light degrading up to 45% of the initial concentration of TCS and showed a reaction rate constant two times higher than pristine zinc oxide. This study allowed us to propose the photocatalytic mechanism of ZnO/GO hybrid photocatalysts to degrade TCS. In addition, this research contributes to the understanding of the enhancement of the efficiency of ZnO/GO hybrids and contributes to obtaining a photoactive material with promising use under natural light radiation in an Advance Oxidation Process to eliminate endocrine-disrupting compounds such as triclosan.

1. Introduction

In recent years, a growing problem with water treatment has arisen due to the presence of endocrine disrupting compounds (EDC), which persist in surface, waste, and drinking water. The term endocrine disrupting compounds defines a diverse and heterogeneous group of chemicals that can alter hormonal balance [1], which means that they interfere in the normal functions of the hormonal processes of living beings. Such chemical compounds can mimic hormones, due to their similar chemical structure, but they do not act as hormones and are responsible for the homeostasis, reproduction, and developmental process in living beings [2,3]. The ways to exposure with EDCs occurs through drinking contaminated water, breathing contaminated air, ingesting food, or coming into contact with contaminated soil.

A significant example of EDC is triclosan (TCS), a bactericidal widely used in deodorant formulations, toothpastes, soaps, powders, cosmetics, textiles, plastics, polymers, fibres, and medical implant devices. Then, given the use of these products, triclosan has been directly discharged into wastewater, although it has also been detected in surface water, sludge, sediment, and drinking water, and several studies have reported its presence in waters and wastewaters in the US and Europe at a very low concentration in the range of ng.L^{-1}. Moreover, it has been stated that when irradiated by UV light, triclosan (in its anionic form) is involved in an efficient ring closure. It leads to the formation of highly toxic compounds like chlorodioxins [4].

The treatment of water, by conventional methods, removes in some cases up to 90% of EDC. However, with such residual concentrations of triclosan it is necessary to develop methods to remove even trace concentrations of these pollutants.

Advanced Oxidation Processes (AOPs) is one of the most effective method due to the high oxidising power of free radicals generated during such processes, like hydroxyl radical (˙OH), which is able to mineralise compounds that cannot be oxidised by oxidising agents such as oxygen, ozone, and chlorine [4].

* Corresponding author.
E-mail address: vladimir.escobar@ipicyt.edu.mx (V. Escobar Barrios).

https://doi.org/10.1016/j.jece.2018.09.064
Received 26 June 2018; Received in revised form 27 September 2018; Accepted 29 September 2018
Available online 05 October 2018
2213-3437/

Among the methodologies to generate hydroxyl free radicals, we can find the heterogeneous photocatalysis, which is usually carried out under ultraviolet radiation in order to activate the semiconductor and thereby to trigger reduction and oxidation reactions that are responsible for degrading and mineralising organic compounds, such as triclosan.

Generally, the semiconductors used for this purpose are cheap, non-toxic, and can be regenerated without losing their photocatalytic activity [5,6]. Examples of the most used semiconductors in heterogeneous photocatalysis for organic compounds are titanium dioxide, zinc oxide, tellurium cadmium, and zinc selenide, although the titanium dioxide is the material that has gained much attention and we can find extensive literature regarding this compound.

However, in the case of TiO_2, its oxidative degradation, by the effect of a high recombination of electrons, limits its use at industrial scale. On the other hand, ZnO has attracted much attention in the degradation of various pollutants due to its high photosensitivity. The ZnO has wide band gap (3.37 eV), large excitation binding energy (60 MeV) and low threshold power for optical pumping and is thus considered a low cost alternative photocatalyst to TiO_2 for the degradation of organic compounds in aqueous solution [7,8].

In addition, ZnO absorbs a greater fraction of the radiation spectrum for the photocatalytic process and, therefore, it has been used in the manufacture of solar panels and for opto-electronic applications. This characteristic of ZnO to absorb a larger fraction of the radiation spectrum and its chemical resistance opens the possibility to use this material in water treatment to degrade EDC, such as triclosan.

The photodegradation of triclosan, until complete mineralisation, has been studied in hybrid systems, especially binary ones, such as TiO_2/UV [9]. Despite the advantages of ZnO and its promising application in photocatalytic degradation using sunlight, there are questions to be answered regarding the degradation of EDC, such as triclosan, because the main problem that affects the photocatalytic efficiency of semiconductors as ZnO is the recombination of excited electrons, which decreases the formation of hydroxyl free radicals and, hence, there is a decrement of the efficiency of pollutant degradation. Thus, some strategies have been focused to reduce the recombination of excited electrons, such as the modification of ZnO nanoparticles with metal, thereby forming hetero-structure. The obtained results by other researchers show the relevance of modifying the ZnO with gold [10], silver [11] and platinum [12] nanoparticles for the photodegradation of different organic pollutants as dyes [13,14], considering that they are good electron conductors, property that imparts to the ZnO a delayed recombination of excited electrons.

However, metals are not the only materials that exhibit good electrical properties to retard the electron recombination process occurring in photocatalysts. Recently, graphene oxide (GO) has been used for the development of new materials by its incorporation in polymeric matrices, due to its chemical surface properties (functional groups), which promote the interactions between GO and polymer [15].

Furthermore, the graphene oxide may exceed the electron transport property, a key characteristic of metals, depending on the amount of functional groups present on its surface [16]. Studies show excellent chemical properties of GO to form compounds with other materials due to its surface chemistry as well as having the ability to be reduced to graphene using ultraviolet radiation [17]. Thus, it is possible to obtain compounds of ZnO/GO or ZnO/Graphene with high thermal and electrical conductivity (higher than the pure semiconductor or metal), which delay the recombination process. These important chemical and electrical characteristics do impart to this material certain attractiveness for potential applications such as photocatalysis.

In this study, we focused on the evaluation of the effect of graphene oxide content on the photocatalytic activity of ZnO/GO hybrid materials for the photodegradation of triclosan in solution by UV and visible light. Furthermore, we describe the mechanism of action during the degradation of TCS.

Table 1
Synthesised ZnO/GO photocatalysts.

Sample	GO Concentration (% w/w)
ZnO/GO 0.10%	0.10
ZnO/GO 0.25%	0.25
ZnO/GO 0.50%	0.50

2. Materials and methods

2.1. Materials

Zinc oxide was obtained from Degussa (Germany) under name VP AdNano ZnO 20, the graphene oxide HC (5 g/L) was purchased from Supermarket Company. Triclosan (≥97%), pure ethanol, 5.5´-dimethyl-1-pirrolidone-*N*-oxide (DMPO) and 2-propanol (≥99% purity) were purchased from Sigma-Aldrich. Deionised water used in the work was purified and its conductivity was 17.5 siemens m^{-1}. All of the materials purchased were used as received, without any further purification.

2.2. Methods

2.2.1. Preparation of ZnO/GO samples

ZnO/GO hybrid catalysts were prepared following the photo-irradiation (FI) method previously reported [18]. The ZnO solutions (1% w/w) were prepared using isopropanol. Then, graphene oxide was added with different concentrations regarding the ZnO weight (Table 1) in order to evaluate the effect of graphene oxide in the overall photocatalytic process to degrade triclosan. The resulting ZnO/GO solutions were sonicated for one hour and after that they were exposed to UV radiation (205 nm) and mixed continuously by magnetic stirring for 2 hours. Finally, the obtained materials were recovered by centrifugation (3200 rpm for 10 minutes) and oven dried at 50 °C for 12 hours, and then stored for use.

2.2.2. Photodegradation of triclosan

The treatment of TCS was conducted by batch-type experiments. The reactor system consisted in a top open glass reactor of 150 mL capacity. The lamps for irradiation (UV or visible) were put on top of the reactor at 8 cm distance. All the mixtures were stirred for mechanical mixing. Typically, the required amount of catalyst (1 g/L) was added firstly to 100 mL of the TCS solution with an initial concentration of 8 mgL^{-1} and subsequently exposed to the light illumination source over a period of 3 hours, UV light (254 nm with intensity of 858 $mW.cm^{-2}$) or visible radiation (150 W halogen lamp with light intensity of 308 $mW.cm^{-2}$). Samples of 1 mL were withdrawn from the reactor at set intervals and filtered immediately through a 0.22 μm filter film.

The adsorption tests by the investigated photocatalysts were conducted in dark conditions; such tests were carried out before photocatalysis and it was established that adsorption takes place during the first one hour of contact between triclosan solution and photocatalyst. Thus, all the experiments began with adsorption process during one hour in dark conditions just before the photocatalytic process started.

In addition, cycling experiments were carried out to verify the photocatalyst stability. For this purpose, after each run, the catalyst was recovered, washed and reused in the subsequent run. The recovered catalysts were collected and dried to evaluate the weight loss.

As it has been by other researchers [19] the photocatalytic process using heterogeneous catalyst can be described using the Langmuir-Hinshelwood model, which was simplified to the pseudo-first order as shown in Eq. (1), was adapted to describe the photocatalytic kinetic behaviours of triclosan through the as-prepared materials.

$$ln\frac{C}{C_0} = -k_{app}t \quad (1)$$

where C ($mg.L^{-1}$) is the triclosan concentration at a given period of time t during photodegradation, Co ($mg.L^{-1}$) is the triclosan concentration at the adsorption equilibrium, t (min) is the degradation time, and k_{app} (min^{-1}) is the apparent reaction rate constant.

2.3. Characterisation techniques

2.3.1. Scanning Electron Microscopy (SEM)

Scanning Electron Microscopy (SEM) was used to characterise the morphology and chemical composition of the ZnO/GO nanocomposites. In order to carry out the analysis, carbon membrane grids were used and over which the samples were directly deposited. A microscope FEI-FIB Dual Beam Helios Nanolab 600 was used for this purpose.

2.3.2. Transmission Electron Microscopy (TEM)

Transmission Electron Microscopy (TEM) was used to determine the structure and morphology of the hybrid ZnO/GO compounds. For this study, a TEM Tecnai (300 keV) type FEG model (FEI Company) microscope was used with a resolution of 1.8 Å point to point in HRTEM and 3 Å in contrast Z, while the resolution of EDS analysis in the bright field is 20 nm and 1 nm in contrast Z. The samples were supported on copper grids with carbon membrane.

2.3.3. Fourier transform infrared spectroscopy (FTIR)

The equipment model Nicolet iS10 (Thermo Scientific) was used for this characterisation with measurements in the wavenumber range from 400 to 4000 cm^{-1}. All the analysed samples were powdered and analysed using the ATR mode.

2.3.4. Raman spectroscopy

Raman spectroscopy was used to provide an overview of the potential interaction between the pristine ZnO and GO materials in the investigated composite (ZnO/GO). The equipment InVia Microraman-Renishaw was used for this purpose using a green laser (532 nm wavelength).

2.3.5. Zeta potential

This analysis was carried out using a Zetasizer Nanoseries (Malvern) in order to obtain the surface zeta potential and the average size of the synthesised samples. Solutions of H_2SO_4 (0.1 M) and NaOH (0.1 M) were used for this analysis.

2.3.6. X-ray diffraction (XRD)

In order to determine the crystal structure of the synthesised hybrid materials and the pure ZnO and GO, the X-ray diffractmeter D8 Advance model (Bruker) was used. The conditions were at 2θ angular interval from 10 to 90 using a step size of 0.02°.

2.3.7. UV–vis spectroscopy

This technique was used to determine the band gap based on absorption spectra of the ZnO and ZnO/GO photocatalysts. The equipment Cary 5000 UV–vis-NIR with high resolution (< 0.047 nm) was used in wavelength range of 190–3300 nm.

2.3.8. Nitrogen physisorption

For this analysis, a Micromeritics TriStar II Plus analyser was used to obtain the pore dimension and surface area of the ZnO/GO hybrid catalysts and the pristine materials, ZnO and GO. All the studied materials were pre-degassed in vacuum at 120 °C for 5 h. The specific surface area was determined using the classical BET model.

2.3.9. High performance liquid chromatography (HPLC)

The concentration of triclosan was quantified by a Shimadzu liquid chromatography equipped with UV detector. The column used was a Kinete x 5 µm EVO C18 100 Å, LC Column 150 × 4.6 mm (Phenomenex). A mobile phase consisting of 70% acetonitrile and 30% water was pumped with flow of 1 mL min^{-1}. The detector SPD-20AV UV wavelength was set at 254 nm. The sample was injected through auto sampler and the injection volume was 50 µL.

2.3.10. Electro spin resonance (ESR)

The Electro Spin Resonance (ESR) signals for radicals spin-trapped were examined using an ADANI CMS Model 8400 spectrometer, using as spin-trap reagent the 5,5´-dimethyl-1-pirrolidone-*N*-oxide (DMPO). In order to minimise experimental errors, the same type of quartz capillary tube was used for all the ESR measurements. The magnetic parameters of the radicals detected were obtained from direct measurements of magnetic field and microwave frequency.

3. Results and discussion

The results are presented and discussed according to the characterisation carried out and correlated with the photocatalytic performance of the synthesised photocatalyst.

3.1. Photocatalysts characterisation

3.1.1. Electron microscopy

Fig. 1 shows SEM images of pristine zinc and graphene oxide along with the corresponding size distribution of ZnO particles obtained by zeta potential.

Fig. 1-a shows different morphologies of the ZnO particles, including prisms, spheroids and tetrapods, mainly. Moreover, different particle sizes were determined, which ranged from 30 to 120 nm as it was confirmed by zeta potential (Fig. 1-b). In addition, small agglomerates of ZnO particles with sizes up to 500 nm were observed.

Fig. 1c and d show the images obtained by SEM for the graphene oxide sheets, with a semi-transparent continuous surface that has slight folds on it, probably as a consequence of sheet stacking.

Based on these size observations, it is suggested that obtained ZnO/GO hybrid photocatalysts are GO covered by ZnO nanoparticles and/or their agglomerates.

The following image (Fig. 2-a) corresponds to ZnO/GO hybrid photocatalyst prepared by the photoirradiation method loaded with 0.25% w/w of graphene oxide.

Fig. 2-a reveals the decoration on the surface of graphene oxide sheets with zinc oxide nanoparticles, which are homogeneously distributed. Zinc oxide particles exhibited the same shapes as those observed in the pure material (Fig. 1-a). It must be pointed out that complete distribution of zinc oxide nanoparticles enabled the reduction of their agglomeration and enabled a good wrapped morphology of graphene sheets by ZnO particles.

The homogeneous distribution of ZnO nanoparticles on the surface of GO is probably ascribed to the photoirradiation method, since the energy used during the synthesis of hybrid photocatalysts would induce a polarity effect to ZnO, as it has been reported by Nikolai Kislov et al. in 2009 and other authors [20–22]. Thus, the polarization favours the homogeneous distribution of ZnO nanoparticles to decorate graphene oxide sheets and promotes the contact and interaction between both materials rather well, characteristically playing an important role in a photocatalytic process. The particle size of ZnO/GO hybrids synthesised in this work was between 1 and 2 µm independently of GO concentrations (0.1% w/w, 0.25% w/w or 0.5% w/w). This result was confirmed with size distribution obtained by zeta potential (Fig. 2-b).

Fig. 3 shows TEM images of pristine graphene oxide and the ZnO/GO hybrid photocatalyst. The observed topology, in Fig. 3-a, of the GO surface is irregular and also has a clear laminate-like aggregation.

Furthermore, the approximate number of graphene layers in the analysed samples was determined, which was around 6-stacked

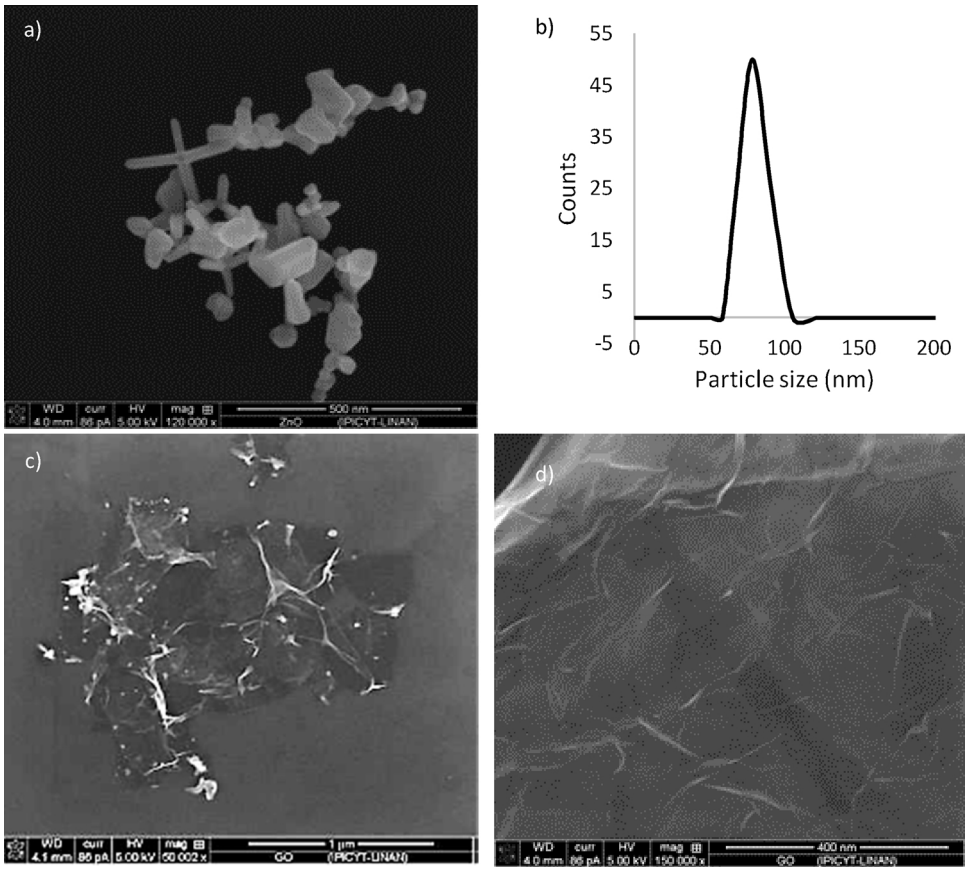

Fig. 1. SEM images of a) pristine zinc oxide (120,000 x), b) size distribution of pure ZnO particles obtained by zeta potential, c) pure graphene oxide (50,000 x) and d) zoom of surface (150000 x).
Based on these size observations, it is suggested that obtained ZnO/GO hybrid photocatalysts are GO covered by ZnO nanoparticles and/or their agglomerates.

graphene layers as shown in Fig. 3-b.

Fig. 3-c and d display the sample TEM images of the final ZnO/GO hybrid photocatalyst compound loading with the highest concentration of graphene oxide (0.5% w/w). These images confirm the dimensions of these compounds, as determined by SEM (between 1 μm and 2 μm), in addition to the information related with zinc oxide nanoparticles distribution on the graphene oxide sheets. It was corroborated the effect of photoirradiation method in the homogenous distribution of ZnO nanoparticles on graphene oxide material.

It is noteworthy that the dimensions of pure GO are higher than those present in the hybrid ZnO/GO compounds, due to the ultrasonication that was carried out during the synthesis of ZnO/GO hybrids, which reduces the GO particle size.

3.1.2. Physisorption

The specific area of ZnO, graphene oxide and ZnO/GO hybrid photocatalysts was determined via N_2 adsorption isotherms using the Brunauer Emmett Teller (BET) method.

Table 2 summarises the BET results of the surface area, pore diameter and pore volume for pristine ZnO and graphene oxide and their corresponding composites. The values of average pore diameter and pore volume were determined using the Barrett-Joyner-Halenda (BJH) method.

The results revealed that the graphene oxide showed the highest

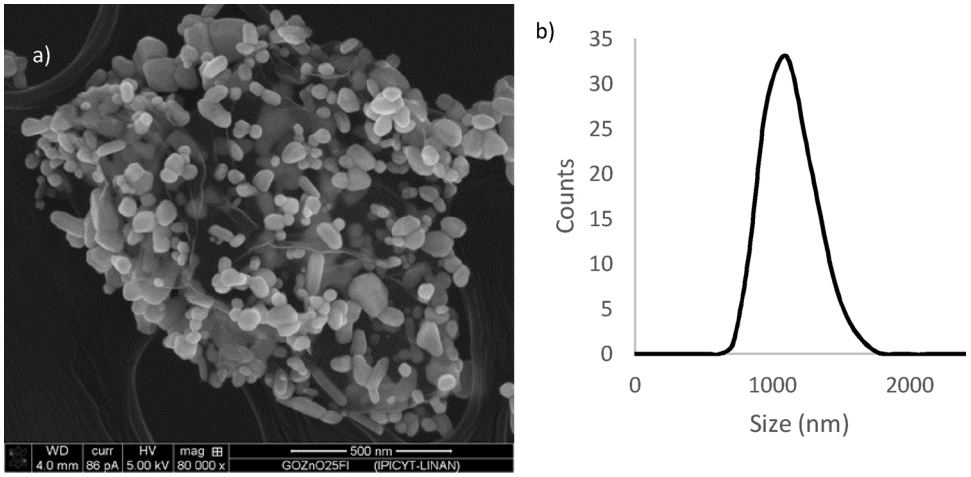

Fig. 2. a) SEM images of Zn/GO hybrid material (0.25% w/w) synthesised by photoirradiation method. Magnification 80,000 × . b) Size distribution of ZnO/GO particles.

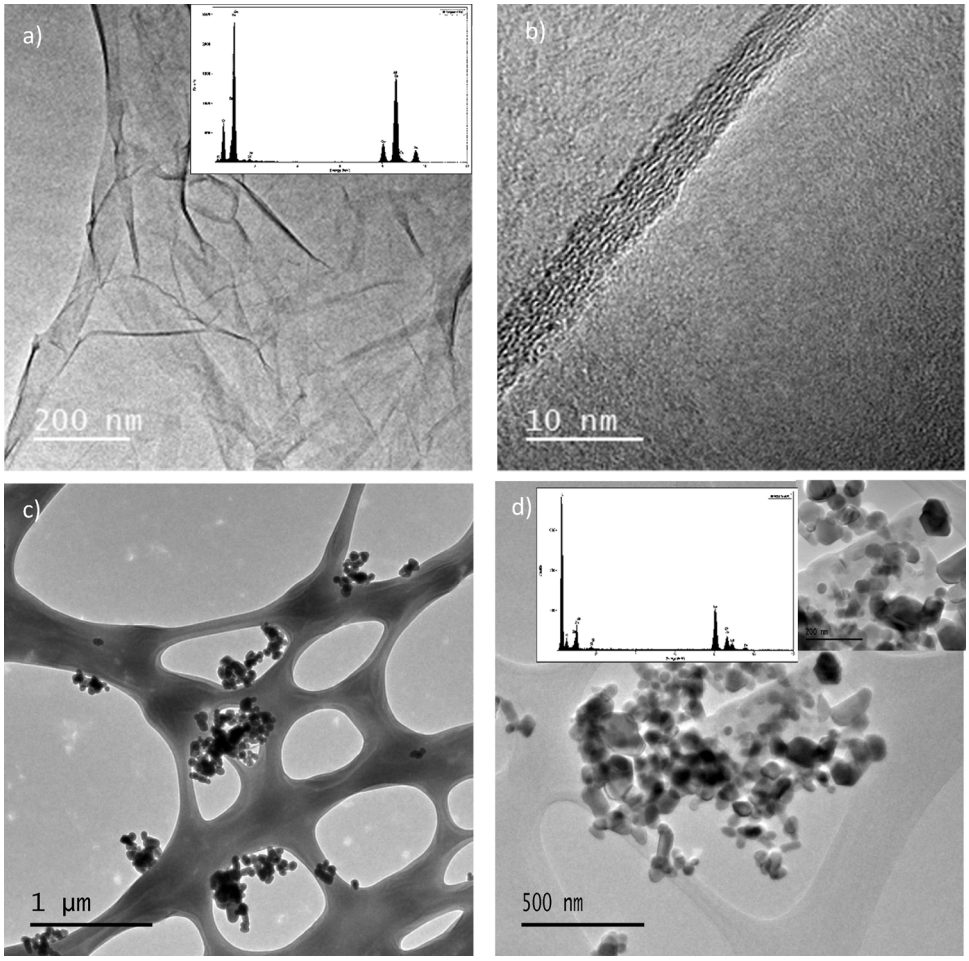

Fig. 3. TEM images of a) pristine graphene oxide and b) graphene layers in GO sample c) Zn/GO photocatalysts (0.5% w/w) synthesised by the photoirradiation method with indicated scale and d) zoom of ZnO/GO photocatalyst with indicated scale (insert scale of 290 nm).

Table 2
Surface area, pore diameter and pore volume of pristine ZnO and GO materials and ZnO/GO hybrid compounds.

Sample	BET Area (m^2/g)	Pore Diameter (Å)	Pore Volume (cm^3/g)
ZnO	10.8	183.4	0.024
GO	46.81	682.8	0.012
ZnO/GO 0.1% w/w-FI	13.3	398.6	0.060
ZnO/GO 0.25% w/w-FI	15.8	306.5	0.073
ZnO/GO 0.5% w/w-FI	17.0	219.9	0.089

surface area for pristine materials, as it can be seen in Table 2. Among the three investigated composites, the photocatalyst loaded with 0.5% w/w of GO had the highest surface area, followed by ZnO/GO 0.25% and ZnO/GO 0.1% catalysts as it was expected. Thus, the addition of GO increases the surface area of hybrid ZnO/GO catalysts up to 57% of the initial area of zinc oxide as a consequence of good dispersion of such nanoparticles, indicating that graphene oxide is an excellent surface hybrid material to support ZnO particles. The increase in surface area is one of the most important properties of a photocatalyst to improve its efficiency.

The pore diameter values for the hybrid catalysts with values between those of base materials, ZnO (183.4 Å) and GO (682.8 Å), increasing up to 2.17 times compared with ZnO when adding a small amount of GO (0.1% w/w) and then as the GO content increases the pore diameter is reduced, and might be ascribed to the obstruction of ZnO nanoparticles surface when they interact with GO. In accordance with the last results, the pore volume varies and depends on the quantity of GO being the highest value for ZnO/GO 0.5%, then ZnO/GO 0.25% and finally ZnO/GO 0.1%, all of them present higher values than the pristine materials ZnO and GO. Such dimensions are indicative of the interaction between the ZnO and graphene oxide.

Figs. 4–7 show the isotherms for pristine ZnO, ZnO/GO 0.1%; ZnO/GO 0.25% and ZnO/GO 0.5%, respectively.

As it can be seen from Figs. 4–7 Isotherms type II with H3-type hysteresis loop were obtained for all the samples, which correspond to a

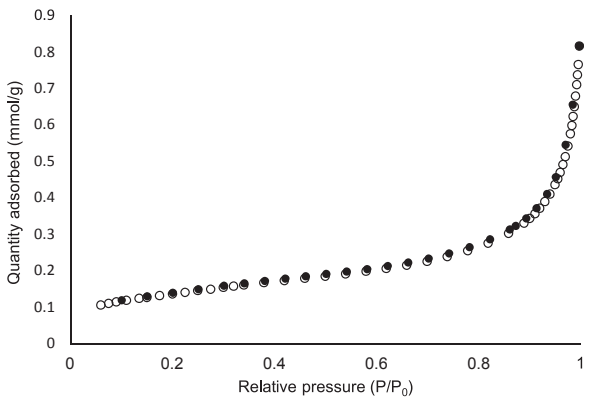

Fig. 4. Physisorption isotherm for pristine ZnO.

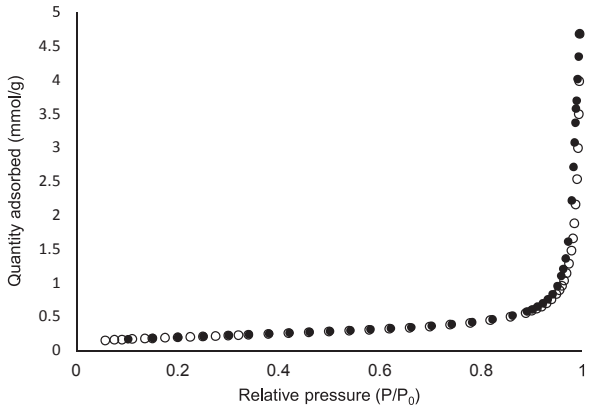

Fig. 5. Physisorption isotherm for ZnO/GO 0.1%.

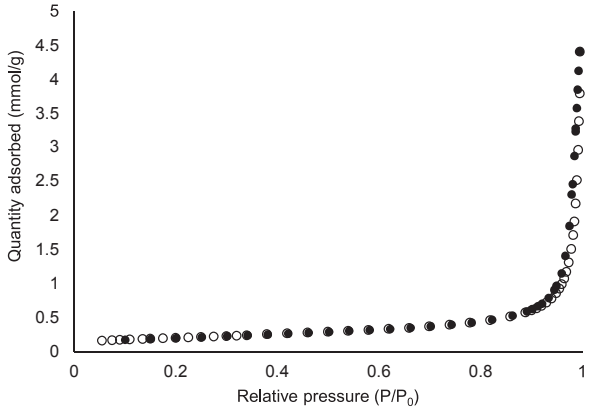

Fig. 6. Physisorption isotherm for ZnO/GO 0.25%.

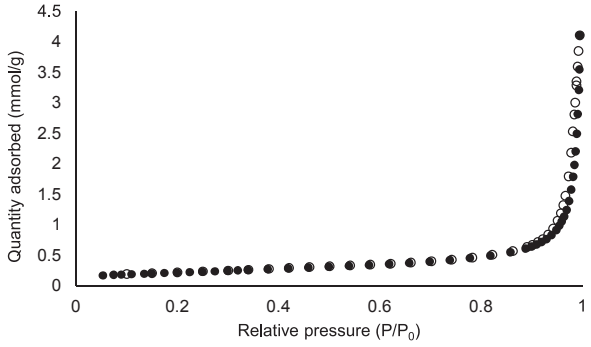

Fig. 7. Physisorption isotherm for ZnO/GO 0.5%.

microstructure containing macropores or micrometric cavities in the case of ZnO/GO samples.

3.1.3. X-ray diffraction

The X-ray diffraction characterisation was used to confirm the presence of graphene oxide in the ZnO/GO hybrid photocatalysts and also to verify the possible reduction of graphene oxide during the synthesis of ZnO/GO composites under high energy (UV radiation) as previously has been reported [23–25]. Fig. 8 shows the XRD patterns of pristine materials; ZnO and graphene oxide, and ZnO/GO composites synthesised in this work.

In Fig. 8, it is concluded that there are no changes in the geometry observed in the diffraction directions, which are related to the size and shape of the crystal unit cell of the characterised samples, which provides information on the crystalline system studied. The ZnO pattern is identified by the characteristic peaks of the crystalline phases of hexagonal wurtzite type structure, corresponding to (100), (002), (101), (102) and (103) planes [18]. The results of the peak intensities for each analysed sample are reported in Table 3.

As can be observed from Table 3 and Fig. 8, there are slight intensity changes between the patterns of the ZnO/GO hybrid photocatalysts and ZnO, in the region between 70 and 85 degrees suggesting a different position of the atoms on the surface of the crystal lattice of the ZnO due to the interactions between this compound with graphene oxide.

Regarding the diffraction pattern of GO, based on bibliographic information referring to characteristic diffraction peaks of three crystal planes of this material, the first one corresponds to the plane 001 at 13°, the second located at 32°, which corresponds to the plane 002 and the third located at 45° for the plane 100 [26,27].

The samples ZnO and ZnO/GO hybrid composites exhibit the typical XRD diffraction related to wurtzite structure. However, no characteristic peak of graphene oxide is observed for either ZnO/GO hybrid photocatalyst in the corresponding region, which may arise by the low content of GO in ZnO/GO hybrids.

Furthermore, the diffraction peaks of the hybrid composites are mostly unchanged compared to that of pure ZnO, which indicates that the lattice constants of ZnO have unchanged because of surface hybridisation of the carbonaceous material [28].

3.1.4. Fourier transform infrared

The FTIR spectra of pristine ZnO and GO, and ZnO/GO hybrid material (0.5% w/w) are shown in Fig. 9.

Fig. 9 shows the typical fingerprint groups of graphene oxide, including the hydroxyl, carboxyl and alkoxy species. The band located around 3400 cm^{-1} corresponds to the stretching vibrations of the −OH group.

The band around 1711 cm^{-1} corresponds to the C═O bond of carbonyls while the band located approximately at 1612 cm^{-1} is attributed to the vibration of the C═C bond and, finally, the characteristic vibration band associated with alkoxy C−O stretches bond is located around 1031 cm^{-1}.

The band located around 699 cm^{-1} corresponding to the Zn−O bond, is preserved in the spectrum of ZnO/GO composite. It is also noted that vibrations corresponding to the epoxy, carbonyl and carboxyl bonds of the GO drastically decrease or disappear; this is due to two possibilities a) low concentration of GO in ZnO/GO samples or b) indicating the reduction of GO during the synthesis of these materials.

In particular, it should be noticed that a specific adsorption band appearing at 1386 cm^{-1} that has been observed only in the ZnO/GO hybrid photocatalyst. This peak could be ascribed to the vibration of the C−O bonds formed between GO and ZnO, such a hybridisation interaction between ZnO and GO with a π-conjugative 2D system that could reduce the activation of surface oxygen atoms of ZnO, by which the photocorrosion of zinc oxide could be significantly inhibited. This phenomenon has been described in a previous research about C60-ZnO composites photocatalysts [29]. Moreover, there is a shift in the C═O band located at 1711 cm^{-1} that implies the hybridisation of ZnO/GO photocatalysts [30].

3.1.5. Raman spectroscopy

The Raman spectra of zinc oxide, graphene oxide and ZnO/GO photocatalyst are shown in Fig. 10, from which it can be seen that the pristine zinc oxide shows an intense peak at 438 cm^{-1} corresponding to E_2 crystal mode of wurtzite structure. The D and G bands of graphene oxide were identified at 1350 cm^{-1} and l593 cm^{-1}, respectively. The Raman-reactive G mode at 1593 cm^{-1} is attributed to all sp^2 carbon-type structures and provides information on the in-plane vibration of sp^2 bonded carbon atoms while D band suggests the presence of sp^3 defects in the hexagonal graphitic layers [31]. The G band has been identified within the ZnO/GO samples and is related with carbon-hybridised bonds in these composites. A slightly blue shift by 9 cm^{-1} in the D band of hybrid photocatalyst compared with D band of graphene

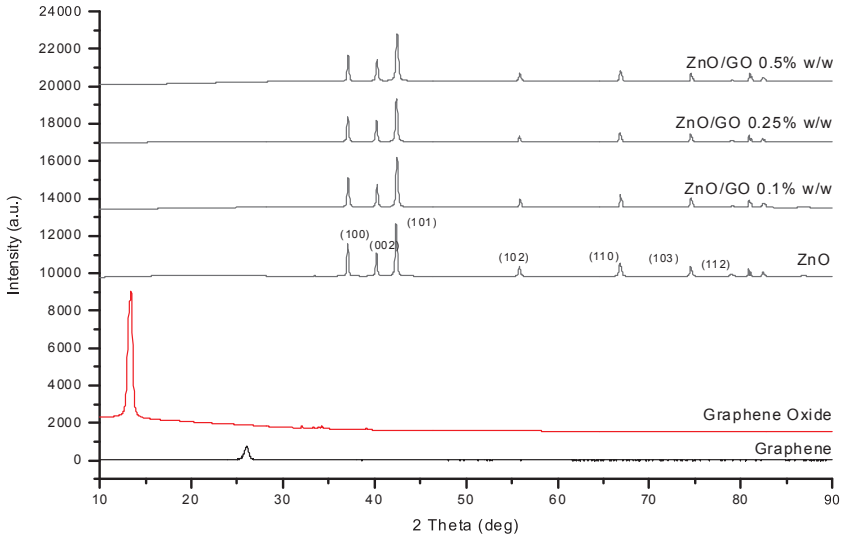

Fig. 8. XRD patterns of pristine ZnO and graphene oxide; and the as-prepared ZnO/GO hybrid photocatalysts loaded with 0.1% w/w, 0.25% w/w and 0.5% w/w.

Table 3
Data of peak intensities corresponding to the XRD patterns of pristine ZnO and graphene oxide and ZnO/GO composites synthesised by the photoirradiation method for two hours.

2θ (deg)	Intensity (a. u.)	2θ (deg)	Intensity (a. u.)	2θ (deg)	Intensity (a. u.)
Graphene		Graphene Oxide		ZnO	
26.01	792.6	13.46	7577.1	37.05	2219.9
43.82	26.8	32.06	403.12	40.18	1749.8
54.23	72.1	33.33	372.4	42.33	3318.1
77.70	37.8	34.22	359.2	55.79	986.8
83.32	49.4	39.06	280.4	66.77	1201.1
		45.98	188.5	74.49	1035.6
		53.91	171.1	78.95	571.9
		54.71	162.6	80.85	864.4
		55.75	153.6	82.37	718.3
				86.79	517.8
ZnO/GO 0.1% w/w		ZnO/GO 0.25% w/w		ZnO/GO 0.5% w/w	
37.10	2038.2	37.06	1825.1	37.10	1912.4
40.25	1684.6	40.19	1624.8	40.25	1690.6
42.42	3171.2	42.37	2757.2	42.44	3080.1
55.88	921.1	55.79	769.9	55.84	938.9
66.84	1148.8	66.77	975.3	66.82	1103.2
74.54	978.5	74.49	887.1	74.50	966.6
79.03	562.5	78.96	521.2	79.06	916.1
80.91	893.3	80.90	863.3	80.96	574.4
82.44	699.2	82.35	657.8	82.40	921.05
86.80	506.1			86.91	528.8

oxide and a red shift in the G band of 8 cm^{-1} was observed. These shifts in the Raman peak could be attributed to the chemical interaction between ZnO and graphene oxide as was suggested by FTIR.

In addition, the D/G intensities ratio is a measure of the defects in the structure of graphitic materials. Regarding the sp^3 and sp^2 hybridisations ID/IG value, in the case of pure graphene oxide is 0.93, indicating that the intensity of the G band is higher than D band which results in a lower amount of sp^3 defects and less structural disorder in this material.

Compared with graphene oxide (0.93), the reduction ID/IG intensity ratio for ZnO/GO 0.5% hybrid photocatalyst (ID/IG = 0.91) is observed, implying a reduction of sp^3 defects compared with pure graphene oxide. This fact confirms the interaction between ZnO and GO given by sp^3 defects. The results given herein above are consistent with the results in FTIR characterisation, revealing the reestablishment of the conjugated graphene oxide network.

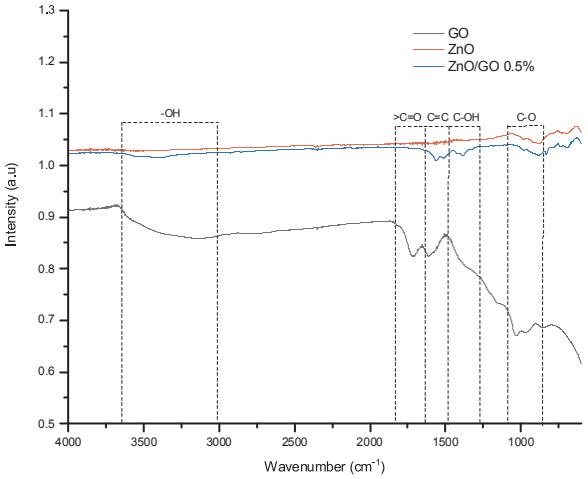

Fig. 9. IR spectra of pure ZnO, pure GO and ZnO/GO nanocomposite (0.5% w/w) synthesised by the photoirradiation method.

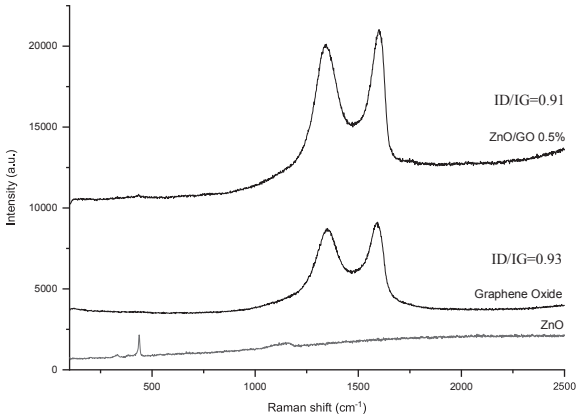

Fig. 10. Raman spectra of pure ZnO, pure graphene oxide and ZnO/GO hybrid composite loaded with 0.5% w/w of graphene oxide and synthesised by the photoirradiation method.

3.1.6. UV–vis spectroscopy

The absorption range of light plays an important role in photocatalysis. Fig. 11 shows the UV–vis diffuse reflectance spectroscopy of the samples. The Band gap values of the different synthesised

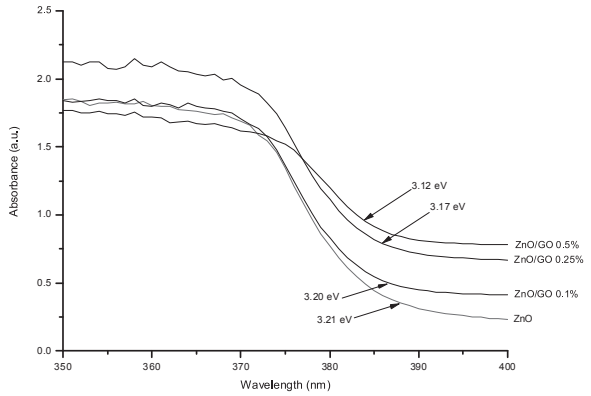

Fig. 11. UV–vis spectra of ZnO and ZnO/GO hybrids compounds with different content of GO 0.1% w/w, 0.25% w/w and 0.5% w/w.

Table 4
Band gap of pristine ZnO photocatalyst and ZnO/GO hybrid materials with a different content of GO (0.1%, 0.25% and ZnO/GO 0.5%) obtained by UV–vis spectrophotometry.

Photocatalyst	Band Gap (eV)	λ (nm)
ZnO	3.21	386
ZnO/GO 0.10%	3.20	387
ZnO/GO 0.25%	3.17	385
ZnO/GO 0.5%	3.12	384

Table 5
Initial concentration for the different photocatalyst samples.

Photocatalyst	Triclosan "initial concentration" for photocatalysis process, mgL^{-1}	Amount of Triclosan adsorbed by photocatalyst, before photocatalysis, mg
ZnO	5.6	0.24
ZnO/GO 0.10%	5.4	0.26
ZnO/GO 0.25%	5.2	0.28
ZnO/GO 0.5%	5.1	0.29

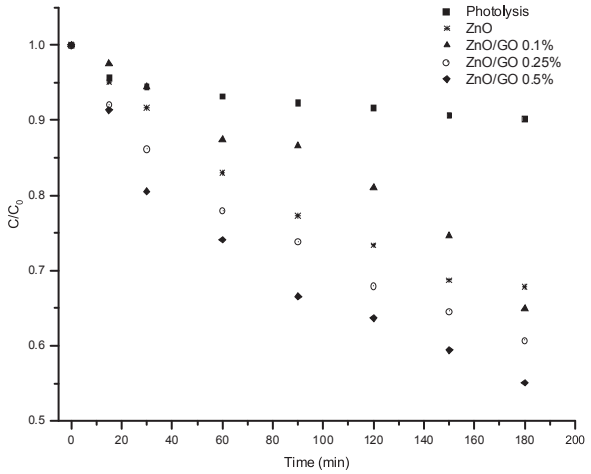

Fig. 12. TCS degradation curves under visible light radiation using pristine ZnO, ZnO/GO 0.1%, ZnO/GO 0.25%, ZnO/GO 0.5% synthesised by the photoirradiation method. Conditions: pH = 7, T = 23 °C.

photocatalysts were estimated using UV Spectroscopy based on the absorption spectra collected in a wavelength range from 200 to 800 nm. The information that provides the interaction between light and the surface of the samples analysed defines their photocatalytic performance. In Fig. 11, a peak in 360 nm corresponding to the absorbance of ZnO due to the optical transition of electrons from valence to conduction band can be observed. The band gap (Eg) values were estimated using the wavelength (nm) of the intersection between the slope of each curve and the Y-axis based on the following equation [18,32]

$$Eg = \frac{hc}{\lambda} \quad (2)$$

Based on this calculation, the Band Gap value for pristine ZnO was obtained, which is 3.21 eV and in the case of ZnO/GO compounds with 0.1%, 0.25% and 0.5% of GO the values obtained are 3.20 eV, 3.17 eV and 3.12 eV, respectively (Table 4)

A decrement of the band gap values of ZnO hybridised materials, regarding the pristine ZnO catalyst, has the following order ZnO > ZnO/GO 0.1% > ZnO/GO 0.25% > ZnO/GO 0.5% (Table 4).

The obtained Eg values imply an increase in light absorption intensity in the visible region due to the presence of GO, which possibly enhances the anti-photocorrosion of ZnO and increases the retention time of the electrons that are promoted from the valance band to the conductive band in ZnO semiconductor.

The stronger absorption intensity in the visible region for ZnO/GO hybrid photocatalysts is a key factor for higher photocatalytic activity even at low concentrations of GO. It can also be clearly observed that hybridised ZnO with graphene oxide showed an enhanced intensity of light absorption.

Therefore, it is possible to activate ZnO/GO hybrid photocatalysts under visible light resulting in an opportunity to use these materials under such radiation, a fact that could have an impact on reducing the operating costs in water treatment systems. Regarding the method, the photoirradiation process is an easy and simple alternative to synthesise effective ZnO/GO photoactive composites with a homogeneous distribution of ZnO particles.

3.1.7. Zeta potential

Finally, zinc oxide and graphene oxide were evaluated by zeta potential, before and after they were photoirradiated with UV light as they were irradiated for the synthesis of the ZnO/GO photocatalysts. This experiment was carried out in order to determine and elucidate about polarisation effect during a photoirradiation method as it has been reported [33]. It is important to mention that both samples, previously to be evaluated, were thoroughly distillate-water washed and there was no control on pH during evaluation. It is important to have in mind that zeta potential for ZnO and GO were evaluated in water solution, as they were photoirradiated using UV light, and just polarisation it was we are focused on.

The results of this experiment showed positive zeta potential values for ZnO particles, before and after being exposed to UV radiation. These values were 58.48 mV and 50.43 mV, respectively. This first result means a partial negative polarisation of the zinc oxide particles when they are exposed to UV radiation during two hours since there was a reduction of potentiometric value in comparison with the initial obtained value in the sample.

On the other hand, for the graphene oxide sample, an initial (before photoirradiation process) negative value of zeta potential (-40.61 mV) was obtained. Then, the GO sample was irradiated, and a positive value (36.35 mV) was determined.

With this result, it is inferred that the carbon material is chemically reduced when it is subjected to UV radiation, as it has been suggested by XRD and FTIR.

Based on these results, it is concluded that the photoirradiation method promotes the interaction between graphene and zinc oxide by a negative polarisation of ZnO nanoparticles as we suggested by TEM and SEM observations and, further, the electrical conductivity of these hybrid catalysts is improved by the chemical reduction of GO particles.

Both aspects improve the properties of ZnO/GO photocatalysts

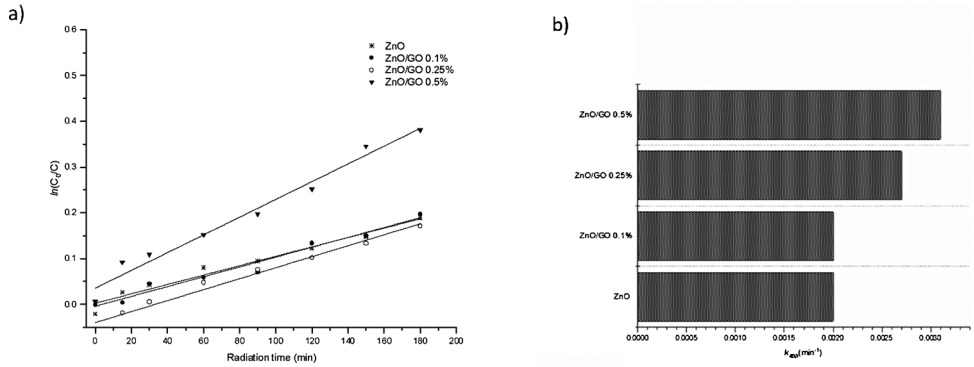

Fig. 13. a) The pseudo-first-order adjustment to experimental values and b) apparent rate constants (k_{app}) for triclosan degradation under visible light with as-prepared samples ZnO/GO loaded with 0.5%, 0.25% and 0.1% of graphene oxide and pristine ZnO.

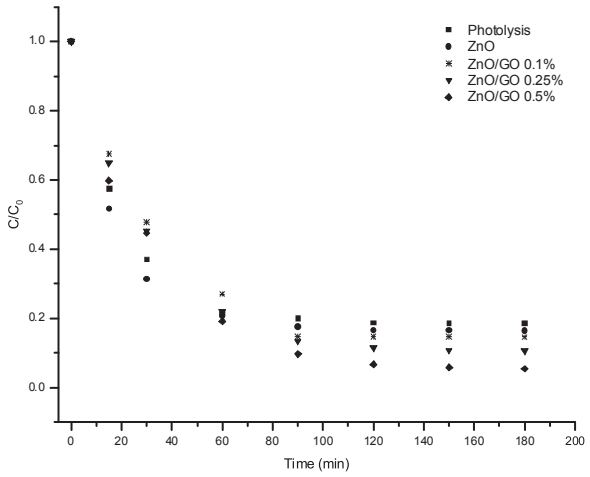

Fig. 14. TCS degradation curves under UV-radiation (254 nm) using pristine ZnO, ZnO/GO 0.1% w/w, ZnO/GO 0.25% w/w, ZnO/GO 0.5% w/w and in absence of catalyst (photolysis). Conditions: pH = 7, T = 23 °C.

synthesised by the photoirradiation method and their performance during the degradation of TCS.

3.2. Photocatalytic performance

In order to evaluate the photocatalytic performance of ZnO/GO photocatalysts, triclosan degradation experiments were conducted in batch systems, using visible light radiation (Halogen lamp, 150 W). The catalyst adsorption capacity for all the photocatalysts was determined previously in dark conditions, and it was determined that the adsorption phenomena for all the different materials takes place in one hour. Thus, after this time (1 hour), it is feasible to evaluate the TCS degradation to exclude the effect of adsorption in the photocatalytic performance of ZnO and ZnO/GO hybrid photocatalysts.

The considered "initial concentration of Triclosan" for the photocatalysis process, with the different photocatalysts, is reported in Table 5. Such "initial concentration" was obtained once the solution has been in dark during 1 h, in order to achieve the sorption equilibrium. In addition, before the sorption process takes place, the Triclosan concentration for all the solutions (with different photocatalyst type) was 8 mgL^{-1}, as it was mentioned in Section 2.2.2., previously.

The photocatalytic activities of the ZnO/GO hybrid materials with different loading amounts of graphene oxide, using the photodegradation of triclosan as a model reaction under visible light are shown in Fig. 12, including that for the photolysis process (degradation in the absence of catalyst) and for the pristine ZnO.

It is clearly noticed that all the ZnO/GO photocatalysts exhibit much higher photocatalytic activities than photolysis (which degraded just 1% of the initial concentration of TCS) and ZnO sample. The ZnO/GO 0.5% photocatalyst exhibits the maximum degradation of triclosan (45%), while the photocatalyst ZnO/GO 0.25% degraded up to 39% of the TCS. Finally, the photocatalyst synthesised with the lowest amount of GO (0.1% w/w) and the pristine ZnO catalyst exhibited degradation percentages of 35% and 32%, respectively. Thus, graphene oxide is beneficial for charge separation and increases the electrons lifetime promoted from the valance band to conductive band reducing the recombination process in ZnO catalyst. The optimal loading amount of graphene oxide in ZnO/GO hybrid photocatalysts, for the studied range, was 0.5% w/w. This percentage is much lower quantities than those that have been reported for synthesised graphene oxide composites

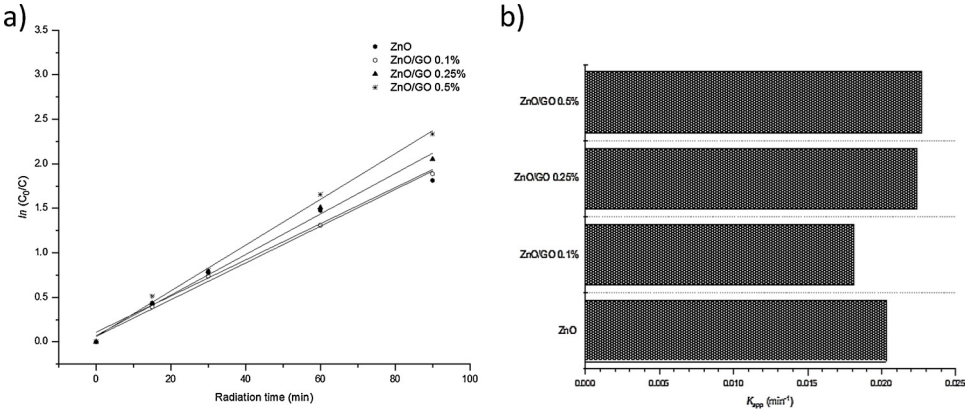

Fig. 15. a) The pseudo-first-order adjustment to experimental values and b) apparent rate constants (k_{app}) for triclosan degradation under UV light irradiation (254 nm) with as-prepared samples ZnO/GO loaded with 0.5%, 0.25% and 0.1% of graphene oxide and pristine ZnO.

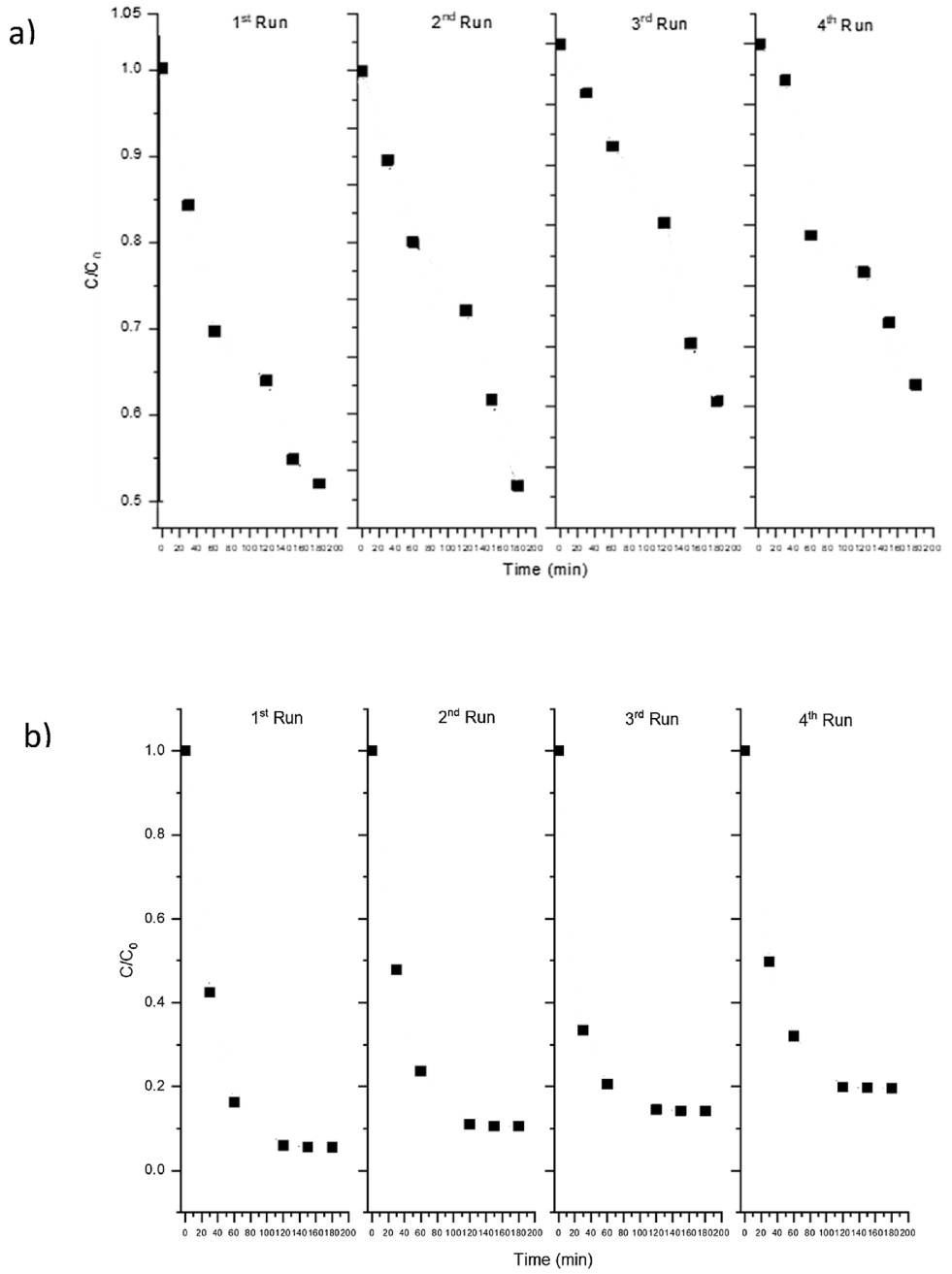

Fig. 16. Cycling experiment for the photocatalytic degradation of triclosan by the prepared ZnO/GO 0.5% composite under a) visible light and b) UV radiation.

(mainly by solvothermal synthesis), which reach up to 5% [33,34].

This result is an important approximation to achieve a good photocatalyst to be used under visible light synthesised by the photo-irradiation method, a promising, facile and friendly technique to synthesise active photocatalysts under visible and solar light radiation.

Regarding the degradation kinetics, the Fig. 13 shows the TCS photodegradation apparent rate constants k_{app} on ZnO/GO hybrid photocatalysts under visible light radiation. The degradation kinetic data were fitted using a pseudo-first-order equation. The introduction of graphene oxide into ZnO increased the rate constant. The photocatalytic activity follows the order ZnO/GO 0.5% > ZnO/GO 0.25% > ZnO/GO 0.1% > ZnO, while the sample ZnO/GO 0.5% shows the highest reaction rate constant of 0.0031 min^{-1} followed by ZnO/GO loaded with 0.25% w/w of graphene oxide (0.0027 min^{-1}). Less graphene oxide leads to a decrement of photocatalytic activity up to 0.0021 min^{-1}, corresponding to ZnO/GO 0.1% hybrid material. Pristine ZnO showed a rate reaction constant of 0.0020 min^{-1}.

The kinetic rate constants of ZnO/GO 0.5% and 0.25% were 55% and 27% higher than the rate constants exhibit by ZnO, respectively.

The ZnO/GO hybrid materials are able to improve the efficiency degradation of triclosan due to the presence of GO that confirms the role of graphene oxide as an electron tramp that retains the electrons promoted from the valance to conductive band in ZnO, which is a situation that improves the generation of a higher amount of radicals, species responsible for efficiently degrading organic molecules such as TCS.

This result contributes to the development of new active photocatalysts under visible light as has been investigated and reported in several studies that have demonstrated the possibility of the photodegradation of triclosan up to 47% using photocatalysts based on rare-earth elements such as Ceria (47%) [35], metals such as Au (10% after 5 h) [36], silver [37] and Cu [38]; and others, such as MgO, WO_3, TiO_2,

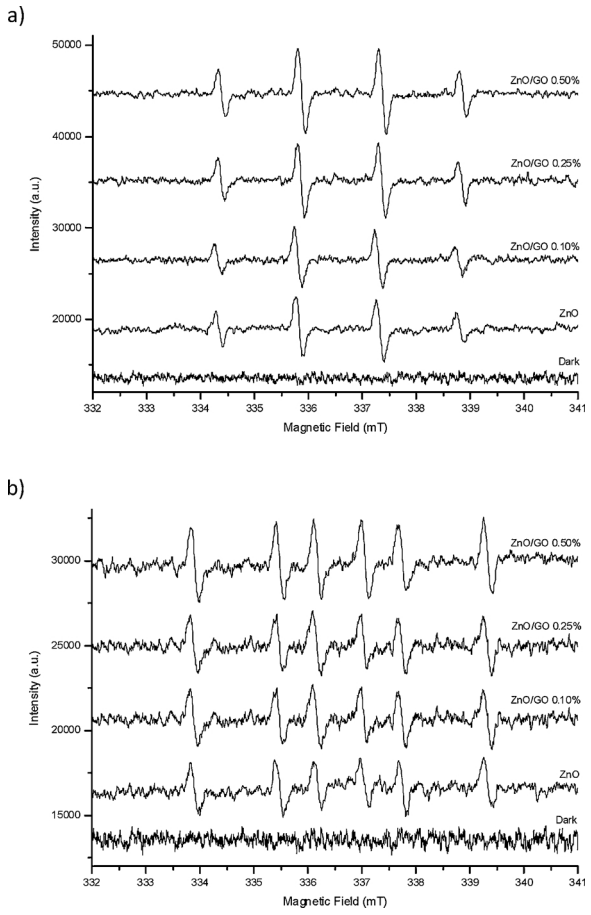

Fig. 17. ESR analysis in dark conditions and visible light radiation of pristine ZnO and ZnO/GO hybrid photocatalysts in a) water and b) ethanol. DMPO was used as the radical trapper.

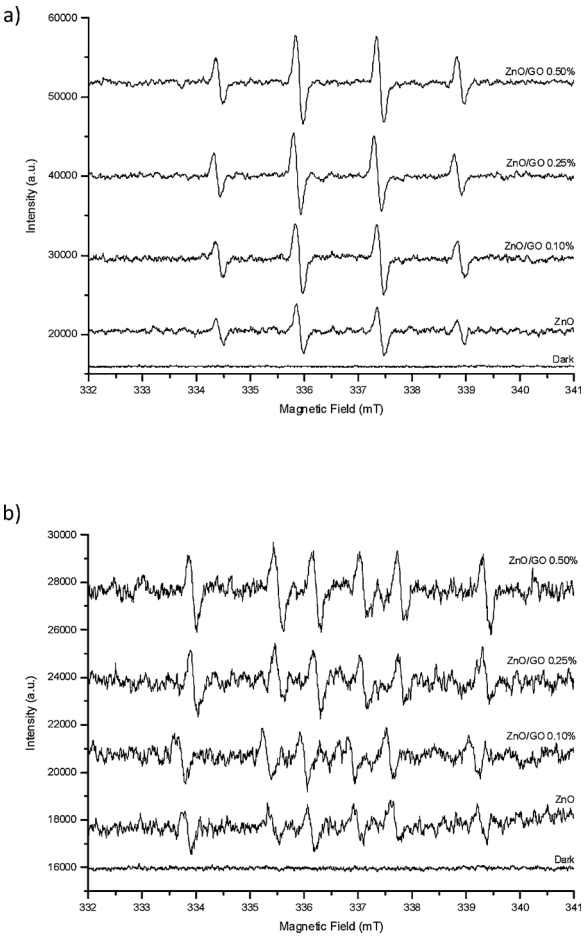

Fig. 18. ESR spectra in dark conditions and UV radiation of the pure ZnO and ZnO/GO hybrid photocatalysts in a) water and b) ethanol. DMPO was used as the radical trapper.

ZnO or GO [39].

In order to compare the photoactivity of the as-prepared ZnO/GO hybrid photocatalyst using higher irradiation, experiments were carried out under UV light (254 nm). Fig. 14 shows that ZnO/GO hybrids possess improved UV light photocatalytic activity versus the commercial ZnO and without the presence of catalyst (photolysis). The result illustrates that the ZnO/GO 0.5% hybrid photocatalyst exhibits the best performance, degrading 95% of the initial concentration of TCS, while ZnO/GO 0.25% gives 89% of degradation.

Finally, the ZnO based catalyst and ZnO/GO 0.1% degraded 83% and 85%, respectively, giving the lowest photocatalytic performance. The amounts of triclosan degraded by ZnO/GO photocatalysts are slightly better than the degradation of TCS via photolysis and ZnO.

It is important to mention that such values of removal of triclosan (up to 95%) are very convenient to improve the water quality and it is very important since the conventional water treatment methods are not high enough (< 95%) so that the residual triclosan is still enough to impact the environment and affect the health of living beings

The apparent rate constants for the degradation of triclosan under UV light were determined and the results are shown in Fig. 15, which reveals a linear relationship between ln (C_0/C) and reaction time over as-prepared samples according to the pseudo-first-order kinetics plot (Fig. 15-a).

The apparent reaction rate constant (k_{app}) values were enhanced through the introduction of graphene oxide in ZnO catalyst. The ZnO/GO 0.5% (0.0227 min^{-1}) exhibited the highest k_{app} value among all the samples.

This result suggests the improvement of the photodegradation efficiency of the ZnO semiconductor due to the presence of graphene oxide which acts as an electron trap enhancing the photodegradation performance of ZnO/GO photocatalysts except the hybrid material with the lowest amount of GO (0.1%) which showed a slightly decrease in the slop degradation kinetic behaviour.

These results are in accordance with those obtained under visible light radiation and demonstrate the enhancement of the photoactivity of ZnO due to the presence of graphene oxide.

On the other hand, the capacity of being reused is a very important feature for photocatalyst. In order to determine the photocatalytic reusability of ZnO/GO 0.5% sample using visible and UV light radiation, four degradation cycles were carried out. After each cycle, the photocatalyst was filtered and dried thoroughly, and then fresh TCS solution was added.

In Fig. 16, we can clearly see that during four cycles the photoactivity test for the degradation of TCS under visible radiation with the ZnO/GO 0.5% the efficiency is reduced up to 27% of the initial activity and under UV light, the same photocatalyst, displays a slight decrease and shows almost no deactivation.

This observation could be attributed to no degraded TCS that is adsorbed in the surface of ZnO/GO photocatalyst which reduce the efficiency of this semiconductor.

3.3. Mechanistic study

Surface area, phase structure, crystallinity and separation efficiency of photogenerated charges are crucial factors for photocatalytic activity [40]. Therefore, in the as-prepared ZnO/GO hybrid samples, the enhancement of their photocatalytic activity is attributed mainly to the

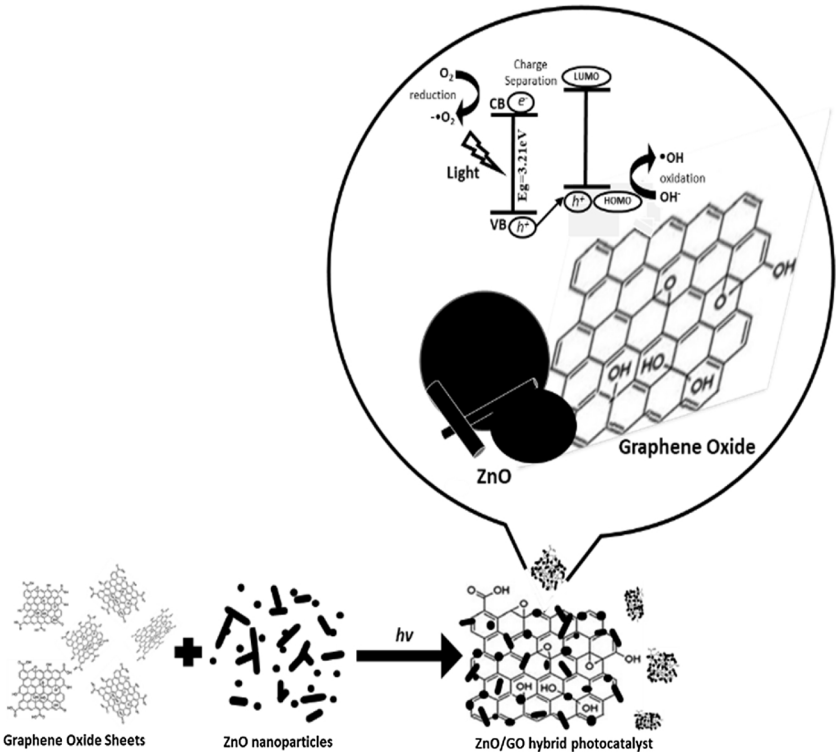

Scheme 1. Interaction of ZnO/GO hybrid photocatalyst during photocatalysis process.

effective separation of the photogenerated electron-hole pairs.

In order to confirm the mechanism further, the ESR technique and trapping experiments of radicals were performed. ESR results are shown in Figs. 17 and 18 under visible light and UV radiation, respectively. The hydroxyl radicals (DMPO-•OH) and superoxide radicals (DMPO-$O_2\bullet^-$) for ZnO and ZnO/GO hybrid photocatalysts in H_2O (four characteristic signals) and ethanol (six signals) using visible light are observed in Fig. 17.

In both cases, it is noticed that the signals for ZnO/GO hybrid materials are more pronounced than those for the ZnO pristine sample, thus accounting for the higher photocatalytic performance of ZnO/GO loaded with 0.5% w/w of graphene oxide than the bare ZnO photocatalyst towards the degradation of triclosan.

Thus, the enhanced photocatalytic activity of ZnO/GO, at any composition, but especially 0.5% compared with pure ZnO, is due to the introduction of graphene oxide, which promotes an increase in charge separation to effective utilisation of electrons to stabilize the $^{\cdot}OH$ and $O_2^{\cdot -}$ radicals. In this case, the signals of $^{\cdot}OH$ (Fig. 17-a) radicals are stronger than those for $O_2^{\cdot -}$ (Fig. 17-b), which suggest the predominance of oxidative reactions whose holes are responsible for the degradation of triclosan.

Furthermore, ZnO photocatalyst present visible light photocatalytic activity but generate better performance under visible light after graphene oxide hybridisation, showing that graphene oxide is responsible for the injection of an excited electron from the LUMO (Lowest Unoccupied Molecular Orbit) orbit of graphene to the CB (Conduction Band) of ZnO [36].

The introduction of the graphene oxide can possibly cause the rapid separation of electron-hole pairs during irradiation [41] prolonging the electron-hole pair lifetime and accelerating the transfer rate of electrons [42] as shown in Scheme 1.

The ESR spectra corresponding to the experiments performed in water and ethanol solvents using UV radiation are shown in Fig. 18. Fig. 18-a corresponds to the hydroxyl radicals generated by the analysed samples and Fig. 18-b shows the superoxide radicals. The same behaviour as observed under visible light radiation, higher signals of the hydroxyl radicals than superoxide radicals, occurred in the case of UV radiation.

It is known that ZnO absorbs light to produce photogenerated electron-hole pairs. Since the valance band (VB) position of ZnO is lower than the HOMO (Highest Occupied Molecular Orbital) orbit of graphene, the photogenerated holes on ZnO could transfer easily to graphene oxide sheets via the well-developed interface.

Meanwhile, the CB position of ZnO is lower than the LUMO orbit of graphene, and the photogenerated electrons on graphene can directly inject to the CB band of ZnO, giving a more efficient charge separation and reducing the probability of recombination, and consequently, enhancing the photocatalytic activity.

As shown in Scheme 1, the high separation efficiency of photo-induced electron-hole pairs is supposed to be responsible for the enhanced UV and visible light photocatalytic activity, resulting in an increase in the number of holes participating in the photo-oxidation process.

These electrons could easily migrate from the inner region to the surface to participate in oxidation and reduction reactions to generate radicals which are prolonged and enriched by the presence of chemical and excellent electronic structure of graphene oxide which acts as an electron tramp, thus dramatically improving the visible light activity.

The following reactions, (3)–(9), describe the proposed reaction mechanism.

$$ZnO + h\nu \rightarrow ZnO + e^- h^+ \quad (3)$$

$$ZnO\ (e^-) + GO \rightarrow ZnO\ (h^+) + GO\ (e^-) \quad (4)$$

$$ZnO\ (h^+) + GO\ (e) + H_2O \rightarrow ZnO + GO + {}^{\cdot}OH + H^+ \quad (5)$$

$$ZnO\ (h^+) + GO\ (e) + {}^-OH \rightarrow ZnO + GO + {}^{\cdot}OH \quad (6)$$

$$ZnO + GO + {}^{\cdot}OH + RH \rightarrow ZnO + GO + H_2O + R^{\cdot} \quad (7)$$

$$ZnO + GO + R^{\cdot} + O_2 \rightarrow ZnO + GO + ROO^{\cdot} \quad (8)$$

$$ZnO + GO + ROO^{\cdot} + O_2 \rightarrow ZnO + GO + CO_2 + H_2O \quad (9)$$

Such reactions describe the transportation of electron-hole pairs between ZnO and graphene oxide sheets. Thus, the photocatalytic degradation of triclosan is enhanced.

4. Conclusions

The photoirradiation method allows a homogeneous distribution of the ZnO particles on the graphene sheets surface due to the surface polarisation of ZnO nanoparticles by the high energy (UV) used during the photocatalyst synthesis process.

There is a good interaction between the ZnO and GO through sp^3 hybridisations of the graphene oxide that improves the photocatalytic efficiency of ZnO/GO photocatalysts.

It is possible to degrade up to 45% of triclosan (5.1–5.6 $mg.L^{-1}$) under visible light radiation using ZnO/GO hybrid photocatalyst even loaded at low concentrations as 0.5% w/w.

GO acts as electron scavenger reducing the recombination process and promotes the charge separation in the ZnO semiconductor between the balance and conductive band that increases the generation of $^{\cdot}OH$ radicals, resulting in the increase of the apparent constant rate up to 55% in ZnO/GO hybrid photocatalyst compared to the apparent rate constant of pristine ZnO.

The ZnO/GO hybrid photocatalyst can be used in a cyclic way without a significant reduction of its efficiency to degrade triclosan.

Acknowledgements

The authors would like to thank the National Science and Technology Council of Mexico for the PhD fellowship to NCR (CONACYT-253175). The authors would also like to thank Gladys Labrada for the SEM analysis, Beatriz Rivera for the Raman and XRD analysis, Héctor Silva for the TEM analysis and Sidra Iftekhar for the ESR analysis. We acknowledge using the facilities of the national laboratory of LINAN at the IPICYT, México, and using the facilities of the Laboratory of Green Chemistry of the Lappeenranta University of Technology, Finland.

References

[1] T. Colborn, F.S. Vom Saal, A.M. Soto, Developmental effects of endocrine-disrupting chemicals in wildlife and humans, Environ. Health Perspect. 101 (1993) 378–384.
[2] E. Diamanti-Kandarakis, J.P. Bourguignon, L.C. Giudice, et al., Endocrine-disrupting chemicals: an endocrine society scientific statement, Endocr. Rev. 30 (2009) 293–342, https://doi.org/10.1210/er.2009-0002.
[3] A. Stolz, G. Schönfelder, M.R. Schneider, Endocrine disruptors: adverse health effects mediated by EGFR?, trends endocrinol, Metabolism 29 (2018) 69–71, https://doi.org/10.1016/j.tem.2017.12.003.
[4] S. Rafqah, P. Wong-Wah-Chung, S. Nelieu, J. Einhorn, M. Sarakha, Phototransformation of triclosan in the presence of TiO2 in aqueous suspension: mechanistic approach, App. Catal. B Environ. 66 (2006) 119–125, https://doi.org/10.1016/j.apcatb.2006.03.004.
[5] J.M. Poyatos, M.M. Muñio, M.C. Almecija, J.C. Torres, E. Hontoria, F. Osorio, Advanced oxidation processes for wastewater treatment: state of the art, Water Air Soil Pollut. 205 (2010) 187–204, https://doi.org/10.1007/s11270-009-0065-1.
[6] M.A. Fox, M.T. Dulay, Heterogeneous photocatalysis, Chem. Rev. 93 (1993) 341–357, https://doi.org/10.1021/cr00017a016.
[7] S.K. Pardeshi, A.B. Patil, Solar photocatalytic degradation of resorcinol a model endocrine disrupter in water using zinc oxide, J. Hazard. Mater. 163 (2009) 403–409, https://doi.org/10.1016/j.jhazmat.2008.06.111.
[8] M. Kamaraj, K.S. Ranjith, S. Rajeshwari, R.T. Rajendra, H.A. Salam, Photocatalytic degradation of endocrine disruptor Bisphenol-A in the presence of prepared $Ce_xZn_{1-x}O$ nanocomposites under irradiation of sunlight, J. Environ. Sci. 26 (2014) 2362–2368, https://doi.org/10.1016/j.jes.2014.09.022.
[9] C.J. Yu, T.Y. Kwong, Q. Luo, Z. Cai, Photocatalytic oxidation of triclosan, Chemosphere 65 (2006) 390–399, https://doi.org/10.1016/j.chemosphere.2006.02.011.
[10] P. Georgiev, N. Kaneva, A. Bojinova, K. Papazova, K. Mircheva, K. Balashev, Effect of gold nanoparticles on the photocatalytic efficiency of ZnO films, Colloids Surf. A Physicochem. Eng. Asp. 460 (2014) 240–247, https://doi.org/10.1016/j.colsurfa.2014.02.004.
[11] Y. Zheng, C. Chen, Y. Zhan, X. Lin, Q. Zheng, K. Wei, J. Zhu, Photocatalytic activity of Ag/ZnO heterostructure nanocatalyst: correlation between structure and property, J. Phys. Chem. C 112 (2008) 10773–10777, https://doi.org/10.1021/jp8027275.
[12] M. Hosseini-Sarvari, Z. Bazyar, Visible light driven photocatalytic cross-coupling reactions on nano Pd/ZnO photocatalyst at room-temperature, ChemistrySelect 3 (2018) 1898–1907, https://doi.org/10.1002/slct.201702219.
[13] J. Shah, M.R. Jan, F. Khitab, Sonophotocatalytic Degradation of Textile dyes over Cu impregnated ZnO catalyst in aqueous solution, Process Saf. Environ. Prot. 116 (2018) 149–158, https://doi.org/10.1016/j.psep.2018.01.008.
[14] J. Wenwen, S. Yongchen, L. Gong, X. Chen, Synthesis of Al-ZnO nanocomposite and its potential application in photocatalysis and electrochemistry, Inorg. Chem. Commun. 88 (2018) 51–55, https://doi.org/10.1016/j.inoche.2017.12.013.
[15] J. Park, Visible and near infrared light active photocatalysis based on conjugated polymers, J. Ind. Eng, Chem 51 (2017) 27–43, https://doi.org/10.1016/j.jiec.2017.03.022.
[16] P.T. Kurnianditia, T. Lling-Lling, W. Ong, W.S. Chang, S. Chai, Graphene oxide: exploiting its unique properties toward visible-light-driven photocatalysis, Appl. Mater. Today 4 (2016) 9–16, https://doi.org/10.1016/j.apmt.2016.04.001.
[17] L. Xinjuan, P. Likun, Z. Qingfei, L. Tian, Z. Guang, C. Taiqiang, L. Ting, S. Zhuo, S. Changqing, UV-assisted photocatalytic synthesis of ZnO–reduced graphene oxide composites with enhanced photocatalytic activity in reduction of Cr (VI), Chem. Eng. J. 183 (2012) 238–243, https://doi.org/10.1016/j.cej.2011.12.068.
[18] A.B. Jasso-Salcedo, A.G. Palestino Escobedo, V.A. Escobar Barrios, Effect of Ag, pH, and time on the preparation of Ag-functionalized zinc oxide nanoagglomerates as photocatalysts, J. Catal. 318 (2014) 170–178, https://doi.org/10.1016/j.jcat.2014.06.008.
[19] A.R. Khataee, M. Fathinia, S. Aber, Kinetic modeling of liquid phase photocatalysis on supported TiO_2 nanoparticles in a rectangular flat-plate photoreactor, Ind. Eng. Chem. Res. 49 (2010) 12358–12364, https://doi.org/10.1021/ie101997u.
[20] N. Kislov, J. Lahiri, H. Verma, D.Y. Goswami, E. Stefanokos, M. Batzill, Photocatalytic degradation of methyl orange over single crystalline ZnO: orientation dependence of photoactivity and photostability of ZnO, Lagmuir 25 (2009) 3310–3315, https://doi.org/10.1021/la803845f.
[21] M.M. Tan, K. Ji-Hee, J. MunSeok, T. Anh-Thu, S. Lee Hong, Oriented ZnO nanostructures and their application in photocatalysis, J. Lumin. 185 (2017) 17–22, https://doi.org/10.1016/j.jlumin.2016.12.046.
[22] M. Kenji, S. Noriko, M. Toshitsugu, H. Junichi, I. Miki, H. Hajime, Surface polarity determination of ZnO spherical particles synthesized via solvothermal route, Cryst. Growth Des. 9 (2009) 5014–5016, https://doi.org/10.1021/cg901216g.
[23] K. Ryong, M. Parvez, K. Chhowalla, UV-reduction of graphene oxide and its application as an interfacial layer to reduce the back-transport reactions in dye-sensitized solar cells, Chem. Phys. Lett. 483 (2009) 124–127.
[24] L. Guardia, S. Villar-Rodil, J.I. Paredes, R. Rozada, A. Martínez-Alonso, J.M.D. Tascón, UV light exposure of aqueous graphene oxide suspensions to promote their direct reduction, formation of graphene–metal nanoparticle hybrids and dye degradation, Carbon 50 (2012) 1014–1024, https://doi.org/10.1016/j.carbon.2011.10.005.
[25] J. Tianhao, H. Yongyong, S. Mei, M. Nan, The mechanism of the reaction of graphite oxide to reduced graphene oxide under ultraviolet irradiation, Carbon 54 (2013) 412–418, https://doi.org/10.1016/j.carbon.2012.11.057.
[26] L. Tian, P. Likun, L. Xinjuan, L. Ting, Z. Guang, S. Zhuo, Enhanced photocatalytic degradation of methylene blue by ZnO-reduced graphene oxide composite synthesized via microwave-assisted reaction, J. Alloys Compd. 509 (2011) 10086–10091, https://doi.org/10.1016/j.jallcom.2011.08.045.
[27] L. Benxia, L. Tongxuan, W. Yanfen, W. Zhoufeng, ZnO/graphene-oxide nanocomposite with remarkably enhanced visible-light-driven photocatalytic performance, J. Colloid Interface Sci. 377 (2012) 114–121, https://doi.org/10.1016/j.jcis.2012.03.060.
[28] B. Xiaojuan, S. Changpo, L. Di, L. Xiaohong, W. Jun, W. Nanxi, C. Xiaojiao, Z. Ruilong, Z. Yongfa, Photocatalytic degradation of deoxynivalenol using graphene/ZnO hybrids in aqueous suspension, App. Catal. B Environ. 204 (2017) 11–20, https://doi.org/10.1016/j.apcatb.2016.11.010.
[29] F. Hongbo, X. Tongguang, Z. Shengbao, Z. Yongfa, Photocorrosion inhibition and enhancement of photocatalytic activity for ZnO via hybridization with C_{60}, Environ. Sci. Technol. 42 (2008) 8064–8069, https://doi.org/10.1021/es801484x.
[30] C. Fangyuan, A. Weijia, L. Li, L. Yinghua, C. Wenqua, Highly efficient removal of bisphenol A by a three-dimensional graphene hydrogel-AgBr@rGO exhibiting adsorption/photocatalysis synergy, App. Catal. B: Environ. 217 (2017) 65–80, https://doi.org/10.1016/j.apcatb.2017.05.078.
[31] X. Tongguang, Z. Liwu, C. Hanyun, Z. Yongfa, Significantly enhanced photocatalytic performance of ZnO via graphene hybridization and the mechanism study, Appl. Catal. B Environ. 101 (2011) 382–387, https://doi.org/10.1016/j.apcatb.2010.10.007.
[32] R. López, R. Gómez, Ban gap energy estimation from diffuse reflectance measurements on sol-gel and commercial TiO2: a comparative study, J. Solgel Sci. Technol. 6 (2012) 1–7, https://doi.org/10.1007/s10971-011-2582-9.
[33] G. Williams, B. Seger, K. Prashant, TiO2-graphene nanocomposites. UV-assisted photocatalytic reduction of graphene oxide, ACS Nano 2 (7) (2008) 1487–1491, https://doi.org/10.1021/nn800251f.
[34] H. Kai, C. Guiqiu, Z. Guangming, C. Anwei, H. Zhenzhen, S. Jiangbo, H. Tiantian, P. Min, H. Liang, Three-dimensional graphene supported catalysts for organic dyes, Appl. Catal. B Environ. 228 (2018) 19–28, https://doi.org/10.1016/j.apcatb.2018.01.061.
[35] J. Santiago-Morales, M.J. Gómez, S. Herrera-López, A.R. Fernández-Alba, E. García-Calvo, R. Rosal, Energy efficiency for the removal of non-polar pollutants during ultraviolet irradiation, visible light photocatalysis and ozonation of a wastewater effluent, Water Res. 47 (2013) 5546–5556, https://doi.org/10.1016/j.watres.2013.06.030.
[36] X. Fei, C. Jinfan, S. Kalytchuk, C. Ling, S. Yiru, K. Dexin, C. Kung-Hui, H.L. Sit

Patrick, T. Yang, Supported gold clusters as effective and reusable photocatalysts for the abatement of endocrine-disrupting chemicals under visible light, J. Catal. 354 (2017) 1–12, https://doi.org/10.1016/j.jcat.2017.07.027.
[37] D. Yunrong, Y. Lifeng, Synthesis and photocatalytic activity of Ag–Ti–Si ternary modified α-Bi2O3 nanoporous spheres, Mater. Lett. 142 (2015) 225–228, https://doi.org/10.1016/j.matlet.2014.12.013.
[38] J. Niu, Y. Dai, L. Yin, J. Shang, J.C. Crittenden, Photocatalytic reduction of triclosan on Au–Cu2O nanowire arrays as plasmonic photocatalysts under visible light irradiation, Phys. Chem. 17 (2015) 17421–17428, https://doi.org/10.1039/c5cp02244d.
[39] L. Zhao, J. Deng, P. Sun, J. Liu, Y. Ji, N. Nakada, Z. Qiao, H. Tanaka, Y. Yang, Nanomaterials for treating emerging contaminants in water by adsorption and photocatalysis: systematic review and bibliometric analysis, Sci. Total Environ. 627 (2018) 1253–1263, https://doi.org/10.1016/j.scitotenv.2018.02.006.
[40] X. Bai, L. Wang, Y. Zhu, Visible photocatalytic activity enhancement of $ZnWO_4$ by graphene hybridization, ACS Catal. 2 (2012) 2769–2778, https://doi.org/10.1021/cs3005852.
[41] L.W. Zhang, H.B. Fu, Y.F. Zhu, Efficient TiO2 photocatalysts from surface hybridization of TiO2 particles with graphite-like carbon, Adv. Funct. Mater. 18 (2008) 2180–2189, https://doi.org/10.1002/adfm.200701478.
[42] Y. Zhang, Z.R. Tong, X. Fu, Y.J. Xu, TiO2 graphene nanocomposites for gas phase photocatalytic degradation of volatile aromatic pollutant: is TiO2 Graphene truly different from other TiO2 carbon composite materials? ACS Nano 4 (12) (2010) 7303–7314, https://doi.org/10.1021/nn1024219.

Publication II

Vladimir A. Escobar Barrios, Dalia Verónica Sánchez Rodríguez, Nancy Ayerim Cervantes Rincón, Alma Berenice Jasso-Salcedo.
Modified Metallic Oxides for Efficient Photocatalysis
Reprinted with permission from

Reprinted with permission from
Photocatalysts – Applications and Attributes
Chapter 4, 2018

Chapter 4

Modified Metallic Oxides for Efficient Photocatalysis

Vladimir A. Escobar Barrios,
Dalia Verónica Sánchez Rodríguez,
Nancy Ayerim Cervantes Rincón and
Alma Berenice Jasso-Salcedo

Additional information is available at the end of the chapter

http://dx.doi.org/10.5772/intechopen.80834

Abstract

The aim of the chapter is to present modified materials like alternatives for conventional photocatalyst such as titanium dioxide. Discussion about silver/graphene nanoparticles-modified zinc oxide for the degradation of pollutants like triclosan or bisphenol A, both considered as endocrine disruptors, which affect the hormonal development of humans, is presented. The best conditions to obtain the highest photodegradation degree are established. In addition, the bismuth oxychloride has gained attention during the last 5 years for photocatalysis. In accordance, the obtained results for phenol photodegradation, using such oxychloride, are also presented. In the chapter, the characterization of photocatalyst is reported along with the proposal for mechanisms of action for the modified ZnO photocatalyst and the bismuth oxychloride.

Keywords: ZnO, bismuth oxychloride, silver and graphene doped

1. Introduction

The photocatalysis has become an important research area in the recent years. The interest on such area has accelerated the number of papers, since photocatalysts have diverse applications, for example, the photodegradation of several contaminants that are quite difficult to transform to innocuous substance as water vapor. Other important applications are the development of self-cleaning products as well as the production of highly effective fuels like hydrogen. Nowadays, the technological development based on photocatalysis has an important growth in regions such as Europe and Asia (12% annually), with an estimated market of about € 1500 million in 2015 [1].

Photocatalysts are based on semiconductor materials, which are activated by radiation with higher energy than the bandgap of the used semiconductor, in order to create hole-electron pairs, once the electron passes from valence to conduction band. The promoted electron, toward conduction band, and the hole remained in valence band react in the photocatalyst interface with adsorbed substances in order to create reactive entities (free radicals and/or radical anions), which interact with contaminants to degrade them. All these processes imply the sorption on the photocatalyst's interface, its activation by radiation, creation of reactive species, and the recombination of electron to hole. The last could occur very fast that the creation of reactive species does not take place at great extent, giving ineffective photodegradation process.

In this context, the research regarding photocatalysis, in recent years, is focused to decrease the bandgap of photocatalyst in order to use solar light rather than UV light, which implies additional cost during the treatment process. In addition, minimization of the recombination process, in order to improve the photocatalytic performance, is quite important too. Some approaches to face these issues consider the doping with metals; meanwhile other research groups also consider the modifications with electron-rich species like graphene.

TiO_2 has been the photocatalyst by excellence and has been widely studied in its pristine form and/or doped with metals like gold and other elements. Nevertheless, other metal oxides, such as ZnO, have shown better photocatalytic performance, especially when visible light is used. ZnO has also been doped with metals like gold or silver. More recently, other metal oxides like bismuth oxychloride have gained attention for photocatalytic process.

In this chapter, discussion about the modification of ZnO with graphene is presented and discussed in terms of the implied mechanism (hybridization), in addition to the obtained results when such hybrid photocatalyst was used for the photodegradation of triclosan under visible light. Additionally, the modification method of ZnO with silver nanoparticles and its effect on photocatalytic performance for bisphenol A, Rhodamine B (RhB), and Triclosan is presented.

Finally, the use of an attractive photocatalyst, bismuth oxychloride (BiOCl), and its respective modification with silver and graphene oxide for RhB photodegradation along with the result and mechanism for the photocatalyst based on TiO_2-BiOCl used for photodegradation of phenol is presented and discussed.

The three different photocatalysts show how effective photocatalyst can be obtained and modified. The presented and discussed results contribute to understand some of the key parameters implied in the photocatalysis.

2. Zinc oxide

Zinc oxide (ZnO) is a II-VI group semiconductor with wurtzite structure with lattice parameters a = 0.3296 nm and c = 0.52065 nm. Zn^{2+} atoms are tetrahedrally coordinated with O^{2-} atoms stacked alternately along the *c* axis so that d-electrons of zinc are hybridized with 2p-electrons of oxygen [2]. ZnO has the potential to become an important material for photocatalysis because it is nontoxic (it is often included in pharmaceuticals), photostable, and low cost.

We consider at least three windows of opportunity to boost ZnO as photocatalyst in academy and industry. The first is related to the quantum yield in visible light rather than UV for the efficient utilization of the electron-hole (e^-/h^+) pairs during decomposition of endocrine disruptors and emergent contaminants in water. A second opportunity is the immobilization of the photocatalyst that could make possible its utilization on continuous mode and toward implementation at industrial scale. The third challenge deals with nonlinear mathematical modeling of the factors that rule the photocatalytic kinetics of the metallic-modified ZnO for optimization purposes. This is not a trivial problem in photocatalysis and artificial neural network tools (ANNs) do not demand of academic expertise for a fast implementation; for example, in the industry sector. The reader can consult [3] for the approach that Meimaroglou and collaborators follow to assess ZnO photocatalyst structure-photocatalytic performance associations toward the maximization of the photocatalytic efficiency. The first two challenges are addressed in the present chapter.

2.1. Use of ZnO/graphene photocatalysts

Nowadays, solar energy, radiant light, and heat from the sun are the most abundant available sources of clean energy. Thus, research studies and development of materials that can efficiently harvest solar irradiation and used for green environmental pollution management are essential. Photocatalysis, which could use renewable solar energy to activate the chemical reactions via oxidation and reduction, such as that occurs in advance oxidation processes (AOPs), is a sustainable technology to provide solution for environmental issue. This photocatalysis system has attracted great interest from science community as the most promising way to solve the environmental problems, especially getting rid of residual pollutants from wastewater stream.

In the field of photocatalysis, ZnO has emerged as the leading candidate for green environmental management systems because of its unique characteristics, such as wide bandgap (3.37 eV) in the near-UV spectral region, a large electron exciton binding energy of 60 eV at room temperature, strong oxidation ability, and good photocatalytic property [4]. It is a well-known fact that ZnO occurs as white hexagonal crystal or white powder known as white zinc. ZnO crystallizes in the wurtzite structure and is available as large bulk single crystals [5]. As an important semiconductor material, ZnO has been applied in catalysis, rubber and paint industries, ceramic bodies, varistors, fertilizers, and cosmetics [6].

Recently, the development of ZnO with precisely controllable features has gained significant scientific interest. The electrical, optical, and magnetic properties of ZnO can be altered or improved by the use of ZnO in nanoscale and efforts have been developed to improve the properties of ZnO photocatalyst [7]. Moreover, ZnO is an environmental friendly material as it is compatible with living organisms [8]. Since ZnO has almost the same bandgap energy as TiO_2 (3.2 eV), its photocatalytic capability is anticipated to be similar to that of TiO_2. However, ZnO is relatively cheaper compared to TiO_2, whereby the usage of titanium dioxide is uneconomic for large-scale water treatment operations [9]. The greatest advantage of ZnO is the ability to absorb a wide range of solar spectrum and more light quanta than some semiconducting metal oxides including the capacity to absorb visible light energy, which is due to its

wide band energy. This results in fast recombination of photogenerated charges and thus caused low photocatalytic efficiency.

The recombination of photogenerated hole (hVB^+) and electron (eCB^-) is one of the major disadvantages in semiconductor photocatalysis. This recombination step lowers the quantum yield and causes energy wasting. Therefore, the e^-/h^+ recombination process should be inhibited to ensure efficient photocatalysis. Metal doping could counter the recombination problem with efficient charge separation between electrons and holes in ZnO photocatalyst. In addition, the dopants may trap electrons, reducing the chances of e^-/h^+ recombination that deactivate the photocatalytic system [10]. Furthermore, the generation of hydroxyl radicals and active oxygen species will greatly increase resulting from the enhancement in charge separation efficiency [11]. Semiconductors as graphene have been proven as a couple semiconductor that can improve the visible-light photocatalytic efficiency of ZnO due to its remarkable chemical, physical, and mechanical properties, such as large surface area (2600 m^2/g), excellent electrical and thermal conductivity, high mechanical strength, flexibility, and efficient wide range of light adsorption. Due to the properties of graphene-based materials, several ranges of environmental applications have been developed such as absorption, transformation, and detection [12]. So far, numerous methods have been used to design and synthesize ZnO/graphene hybrid photocatalysts with various morphologies. However, most of these methods rely on chemical and/or high-energy consumption resulting in a costly, environmentally hazardous, and especially inefficient photocatalyst for complete degradation of organic pollutants as triclosan, which has been classified as potential endocrine disrupting compound (EDC). Triclosan was ranked as the most abundant compound among all investigated pharmaceuticals and personal care products with its mean concentration of 12.6 ± 3.8 mg/Kg in 110 biosolids samples collected from 94 US wastewater treatment plants across 32 states and the District of Columbia using EPA Method 1694 [13]. In addition, the highest initial concentrations of triclosan detected in municipal biosolids were 2715 and 1265 μg/Kg [14].

Hydrothermal and chemical reductions have been the main methods studied to obtain ZnO/graphene hybrid photocatalysts. However, photodeposition method [15] has been reported as an efficient method to generate hybrid photocatalyst to degrade pollutants. This study proposes the synthesis of ZnO/graphene semiconductors by developing a facile, cheap, environmentally and high reproducibility approach to obtain an efficient material to degrade organic pollutants, as triclosan (TCS), under visible light. For instance, it has been demonstrated that inductive irradiation method is possible to synthesize ZnO composites due to its polarity [16]. In particular, graphene has the ability to accept electrons efficiently due to the absence of oxygen chemical groups on its surface preventing the recombination and providing a favorable π-π conjugation between TCS and aromatic region of graphene (**Figure 1**). The trapped electrons on graphene react with the dissolved oxygen and water to form reactive superoxide and hydroxyl radicals, which further oxidizes triclosan.

The modified photodeposition method has resulted in a successful process to prepare ZnO/graphene hybrid photocatalysts with enhanced photocatalytic activity under visible light radiation. The obtained results show degradation of 1% of triclosan (8 ppm) in absence of catalyst (photolysis) while this degradation percentage increases up to 42% using 0.5 wt% of

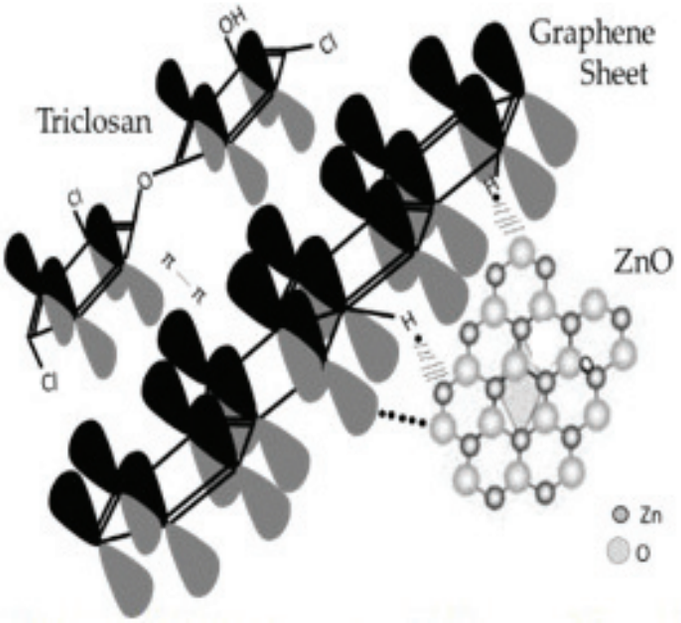

Figure 1. Schematic illustration of the interaction between ZnO photocatalyst doped with graphene sheets and its interaction with triclosan.

graphene sheets as dopant in ZnO nanocatalyst. It is important to mention that wurtzite has been the structure used in this study with a bandgap of 3.21 eV obtained by UV-vis spectrophotometer, while a value of 3.15 eV for ZnO/graphene composite was obtained. This reduction in the bandgap value is associated to a structure based on good interaction between ZnO nanocatalyst and graphene sheets, which creates intermediate energy levels between both materials, a property that allows to transfer the electrons promoted from the valence band to the conductive band of the ZnO semiconductor to graphene sheets that capture and retain the transferred electrons, improving the photocatalytic performance of ZnO as it is illustrated in **Figure 2**. This important first approximation has been the result of the evaluation of the effect of the loaded graphene amount in zinc oxide nano-photocatalyst. Graphene concentrations of 0.25 and 0.5 wt% were evaluated for this purpose and the obtained results showed enhancement of the ZnO photocatalytic activity under visible light radiation even using minimum contents of graphene sheets. Thus, 34 and 36% of the initial concentration of triclosan (8 ppm) was degraded using ZnO/graphene composites loaded with 0.25 and 0.5 wt% of graphene, respectively, and the bandgap values were 3.19 and 3.18 eV, for such ZnO/graphene composites. In contrast with 25% of initial triclosan degraded using pristine ZnO (bandgap: 3.21 eV). These results can be compared with those reported in previous investigations related with the photodegradation of triclosan using dopants such as rare-earth elements as Ce (47%) [17], metals such as Au (10% after 5 h) [18], Ag [19], and Cu [20]; as well as oxide compounds as MgO, WO_3, TiO_2, ZnO, or graphene oxide [21] using dopant contents up to 10%.

The adsorption properties of the as-prepare ZnO/graphene hybrid photocatalysts doped with different amounts of graphene sheets were one of the most important characteristics to improve the degradation efficiency of the ZnO. The specific area of ZnO and ZnO/graphene

hybrid photocatalysts was determined via N_2 adsorption isotherms using the Brunauer Emmett Teller (BET) method. The results revealed that the graphene monolayers (44.2 g/m^2) showed the highest surface area for the analyzed pristine material, while ZnO had a specific area of 10.8 g/m^2. Among the three investigated composites, the photocatalyst loaded with 0.5 wt% of graphene had the highest surface area (18.3 g/m^2), followed by ZnO/graphene 0.25 wt% (14 g/m^2) and ZnO/graphene 0.1 wt% (13.3 g/m^2) catalysts. Thus, the addition of graphene sheets increases the surface area of the hybrid catalysts up to 69% of the initial area of zinc oxide and improve their adsorption capacities, resulting in the first property of the as-prepare hybrid composites to increase the degradation of triclosan, as it has been reported previously [22].

In order to study the effect of the method of synthesis in the ZnO/graphene hybrids, composites were prepared by impregnation method with graphene contents of 0.5 wt% using continuous stirring in the absence of UV radiation. The resultant photocatalysts were tested to degrade triclosan under visible light radiation, and it was obtained that 15% of the initial concentration of triclosan was degraded, 53% less than the composites synthesized by photodeposition method as it can be observed in **Figure 2**.

The hybridization of ZnO with graphene has been studied and confirmed by Raman spectroscopy integrating the intensity ratio of the D to G bands characteristic for carbon materials. The G peak arises from the stretching of C-C bond of graphite materials and is highly sensitive to strain effects in sp^2 system, while D peak is caused by the disordered structure of graphene material. Regarding the sp^3 and sp^2 hybridizations I_D/I_G value, in the case of pristine graphene oxide was 0.93, indicating that the intensity of the G band is higher than D band, which results in a lower amount of sp^3 defects and less structural disorder. Compared with graphene oxide (0.93), the reduction of I_D/I_G ratio for ZnO/GO 0.5 wt% hybrid photocatalyst (I_D/I_G = 0.91) is observed, implying a reduction of sp^3 defects compared with pure graphene oxide. This fact

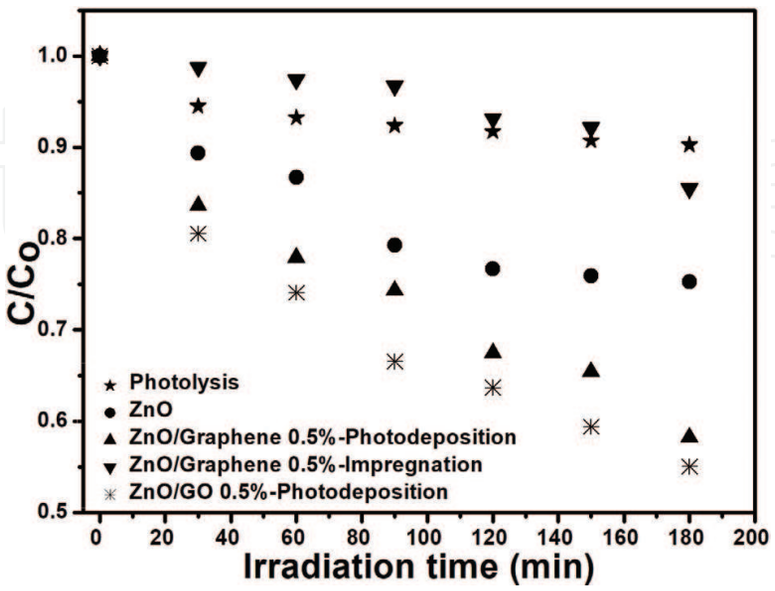

Figure 2. Degradation curves of triclosan under visible light radiation conditions: 23°C, pH = 7.

confirms the interaction between ZnO and GO given by sp^3 defects. The results given hereinabove are consistent with the results in FTIR characterization, revealing the reestablishment of the conjugated graphene oxide network. In contrast, the ratio I_D/I_G for the composite prepared with graphene sheets was calculated and corresponds to the value of 1.04 (higher than I_D/I_G of pristine graphene, 0.36) indicating the presence of more defects in the graphene oxide lattice, which implies a decrease in the size of the in-plane sp^2 domains and formation of the defects and disorders in the graphene sheets, revealing the reestablishment of the conjugated graphene network (sp^2 carbon) [23] in the ZnO/GO photocatalysts due to the hybridization of graphene via photoirradiation method but resulting in a weak interaction due to the absence of chemical groups on the surface of graphene sheets as are presented on GO surface. The interaction between graphene oxide sheets was improved by the interaction of ZnO-polarized structure and the chemical surface of graphene oxide, which contains carbonyl, carboxyl, epoxy, and hydroxyl groups.

The degradation curves of triclosan for ZnO/GO hybrid photocatalyst are presented in **Figure 3**. It is noticed that the composites obtained by the photodeposition method are the materials with the best performance to degrade triclosan under visible light radiation compared with photolysis experiment and with the degradation using the bare ZnO photocatalyst.

In addition to the photodegradation curves presented in **Figure 3**, the rate constants are presented in **Table 1**.

The results show the highest apparent degradation rate constant for the hybrid catalyst synthesized with graphene oxide (0.003 min^{-1}), almost four times higher than the pristine ZnO semiconductor, corroborating the importance of interaction between ZnO and GO.

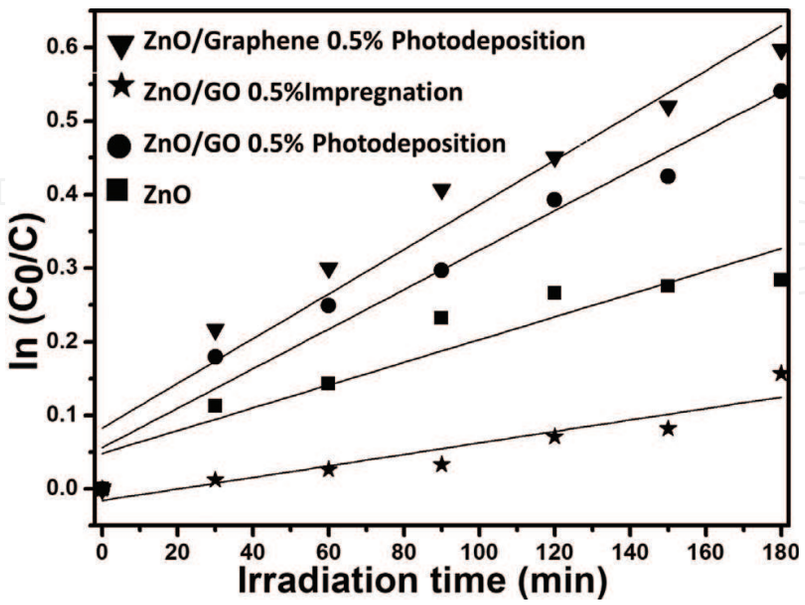

Figure 3. Triclosan photodegradation curves with ZnO/graphene and ZnO/GO hybrid photocatalysts under visible light. Conditions: 23°C, pH = 7.

Photocatalyst	K_{app}, min^{-1}
ZnO	0.00078
ZnO/G_{PD}	0.0016
ZnO/OG_{IMP}	0.0027
ZnO/OG_{PD}	0.003

Table 1. Apparent rate constants for triclosan photodegradation under visible light.

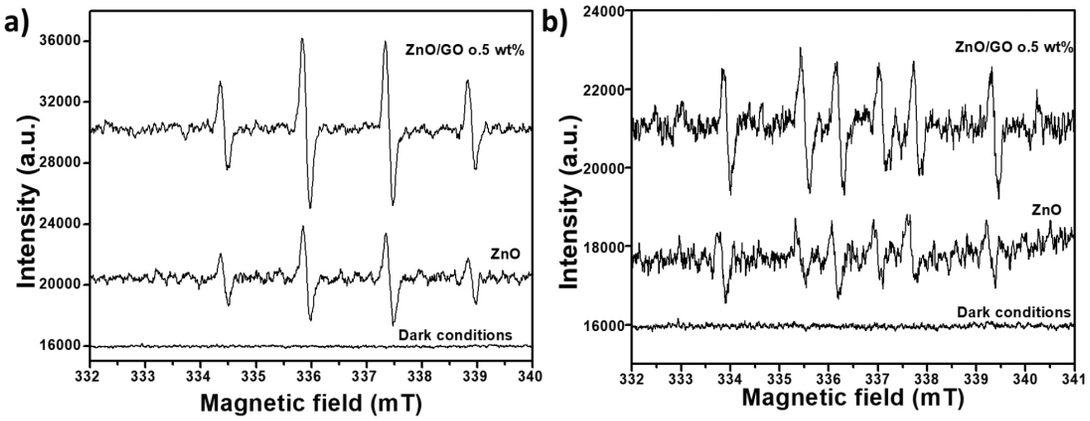

Figure 4. EPR spectra of ZnO/GO hybrid photocatalyst irradiated under visible light in (a) water and (b) ethanol solvents. DMPO was used as a radical trapper.

The mechanism of the best as-prepare ZnO/GO hybrid composite was proposed. Thus, the ESR spin-trap technique (with DMPO) was used to monitor the reactive oxygen species generated during the irradiation of the hybrid photocatalyst and the results are shown in **Figure 4**. Both signals of DMPO-$^{\bullet}$OH and DMPO-$O_2^{\bullet-}$ are clearly observed when pristine ZnO and ZnO/GO were exposed to visible radiation. Therefore, a dual mechanism involving both hydroxyl radicals and superoxide radicals is expected in the photocatalytic process. However, the signals for hybrid photocatalysts are stronger than the signals in pristine ZnO, thus accounting for the higher and stable photocatalytic performance of hybrid composites than bare ZnO toward the degradation of triclosan. The hydroxyl radicals trapped by DMPO (DMPO-$^{\bullet}$OH) and superoxide radicals (DMPO-$O_2^{\bullet-}$) for ZnO and hybrid photocatalysts were characterized by detecting four characteristic signals in water, and six signals in ethanol for DMPO-$^{\bullet}$OH and DMPO-$O_2^{\bullet-}$, respectively. In both cases, it is noticed that the signals for hybrid material are more pronounced than those for the ZnO pristine sample, thus accounting for the better photocatalytic performance.

Thus, the enhanced photocatalytic activity of ZnO/GO photocatalyst is due to the introduction of carbon material, which promotes an increase in charge separation to effective utilization of electrons to produce more $^{\bullet}$OH and $O_2^{\bullet-}$ radicals. In this case, the signals of $^{\bullet}$OH radicals are

stronger than those for $O_2^{\bullet -}$, which suggests the predominance of oxidative reactions whose holes are responsible for the degradation of triclosan. Furthermore, ZnO photocatalyst presents visible light photocatalytic activity but generates stronger visible light after graphene hybridization, showing that graphene oxide is responsible for the visible light performance, which is induced by the injection of an excited electron from the lowest unoccupied molecular orbit (LUMO) of graphene to the conduction band (CB) of ZnO. The introduction of the graphene semiconductors can possibly cause the rapid separation of electron-hole pairs during irradiation [11] prolonging the electron-hole pair lifetime and accelerating the transfer rate of electrons [24] as shown in **Figure 5**.

In conclusion, the adsorption properties, good interaction between ZnO- and graphene-based materials, chemical structure of graphene, method of synthesis, and concentration of the dopant used to hybridize ZnO catalyst are the most important properties that affect the development of ZnO/graphene hybrid photocatalysts.

2.2. ZnO modification by inorganic molecules: silver

Silver nanoparticles are linked to the ZnO surface through the alkanethiol surfactant (**Figure 6a**). The stabilizer ligands COOH-$(CH_2)_n$-S-Ag keep nanoparticles as small as 7 nm in the solution and 15–26 nm in the Ag/ZnO photocatalyst, corroborated by XRD; although TEM analysis shows Ag nanoparticles of spherical shape and defined boundaries smallest as 3 nm over ZnO surface (**Figure 6b-d**). We studied the effect of the pH and time on the functionalization of ZnO nanoagglomerates by two methods denominated as photodeposition (PD) and impregnation (IMP) [15]. We propose to replace the ambiguous terms "doping" with functionalization when spoke of superficial ZnO modification. For instance, the sample 1%Ag/ZnO-PD11,1 synthesized by the PD method using 1 wt.% Ag at pH 11 and 1 h under UV light, a functionalization yield of 100% was corroborated by elemental analysis by inductively coupled plasma spectrometry ICP-OES and SEM-EDX. The UV irradiation produces free radicals ($^{\bullet}OH$, $^{-\bullet}O$) that degrade the ligand and release the silver nanoparticles onto the ZnO surface (**Figure 6c**). Byproducts of surfactant decomposition accumulate in ZnO are observed by IR. This functionalization of the

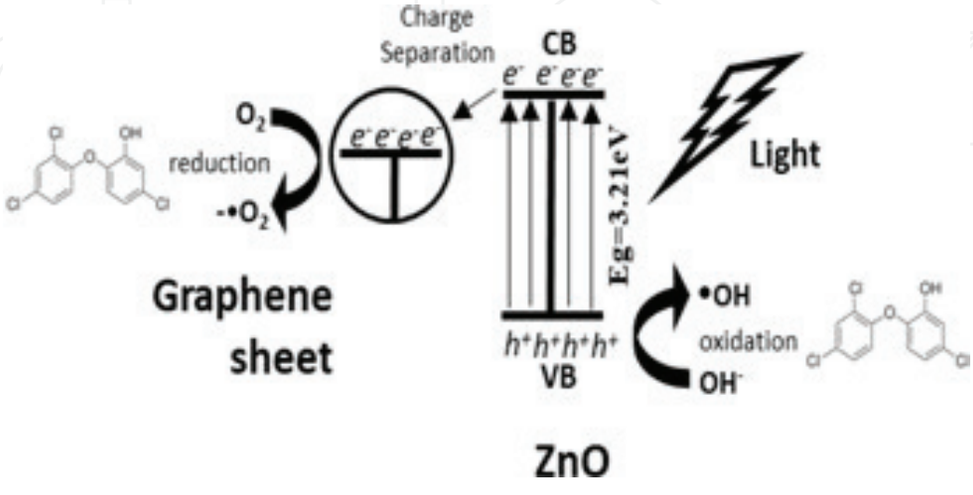

Figure 5. Schematic illustration of the photocatalytic process in the ZnO/GO hybrid semiconductor.

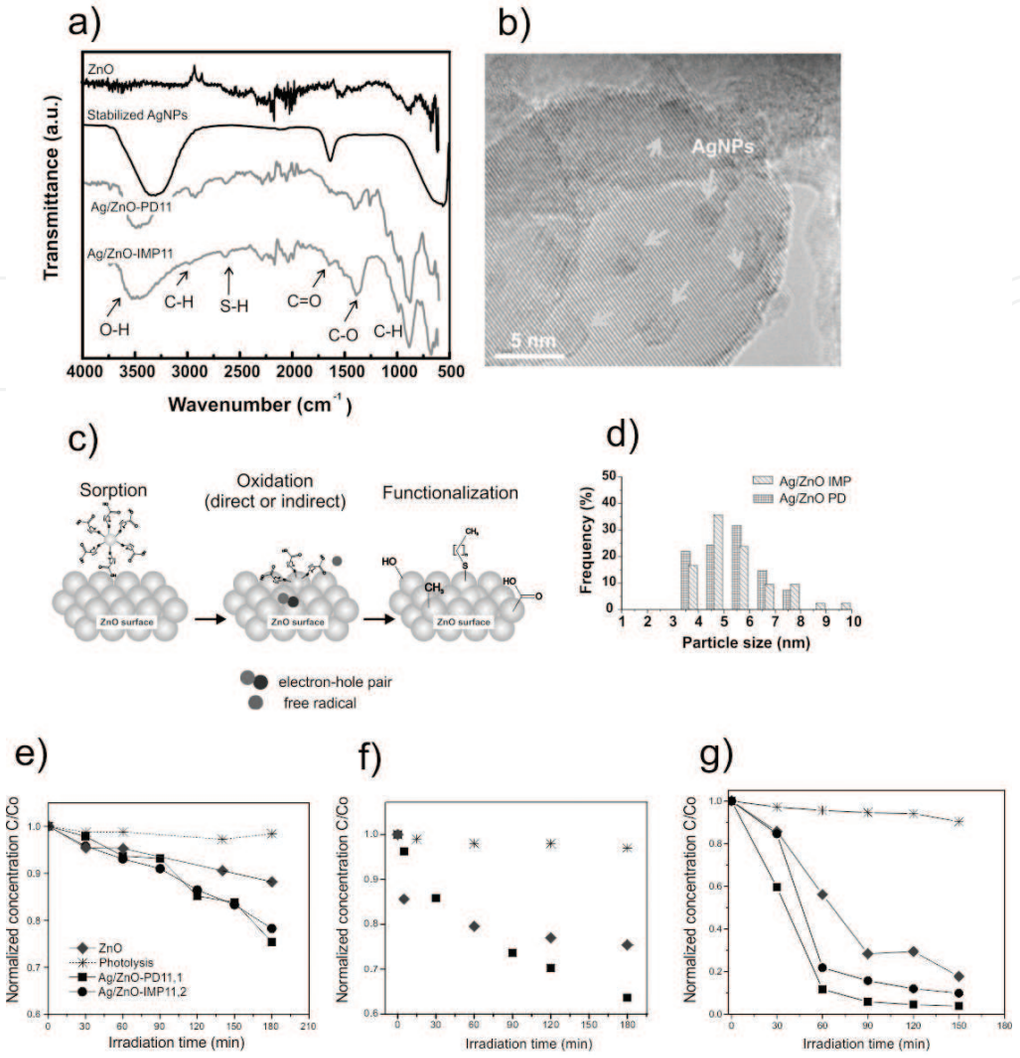

Figure 6. FTIR (a) and TEM image (b) of the as-synthesized photocatalyst functionalized ZnO by silver nanoparticles. Schematic illustration of the functionalization by PD method. (c). Histogram of silver particle size (d). Photocatalytic degradation of bisphenol A (e), triclosan (f), and RhB (g).

photocatalyst surface with S-H, C-O, and hydroxyl groups ($^{-}$OH) creates defect sites advantageous in photocatalysis. Silver-experienced redox processes during PD functionalization, for instance, oxidation (Ag^{+}/Ag^{0}, +0.799 eV vs. SHE) by photogenerated holes (+2.75 eV, vs. SHE) and free radicals. They reduce again into the zero-valence form (Ag^{0}) by photoexcited electrons. This method favors insertion of ionic silver Ag^{+} into ZnO crystalline structure perceived as an expansion of lattice parameters measured by XRD. The new attached silver possibly anchors on the surface defect sites of ZnO [25, 26]. The role of the metallic modifier in Ag/ZnO is to promote the pair electron-hole (e^{-}/h^{+}) separation and to increase the photocatalyst sensitivity toward visible light, in our case, evidenced as an absorption in the visible region by UV-Vis spectroscopy.

The IMP functionalization mechanism is different in the sense that silver nanoparticles and ZnO interaction is a function of the reaction time for an optimum of 2 h. For instance, the sample 1%Ag/ZnO-IMP11,2 synthesized using 1 wt.% Ag at pH 11 and 2 h under vigorous

stirring results in heterogeneously distributed silver nanoparticles of average size of 15 nm determined by Scherrer equation. The surfactant decomposes almost completely during the heating (at 300°C) that releases AgNPs onto ZnO surface. As before, residuals S-H and C-H functionalizing the ZnO surface was observed by IR (**Figure 6a**). Similarly, the as-synthesized 1%Ag/ZnO-IMP samples absorb in visible region of the spectrum and silver nanoparticles induce a surface-localized plasmon resonance.

It is challenging to control the metallic particle size because the nanoparticles have the trend to form agglomerates. The deposition of silver nanoparticles over metallic oxides from pre-formed nanoparticles using, for example, chemical vapor deposition [27] has been used, but IMP and PD methods demonstrate to be a successful bulk functionalization of ZnO at room temperature and atmospheric pressure. The increase of photocatalytic efficiency by silver-modified ZnO is demonstrated on the degradation of endocrine disruptors (i.e., bisphenol-A), an emergent contaminant (i.e., triclosan), and a dye (i.e., RhB) under visible light, which represents an important achievement in the use of solar-driven Ag/ZnO photocatalysts.

Figure 6e-g shows the progress of the contaminant photodegradation under visible light (365 nm, 0.97 mW/cm^2, 8 W 3UV-38 UVP Inc. lamp, lab-made reactor) at 20°C. The results show that 25% of bisphenol-A (10 mg/L) was destroyed after 3 h using Ag/ZnO-PD, and it represents an improvement of 100% compared with ZnO. A total of 35% of initial triclosan (20 mg/L) was destroyed within 3 h using Ag/ZnO-IMP11, represents an improvement of 45% compared with ZnO. Finally, 90% of dye discoloration is obtained with Ag/ZnO-PD11, being only 20% better than ZnO.

Similarly, the photocatalysts were tested under UV light (302 nm). The use of BET surface area normalization of the apparent rate constant (k_{app}/BET ssa) in photocatalysis was proposed to clearly demonstrate that ZnO nanoagglomerates is 400% faster than Pi-25, a TiO_2 well-known and extensively used photocatalyst from Degussa. The bandgap energy of ZnO and titanium dioxide (TiO_2) is basically the same (3.2 eV). However, the valence and conduction bands exhibit differences in electric potential values; whose reported values are in the range of −0.45 to 2.75 eV vs. NHE and − 0.1 to 3.1 eV vs. NHE, for ZnO and TiO_2, respectively [28, 29]. Thus, the photogenerated holes in ZnO have strong enough oxidizing power to decompose most organic compounds. Furthermore, 1%Ag/ZnO-PD11,1 photocatalytic activity is 370% faster than ZnO attributed to the photoexcited electron trapping in the metallic primary (e^-/h^+ pair) and secondary active species (free radicals, i.e., $^{\bullet}OH$) for the oxidation of bisphenol-A. The effect of pH, photocatalyst dosage, and bisphenol-A concentration on the kinetic rate constant were also studied extensively and reported [3].

2.3. ZnO immobilization by organic molecules: poly (acrylic acid)

The utilization of powder photocatalyst may end unpractical for industrial scales because of the technical challenges like efficient dispersion and finally difficult separation of photocatalyst after the reaction that may entail important energetic costs and sometimes even producing a secondary pollution. Besides, photocorrosion is an important drawback in photocatalysis, and the anchoring of silver has been proved to control its progress. The

immobilization of ZnO into organics tends to solve both the difficulty of photocatalyst dispersion and recuperation for a cyclic usage together with an improvement of the photostability [30]. The organics that have been reported for immobilization of TiO_2 comprise polyaniline [31, 32] and polypyrrole [33] that are hydrophobic and opaque, then it is incompatible for aqueous applications. Hydrogels, based on acrylic polymers, allow effective transport of water and other dissolved molecules due to their hydrophilicity and high swelling capacity. This kind of polymers shows stimuli-responsive properties to pH, temperature, solvent composition, and ionic strengths. Hydrogels come to be an ideal choice for Ag/ZnO photocatalyst immobilization since they are colorless and visually transparent, which permits penetration of light (**Figure 7e**).

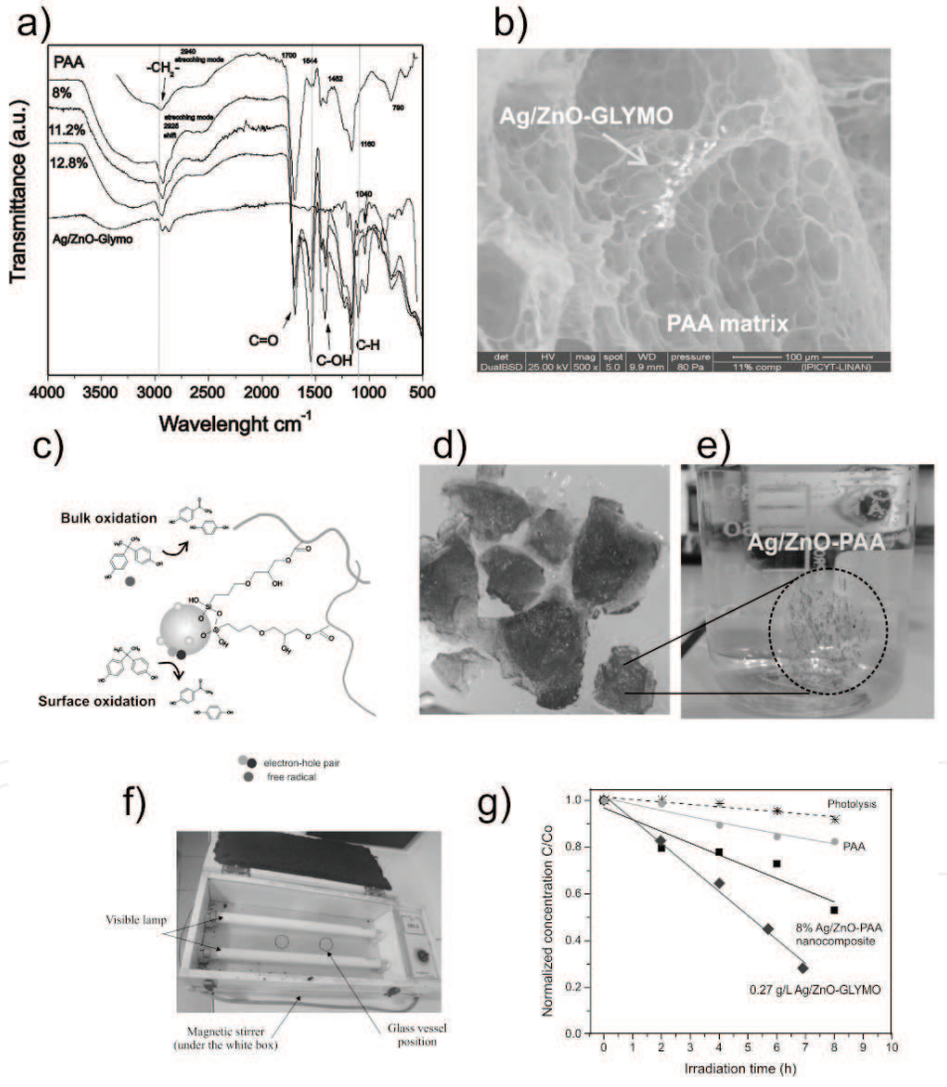

Figure 7. FTIR (a) and E-SEM image (b) of the as-synthesized Ag/ZnO-PAA. Schematic representation of the ligands between photocatalyst pending from the PAA chain and its photocatalytic role (c). Semi-swell Ag/ZnO-PAA composite (d) and reaction vessel containing photocatalyst dissolved in the pollutant solution (e).Home made photocatalytic reactor operated at room temperature and pressure (f). Photocatalytic degradation of bisphenol-A (g).

The general mechanism for the immobilization of Ag/ZnO into a poly (acrylic acid) (PAA) matrix involves the use of GLYMO as photocatalyst stabilizer and coupling agent. Infrared analysis (FTIR) shows characteristic bands at 916 and 1260 cm^{-1} for free epoxide functional groups, in pure GLYMO and Ag/ZnO-GLYMO, meaning that epoxide do not react with Ag/ZnO surface, as desired. Disappearance of bands at 823 and 780 cm^{-1}, corresponding to C-H from the methoxysilyl groups (CH_3O^-) of GLYMO, indicates two processes: hydrolysis of methoxy group and reaction with Ag/ZnO surface by weak bond such as hydrogen bonds. In addition, the peak at 1030 cm^{-1} corresponds to the formation of self-assembled monolayer Si-O-Si on Ag/ZnO surface, and confirms the efficient silanization of the photocatalyst (**Figure 7a**). Lastly, the interaction between the free tail of Ag/ZnO-GLYMO (highly reactive epoxy groups) and the carboxylic groups of PAA gives strong interaction and immobilization into the polymeric matrix.

Two possible arrangements of the photocatalyst bonded to the polymer matrix are proposed: (i) a photocatalyst pending from the PAA chain (**Figure 7c**) and (ii) a cross-linked–like structure, where the photocatalyst is the bridge between two PAA chains.

Environmental SEM chamber allow us for first time to obtain images of 3D network of cross-linked PAA under low vacuum that gives us a time-window of approximately 30 minutes for the analysis before dehydration (**Figure 7b**). SEM-EDX confirms the homogeneous dispersion of photocatalyst within the PAA matrix on 8%Ag/ZnO-PAA composites. The swelling capacity of the composite increases with photocatalyst content (5–13 wt.%) due to the high hydrophilicity of Ag/ZnO (**Figure 7d**). In addition, the composite photostability after 16 h of UV (365 nm) exposure was corroborated by FTIR and TGA analysis.

This enhanced photochemical stability has the potential of use as resistant composite packing material for continuous treatment of water under UV irradiation. This last aspect was first tested in batch experiments toward the degradation of bisphenol-A. Thus, **Figure 7g** shows the time evolution of the bisphenol-A photodegradation under visible light (>450 nm, 8 uW/cm^2, 8 W Hampton Bay lamp, home-made reactor in **Figure 7f**) at 50°C. On the other hand, 47% of the initial concentration of 10 mg/L is degraded within 7 h by 8%Ag/ZnO-PAA composite, it represents a decrease of 50% compared with Ag/ZnO-GLYMO. The composite was reused in a second consecutive cycle without washing that results in an improvement of 40% compared with the first cycle. It is necessary to highlight that the sorption of bisphenol-A in dark conditions was not important; therefore, regeneration of the composite is not necessary in continuous water treatments. Ag/ZnO-PAA composites like those synthesized in this study are less sensitive to saturation compared to zeolites and carbon materials.

3. Bismuth oxychloride (BiOCl)

Bismuth oxyhalides BiOCl (X:Cl, Br, and I) are a new class of semiconductors that have recently attracted attentions in the photocatalytic process due to their relatively slow electron-hole recombination process. BiOXs are conformed by Bi^{3+}, O^{2-}, and halide (X^-) ions stacked in $[X\text{-}Bi\text{-}O\text{-}Bi\text{-}X]_n$ layers, giving a tetragonal structure with no linkers interactions with halide

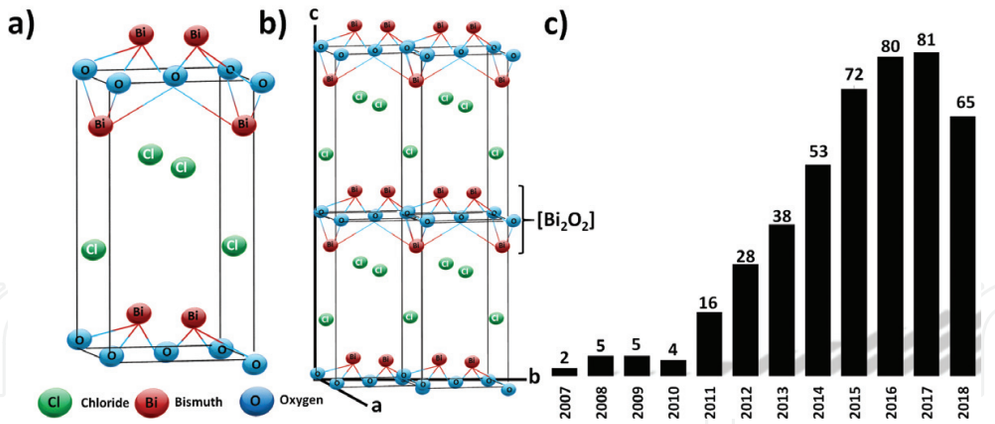

Figure 8. Scheme of unit cell (a), crystal structure BiOCl with {001} facet (b) and growing of articles of BiOCl in the photocatalytic process in later years (c).

along the C axis as showed in **Figure 8a**, **b**. The photocatalytic activity is due to $[Bi_2O_2]$ layers intercalated of double halogen atoms that allow a better separation of the electron-hole pairs. The bismuth oxychloride (BiOCl) is a solid inorganic compound, not toxic, of pearlescent white color and due its brightness has been used in the cosmetic industry. There is a record not greater than 500 articles reported in the Scopus database concerning the use of BiOCl, as photocatalyst; this review was realized in June 2018 (**Figure 8c**) and the first publications appeared in 2007 with a growing interest during the last years.

The BiOCl has a bandgap of 3.2–3.5 eV and the valence band is constituted of O_{2p} and Cl_{3p}; while the conduction band has Bi_{6p} according to density functional theory (DFT), whereby when excited, the electrons from Cl atoms are displaced at bismuth orbital [34].

Most studies of BiOCl photocatalyst are focused on enhancing the photocatalytic activity for environmental remediation, especially for dyes degradation during water treatment. Due to the bandgap, its photocatalytic activity, under UV irradiation, has shown a similar or better photocatalytic activity than TiO_2 [35]. Some "model" dyes used to evaluate the photocatalytic activity with BiOCl are methylene blue, methyl orange [36], and Rh B [37]. In spite of the bandgap of BiOCl, there are reports wherein demonstrate an excellent degradation of RhB under visible light [38].

However, some challenges remain for BiOCl as most photocatalysts also face; one challenge is its activation under visible light due to the limited absorption of such radiation. A variety of strategies have been employed to get better light absorption and to decrease the charge carrier recombination, such as the heterojunction, doping impurity, and metallization of the surface. Modifications consider the presence of metal elements or compounds like Ag [39, 40], AgCl [41], Fe [42], and Bi [43], also with materials carbon-based as graphene [44], graphene oxide [45], and with other semiconductors as Co_3O_4 [46], BiOI [47], and TiO_2 [48–50]. However, most researches evaluated the photocatalytic activity for degradation of dyes, considering the RhB in many cases. Other pollutant photodegradation studies are bisphenol A using Fe-BiOCl under visible light [42], sulfanilamide with BiOCl-RGO [51], and phenol under visible light with BiOCl-TiO_2 composite [50]. Nowadays, the BiOCl is being investigated to reduce of carbon dioxide (CO_2) [52].

3.1. Experimental section for BiOCl

The photocatalytic activity was evaluated using two commercial BiOCl samples, which were modified with silver (Ag), graphene oxide (OG), and TiO_2. The BiOCl samples were named as P2600 and SB. The P2600 sample is a hydrophobic sample while SB sample is hydrophilic sample.

3.1.1. Modification of BiOCl samples

The modification of BiOCl with Ag and OG was carried out by photodeposition method, which consisted in disperse 500 mg of BiOCl (P2600 and SB) in deionized water during 30 minutes, then the particles of the Ag or OG were added in different percentages; in the case of Ag were 2.0, 0.5, and 0.1% w/w and for OG were 0.5 and 0.1% w/w. Then, the sample was irradiated using a Q200 reactor (λ = 250 nm, 304 mW/cm^2) for 3 h with continuous stirring. Later, the samples were centrifuged and thoroughly water washed for several cycles, and finally, they were dried at 70°C for 24 h. The composites with TiO_2 were prepared by solvothermal method with different weight percentages of TiO_2 (25, 50, and 75% w/w).

3.1.2. Characterization

The crystal structure of the synthesized photocatalysts was analyzed by X-ray diffraction (XRD) using a DX8 advance diffractometer (Bruker) with: Cu Kα radiation, 35 kV, 25 mA, λ = 0.15418 nm over the 2θ range of 10–80° in a step of 0.02°s^{-1}. The analysis of surface morphology and microstructure of the samples was carried out by a QUANTA 200 environmental scanning electron microscope.

3.1.3. Photocatalytic activity

The photocatalytic activity was evaluated with two pollutants. The samples modified with Ag and OG were evaluated for RhB degradation under visible light, the RhB degradation was followed by UV-Vis spectrophotometer at 552 nm. The composites with TiO_2 were evaluated for Phenol degradation under visible light (Xenon lamp; Oriel 300 W; λ = 450 nm). Monitoring of phenol degradation was carried out by high performance liquid chromatography (HPLC) using a C18 column with a mobile phase of acetonitrile-water (27–75%) with a flow of 0.5 mL min^{-1}.

3.2. Results and discussion

Both pure BiOCl samples (P2600 and SB) showed overlapping flakes forming flower-like morphology, the size of flakes were of 10–60 microns approximately in P2600 samples (**Figure 9a**), while SB samples displayed a size of flakes about 9–34 microns (**Figure 9b**).

In the Ag-modified samples, small BiOCl-impregnated particles on the flakes were observed, in the case of the modified SB samples, a major impregnation of Ag particles was noticed (**Figure 9c**) in comparison with Ag-P2600 sample (**Figure 9d**); probably due to hydrophobic character of P2600 sample avoiding that Ag particles could have contact with the photocatalyst. Regarding OG-BiOCl samples, in both modified photocatalysts, it was observed

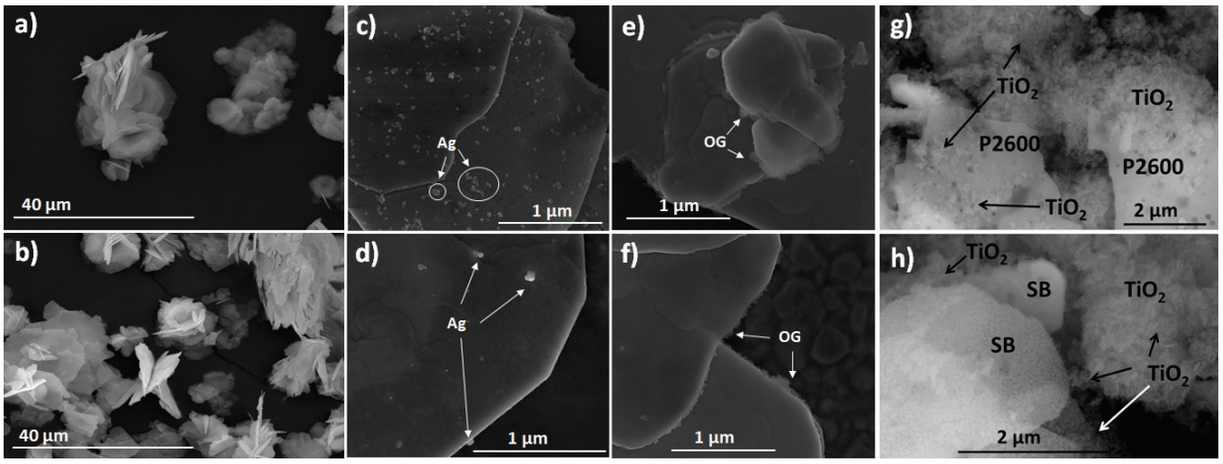

Figure 9. SEM images of BiOCl pure samples; SB (b) and P2600 (a). BiOCl modified with silver; Ag-SB (c) and Ag-P2600 (d). BiOCl modified with graphene oxide; OG-SB (e) and OG-P2600 (f). BiOCl modified with titanium dioxide; TiO_2-SB (g) and TiO_2-P2600 (h).

that small sheet of OG was deposited in the flakes of BiOCl, mainly in the edges of flakes as it is observed in **Figure 9e-f**. While in the composites of TiO_2-BiOCl, the generated TiO_2 was incrusted as small agglomerated particles on the BiOCl flakes (**Figure 9c-d**). Both photocatalysts could promote a better separation of photocharges generated during the reaction and therefore a better photocatalytic activity (**Figure 9g-h**).

The RhB degradation under visible light with Ag-BiOCl is shown in **Figure 10a**, **b**, the maximum degradation of RhB was obtained with pure BiOCl; and 30 and 40% of RhB degradation with P2600 and SB were obtained, respectively. In the case of Ag-SB, as the percentage of Ag increased, the photocatalytic activity decreased, while with Ag-P2600 was observed a greater degradation with 0.5% Ag than with 0.1%Ag. The presence of Ag in the BiOCl generates a decrease of photocatalytic activity, this result may be due to the presence of Ag in two oxidation states (Ag^0 and Ag^{1+}) observed in the XRD specter (**Figure 10c**, **d**), which may be acting as recombination sites. The modification with Ag incites a displacement of the [001] peak in the XRD specter probably due to the change of atoms of Bi by atoms of Ag because both elements have a similar ionic radius. Likewise, change of intensity in the [002] and [101] peaks in the spectra may be associated with a modification of the crystalline phase. This change in the Ag-BiOCl may affect the photocatalytic activity.

With the OG-BiOCl sample, the photocatalytic activity was different, since with low percentage of OG, the photocatalytic activity increased. The OG-SB sample (0.1% of OG) gave the greater degradation of RhB, while the OG-P2600 (0.1% of OG) and pure P2600 had the same degradation percentage (**Figure 11a**, **b**). In the XRD spectra of OG-BiOCl was observed, a decrement in intensities of [001], [102], and [112] peaks, and an intensity increment for [002] peak as the OG percentage increased. This result indicates that OG induces a better orientation of {001} facet in both BiOCls (**Figure 11c**, **d**).

Referring to TiO_2-BiOCl composite, its photocatalytic activity was evaluated for phenol degradation under visible light. The better composites were TiO_2-P2600 (75–25%) giving 45% of

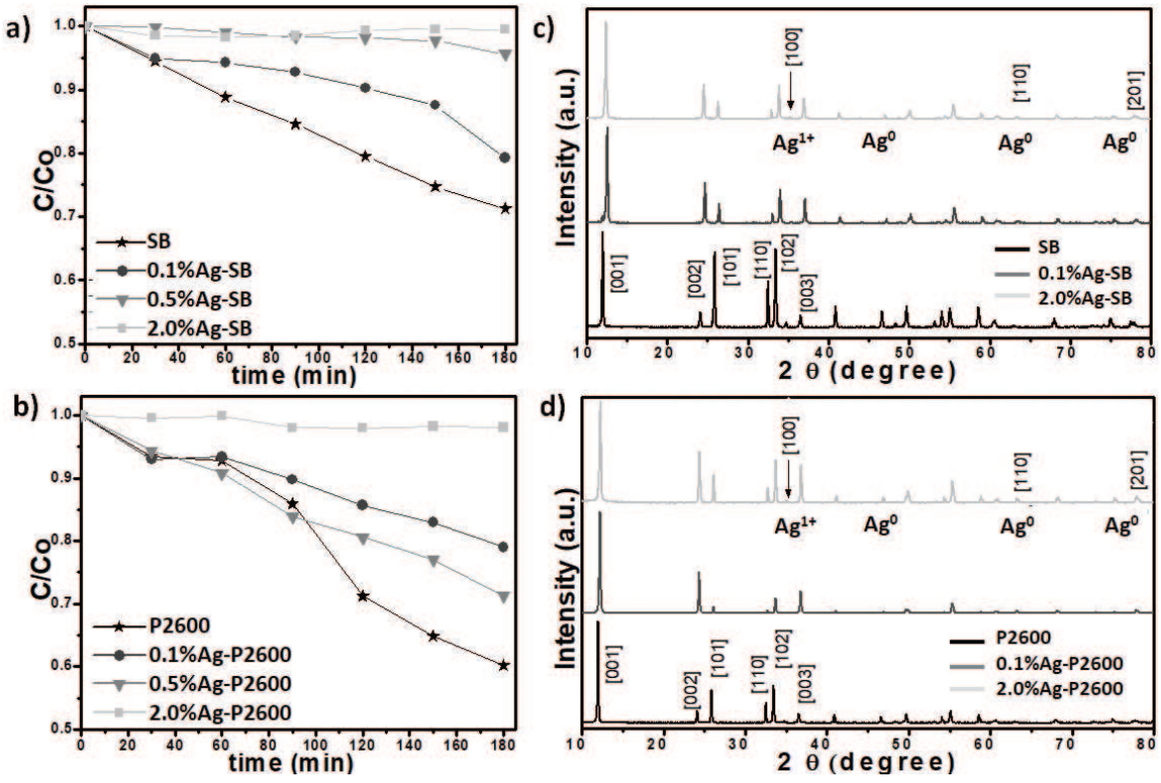

Figure 10. RhB degradation under visible irradiation with BiOCl pure and modified with silver; Ag-SB (a) and Ag-P2600 (b). XRD spectra of BiOCl samples; Ag-SB (c) and Ag-P2600 (d).

phenol degradation and TiO_2-SB (50–50%) giving 36% of phenol degradation during 6 h of reaction (**Figure 12a**, **b**). For the composite TiO_2-P2600 conforming the percentage of TiO_2 decreased, the photocatalytic activity also decreased. Such results confirm that there is a good interaction between both photocatalysts (BiOCl and TiO_2), in the TiO_2-P2600 composites, the size and hydrophobicity of P2600 played an important role in the adsorption of phenol on the surface, and therefore, gave a higher photocatalytic activity. In addition, higher TiO_2 percentage generated the appropriate heterojunction. In the XRD spectrum of TiO_2-BiOCl, the presence of peaks from both photocatalysts was observed (**Figure 12c**, **d**), also an overlap of the peaks [002] and [101] of BiOCl with the peak of [001] of TiO_2. In TiO_2-SB composites, it observed a lower intensity for [001] peak corresponding to BiOCl. Regarding TiO_2-SB composites, the SB exhibited a smaller size and hydrophilic character; then it was necessary that less amount of TiO_2 is active under visible light, and an increment of TiO_2 could generate the recombination of electron-hole pairs decreasing the photocatalytic activity.

The results obtained in our study offer a promising direction for the design of more practical and efficient photocatalysts to be used under visible light. In addition, the photocatalysis using BiOCl is becoming a promising research topic due to its fascinating characteristics, and it is necessary to study and understand the synthesis methods, morphology, predominant facets that improve the photocatalytic activity in all visible irradiations in order to achieve the mineralization of pollutants. Currently, our research group is working with the generation of biofuels by photocatalysis using BiOCl.

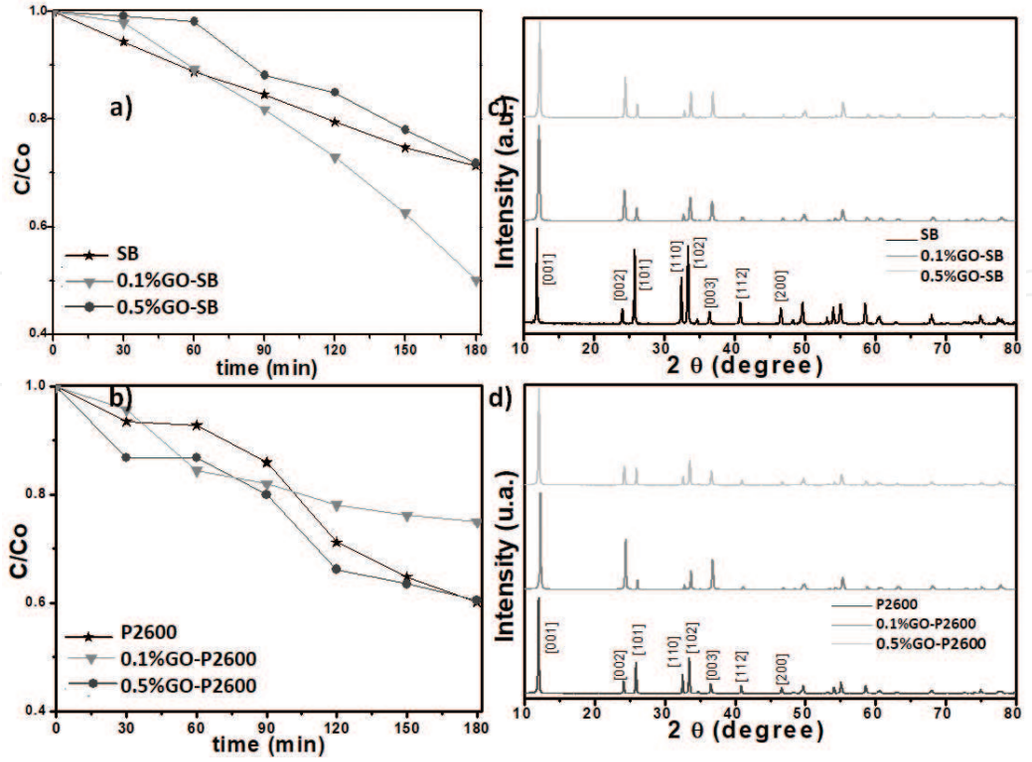

Figure 11. RhB degradation under visible irradiation with BiOCl pure and modified with graphene oxide; OG-SB (a) and OG-P2600 (b). XRD spectra of BiOCl samples; OG-SB (c) and OG-P2600 (d).

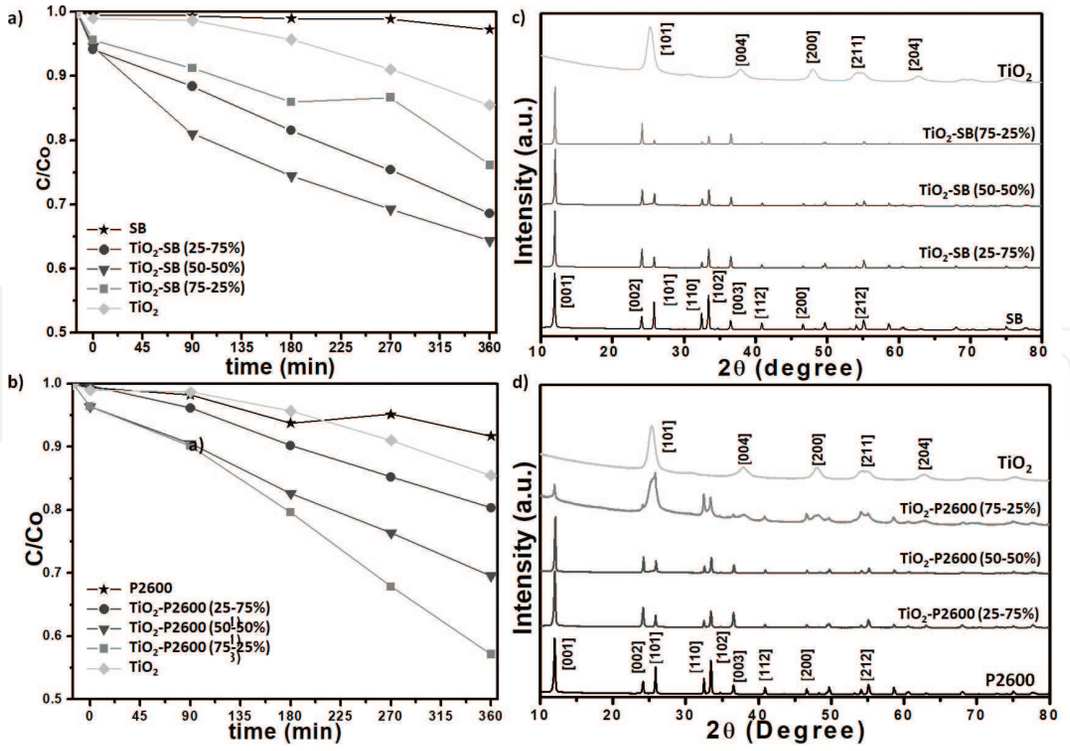

Figure 12. Phenol degradation under visible irradiation with BiOCl pure and modified with titanium dioxide; TiO_2-SB (a) and TiO_2-P2600 (b). XRD spectra of BiOCl samples; TiO_2-SB (c) and TiO_2-P2600 (d).

Author details

Vladimir A. Escobar Barrios[1]*, Dalia Verónica Sánchez Rodríguez[1],
Nancy Ayerim Cervantes Rincón[2] and Alma Berenice Jasso-Salcedo[3]

*Address all correspondence to: vladimir.escobar@ipicyt.edu.mx

1 Instituto Potosino de Investigación Científica y Tecnólogica, A.C. (IPICYT), Advanced Materials Division, San Luis Potosí, México

2 Instituto Potosino de Investigación Científica y Tecnólogica, A.C. (IPICYT), Environmental Sciences Division, San Luis Potosí, México

3 Department of Materials and Environmental Chemistry, Stockholm University, Stockholm, Sweden

References

[1] Lacombe S, Keller N. Photocatalysis: Fundamentals and applications in JEP 2011. Environmental Science and Pollution Research. 2012;**19**:3651-3654. DOI: 10.1007/s11356-012-1040-8

[2] Wang ZL, Kong XY, Ding Y, Gao P, Hughes WL, Yang R, et al. Semiconducting and piezoelectric oxide nanostructures induced by polar surfaces. Advanced Functional Materials. 2004;**14**:943-956. DOI: 10.1002/adfm.200400180

[3] Jasso-Salcedo AB, Hoppe S, Pla F, Escobar-Barrios VA, Camargo M, Meimaroglou D. Modeling and optimization of a photocatalytic process: Degradation of endocrine disruptor compounds by Ag/ZnO. Chemical Engineering Research and Design. 2017;**128**:174-191

[4] Man MT, Kim JH, Jeong MS, Do ATT, Lee HS. Oriented ZnO nanostructures and their application in photocatalysis. Journal of Luminescence. 2017;**185**:17-22. DOI: 10.1016/j.jlumin.2016.12.046

[5] Cantwell G, Harsch WC, Jogai B. Valence-band ordering in ZnO. Physical Review B: Condensed Matter and Materials Physics. 1999;**60**:2340-2344. DOI: 10.1103/PhysRevB.60.2340

[6] Porter F. Modified Metallic Oxides for Efficient Photocatalysis. First edit; 1991

[7] Jia W, Shang Y, Gong L, Chen X. Synthesis of Al-ZnO nanocomposite and its potential application in photocatalysis and electrochemistry. Inorganic Chemistry Communications. 2018;**88**:51-55. DOI: 10.1016/j.inoche.2017.12.013

[8] Schmidt-Mende L, MacManus-Driscoll JL. ZnO–Nanostructures, defects, and devices. Materials Today. 2007;**10**:40-48. DOI: 10.1016/S1369-7021(07)70078-0

[9] Daneshvar N, Aber S, Seyed Dorraji MS, Khataee AR, Rasoulifard MH. Photocatalytic degradation of the insecticide diazinon in the presence of prepared nanocrystalline ZnO

powders under irradiation of UV-C light. Separation and Purification Technology. 2007; **58**:91-98. DOI: 10.1016/j.seppur.2007.07.016

[10] Wang C, Astruc D. Recent developments of metallic nanoparticle-graphene nanocatalysts. Progress in Materials Science. 2018;**94**:306-383. DOI: 10.1016/j.pmatsci.2018.01.003

[11] Bai X, Wang L, Zhu Y. Visible photocatalytic activity enhancement of $ZnWO_4$ by graphene hybridization. ACS Catalysis. 2012;**2**:2769-2778. DOI: 10.1021/cs3005852

[12] Shen Y, Fang Q, Chen B. Environmental applications of three-dimensional graphene-based macrostructures: Adsorption, transformation, and detection. Environmental Science & Technology. 2015;**49**:67-84. DOI: 10.1021/es504421y

[13] McClellan K, Halden RU. Pharmaceuticals and personal care products in archived U.S. biosolids from the 2001 EPA national sewage sludge survey. Water Research. 2010;**44**: 658-668. DOI: 10.1016/j.watres.2009.12.032

[14] Walters E, McClellan K, Halden RU. Occurrence and loss over three years of 72 pharmaceuticals and personal care products from biosolids-soil mixtures in outdoor mesocosms. Water Research. 2010;**44**:6011-6020. DOI: 10.1016/j.watres.2010.07.051

[15] Jasso-Salcedo AB, Palestino G, Escobar-Barrios VA. Effect of Ag, pH, and time on the preparation of Ag-functionalized zinc oxide nanoagglomerates as photocatalysts. Journal of Catalysis. 2014;**318**:170-178

[16] Kislov N, Lahiri J, Verma H, Goswami DY, Stefanakos E, Batzill M. Photocatalytic degradation of methyl orange over single crystalline ZnO: Orientation dependence of photoactivity and photostability of ZnO. 2009;**25**:3310-3315. DOI: 10.1021/la803845f

[17] Santiago-Morales J, Gómez MJ, Herrera-López S, Fernández-Alba AR, García-Calvo E, Rosal R. Energy efficiency for the removal of non-polar pollutants during ultraviolet irradiation, visible light photocatalysis and ozonation of a wastewater effluent. Water Research. 2013;**47**:5546-5556. DOI: 10.1016/j.watres.2013.06.030

[18] Xu F, Chen J, Kalytchuk S, Chu L, Shao Y, Kong D, et al. Supported gold clusters as effective and reusable photocatalysts for the abatement of endocrine-disrupting chemicals under visible light. Journal of Catalysis. 2017;**354**:1-12. DOI: 10.1016/j.jcat.2017.07.027

[19] Dai Y, Yin L. Synthesis and photocatalytic activity of Ag-Ti-Si ternary modified-Bi_2O_3 nanoporous spheres. Materials Letters. 2015;**142**:225-228. DOI: 10.1016/j.matlet.2014.12.013

[20] Niu J, Dai Y, Yin L, Shang J, Crittenden JC. Photocatalytic reduction of triclosan on Au–Cu_2O nanowire arrays as plasmonic photocatalysts under visible light irradiation. Physical Chemistry Chemical Physics. 2015;**17**:17421-17428. DOI: 10.1039/C5CP02244D

[21] Zhao L, Deng J, Sun P, Liu J, Ji Y, Nakada N, et al. Nanomaterials for treating emerging contaminants in water by adsorption and photocatalysis: Systematic review and bibliometric analysis. Science of the Total Environment. 2018;**627**:1253-1263. DOI: 10.1016/j.scitotenv. 2018.02.006

[22] Chen F, An W, Liu L, Liang Y, Cui W. Highly efficient removal of bisphenol A by a three-dimensional graphene hydrogel-AgBr@rGO exhibiting adsorption/photocatalysis synergy. Applied Catalysis B: Environmental. 2017;**217**:65-80. DOI: 10.1016/j.apcatb.2017.05.078

[23] Fu H, Xu T, Zhu S, Zhu Y. Photocorrosion inhibition and enhancement of photocatalytic activity for ZnO via hybridization with C_{60}. Environmental Science & Technology. 2008; **42**:8064-8069. DOI: 10.1021/es801484x

[24] Xu T, Zhang L, Cheng H, Zhu Y. Significantly enhanced photocatalytic performance of ZnO via graphene hybridization and the mechanism study. Applied Catalysis B: Environmental. 2011;**101**:382-387. DOI: 10.1016/j.apcatb.2010.10.007

[25] Xie W, Li Y, Sun W, Huang J, Xie H, Zhao X. Surface modification of ZnO with Ag improves its photocatalytic efficiency and photostability. Journal of Photochemistry and Photobiology A: Chemistry. 2010;**216**:149-155. DOI: http://dx.doi.org/10.1016/j.jphotochem.2010.06.032

[26] Kawano K, Komatsu M, Yajima Y, Haneda H, Maki H, Yamamoto T. Photoreduction of Ag ion on ZnO single crystal. Applied Surface Science. 2002;**189**:265-270

[27] Salaün A, Hamilton JA, Iacopino D, Newcomb SB, Nolan MG, Padmanabhan SC, et al. The incorporation of preformed metal nanoparticles in zinc oxide thin films using aerosol assisted chemical vapour deposition. Thin Solid Films. 2010;**518**:6921-6926

[28] Li B, Cao H. ZnO@graphene composite with enhanced performance for the removal of dye from water. Journal of Materials Chemistry. 2011;**21**:3346-3349. DOI: 10.1039/c0jm03253k

[29] Xiong Z, Zhang LL, Ma J, Zhao XS. Photocatalytic degradation of dyes over graphene-gold nanocomposites under visible light irradiation. Chemical Communications. 2010;**46**: 6099-6101. DOI: 10.1039/c0cc01259a

[30] Jasso-Salcedo AB, Meimaroglou D, Hoppe S, Pla F, Escobar-Barrios VA. Surface modification and immobilization in poly (acrylic acid) of Ag/ZnO for photocatalytic degradation of endocrine-disrupting compounds. Journal of Applied Polymer Science. 2016;**133**:1-12

[31] Leng C, Wei J, Liu Z, Xiong R, Pan C, Shi J. Facile synthesis of PANI-modified $CoFe_2O_4$-TiO_2 hierarchical flower-like nanoarchitectures with high photocatalytic activity. Journal of Nanoparticle Research. 2013;**15**:1643

[32] Zhang H, Zong R, Zhu Y. Photocorrosion inhibition and photoactivity enhancement for zinc oxide via hybridization with monolayer polyaniline. Journal of Physical Chemistry C. 2009;**113**:4605-4611

[33] Lu B, Liu M, Shi H, Huang X, Zhao G. A novel photoelectrochemical sensor for bisphenol A with high sensitivity and selectivity based on surface molecularly imprinted polypyrrole modified TiO_2 nanotubes. Electroanalysis. 2013;**25**:771-779

[34] Yang W, Wen Y, Chen R, Zeng D, Shan B. Study of structural, electronic and optical properties of tungsten doped bismuth oxychloride by DFT calculations. Physical Chemistry Chemical Physics. 2014;**16**:21349-21355. DOI: 10.1039/C4CP02801E

[35] Sun D, Li J, Feng Z, He L, Zhao B, Wang T, et al. Solvothermal synthesis of BiOCl flower-like hierarchical structures with high photocatalytic activity. Catalysis Communications. 2014;**51**:1-4. DOI: 10.1016/j.catcom.2014.03.004

[36] Sarwan B, Pare B, Acharya AD. The effect of oxygen vacancies on the photocatalytic activity of BiOCl nanocrystals prepared by hydrolysis and UV light irradiation. Materials Science in Semiconductor Processing. 2014;**25**:89-97. DOI: 10.1016/j.mssp.2013.09.015

[37] Hao HY, Xu YY, Liu P, Zhang GY. BiOCl nanostructures with different morphologies: Tunable synthesis and visible-light-driven photocatalytic properties. Chinese Chemical Letters. 2015;**26**:133-136. DOI: 10.1016/j.cclet.2014.11.022

[38] Wang Q, Hui J, Huang Y, Ding Y, Cai Y, Yin S, et al. The preparation of BiOCl photocatalyst and its performance of photodegradation on dyes. Materials Science in Semiconductor Processing. 2014;**17**:87-93. DOI: 10.1016/j.mssp.2013.08.018

[39] Gao Y, Wang L, Li Z, Li C, Cao X, Zhou A, et al. Microwave-assisted synthesis of flower-like Ag-BiOCl nanocomposite with enhanced visible-light photocatalytic activity. Materials Letters. 2014;**136**:295-297. DOI: 10.1016/j.matlet.2014.08.026

[40] Zhang Z, Zhou Y, Yu S, Chen M, Wang F. Ag-BiOCl nanocomposites prepared by the oxygen vacancy induced photodeposition method with improved visible light photocatalytic activity. Materials Letters. 2015;**150**:97-100. DOI: 10.1016/j.matlet.2015.03.011

[41] Cheng J, Wang C, Cui Y, Sun Y, Zuo Y, Wang T. Large improvement of visible-light-driven photocatalytic property in AgCl nanoparticles modified black BiOCl microsphere. Materials Letters. 2014;**127**:28-31. DOI: 10.1016/j.matlet.2014.04.012

[42] Xia J, Xu L, Zhang J, Yin S, Li H, Xu H, et al. Improved visible light photocatalytic properties of Fe/BiOCl microspheres synthesized via self-doped reactable ionic liquids. CrystEngComm. 2013;**15**:10132. DOI: 10.1039/c3ce41555d

[43] Hu J, Xu G, Wang J, Lv J, Zhang X, Zheng Z, et al. Photocatalytic properties of Bi/BiOCl heterojunctions synthesized using an in situ reduction method. New Journal of Chemistry. 2014;**38**:4913-4921. DOI: 10.1039/C4NJ00794H

[44] Gao F, Zeng D, Huang Q, Tian S, Xie C. Chemically bonded graphene/BiOCl nanocomposites as high-performance photocatalysts. Physical Chemistry Chemical Physics. 2012;**14**:10572. DOI: 10.1039/c2cp41045a

[45] Kang S, Pawar RC, Pyo Y, Khare V, Lee CS. Size-controlled BiOCl–RGO composites having enhanced photodegradative properties. Journal of Experimental Nanoscience. 2016;**11**:259-275. DOI: 10.1080/17458080.2015.1047420

[46] Tan C, Zhu G, Hojamberdiev M, Okada K, Liang J, Luo X, et al. Co_3O_4 nanoparticles-loaded BiOCl nanoplates with the dominant {001} facets: Efficient photodegradation of organic dyes under visible light. Applied Catalysis B: Environmental. 2014;**152–153**: 425-436. DOI: 10.1016/j.apcatb.2014.01.044

[47] Sun L, Xiang L, Zhao X, Jia CJ, Yang J, Jin Z, et al. Enhanced visible-light photocatalytic activity of BiOI/BiOCl heterojunctions: Key role of crystal facet combination. ACS Catalysis. 2015;**5**:3540-3551. DOI: 10.1021/cs501631n

[48] Liu Z, Xu X, Fang J, Zhu X, Li B. Synergistic degradation of eosin y by photocatalysis and electrocatalysis in UV irradiated solution containing hybrid BiOCl/TiO_2particles. Water, Air, and Soil Pollution. 2012;**223**:2783-2798. DOI: 10.1007/s11270-011-1066-4

[49] Li L, Zhang M, Liu Y, Zhang X. Hierarchical assembly of BiOCl nanosheets onto bicrystalline TiO_2 nanofiber: Enhanced photocatalytic activity based on photoinduced interfacial charge transfer. Journal of Colloid and Interface Science. 2014;**435**:26-33. DOI: 10.1016/j.jcis.2014.08.022

[50] Sánchez-Rodríguez D, Méndez Medrano MG, Remita H, Escobar-Barrios V. Photocatalytic properties of BiOCl-TiO_2 composites for phenol photodegradation. Journal of Environmental Chemical Engineering. 2018;**6**:1601-1612. DOI: 10.1016/j.jece.2018.01.061

[51] Dong S, Pi Y, Li Q, Hu L, Li Y, Han X, et al. Solar photocatalytic degradation of sulfanilamide by BiOCl/reduced graphene oxide nanocomposites: Mechanism and degradation pathways. Journal of Alloys and Compounds. 2016;**663**:1-9. DOI: 10.1016/j.jallcom.2015.12.027

[52] Zhang L, Wang W, Jiang D, Gao E, Sun S. Photoreduction of CO_2 on BiOCl nanoplates with the assistance of photoinduced oxygen vacancies. Nano Research. 2015;**8**:821-831. DOI: 10.1007/s12274-014-0564-2

IntechOpen